Batteries in Electricity Markets: Economic Planning and Operations

Bolun Xu

A dissertation
submitted in partial fulfillment of the
requirements for the degree of

Doctor of Philosophy

University of Washington

2018

Reading Committee:

Daniel S. Kirschen, Chair

Baosen Zhang

Miguel A. Ortega-Vazquez

Venkat Subramanian

Program Authorized to Offer Degree:
Electrical Engineering

University of Washington

Abstract

Batteries in Electricity Markets:
Economic Planning and Operations

Bolun Xu

Chair of the Supervisory Committee:
Professor Daniel S. Kirschen
Department of Electrical Engineering

Batteries have been storing electricity for mankind since 1800, while it is till recently that grid-scale battery energy storage become commercially viable and are seeking merchant opportunities in electricity markets. Battery energy storage have faster ramp speed compared to other types of generation units, and are extremely valuable for facilitating the integration of renewable energy resources. Battery energy storage can provide arbitrage and ancillary services in the electricity market. However, even though nowadays battery energy storage systems are constructed and operated with mature technologies, it remains an open question on how to operates them economically in electricity market to maximize the investment profit.

This dissertation covers the optimal planning, scheduling, and operation for battery energy storage in electricity markets. It shows that the degradation mechanism of electrochemical battery cells must be considered in market bidding and operation strategies to maximize the participant's operating profit, and proposes optimal methods to incorporate the cost of battery degradation into different participation stages and markets.

For frequency regulation markets, this dissertation proposes a real-time control policy that optimally trades-off the performance penalty and the degradation cost in frequency regulation operations. A optimal bidding policy is designed based on the proposed control policy to maximize participant's market profit while maintaining satisfactory operation

performance. For energy markets, this dissertation designs a piece-wise linear model that accurately incorporates battery degradation cost into dispatch optimization and bidding strategies. Finally, this dissertation proposes a bi-level planning model to optimize the location and rating of battery energy storage systems considering both energy and reserve markets. This model ensures the profitability of investments in energy storage by enforcing a rate of return constraint. This model is tested on a 240-bus model of the Western Electricity Coordinating Council (WECC) system, and the result analyzes the effects of different storage technologies, rate of return requirements, and regulation market policies on ES participation on the optimal storage investment decisions.

TABLE OF CONTENTS

Page

List of Figures iv

Chapter 1: Introduction 1
1.1 Batteries for Grid-scale Energy Storage 1
1.2 Participation of Battery Energy Storage in Electricity Markets 3
1.3 Thesis Outline 3

Chapter 2: Cost of Battery Degradation 6
2.1 Battery Operating Cost 6
2.2 Electrochemical Battery Degradation Mechanisms 7
2.3 The Rainflow Counting Algorithm 9

Chapter 3: Battery Real-Time Control 12
3.1 Motivation 12
3.2 Contribution 13
3.3 Modeling 13
3.4 Proposed Online Control Policy 15
3.5 Simulation Results 20
3.6 Summary 22

Chapter 4: Battery Bidding in Regulation Market 26
4.1 Motivation 26
4.2 Contribution 27
4.3 Regulation Market Model 27
4.4 Optimization Problem Formulation 28
4.5 Optimal Control and Bidding Policy 29
4.6 Simulation 34
4.7 Summary 37

Chapter 5: Battery Scheduling in Energy Market 41
5.1 Motivation 41
5.2 Contribution 41
5.3 Marginal Cost of Battery Cycling 42
5.4 Optimizing the BES Dispatch 43
5.5 Case Study 47
5.6 Summary 53

Chapter 6: Battery Planning in Energy and Reserve Markets 56
6.1 Motivation 56
6.2 Contribution 57
6.3 Problem Formulation 58
6.4 Solution Method 63
6.5 Case Study Test System 69
6.6 Simulation Results 74
6.7 Summary 79

Chapter 7: Conclusion 81
7.1 Conclusion 81
7.2 Suggestions for Future Work 82

Bibliography 87

Appendix A: Supplementary Material to Chapter 3 100
A.1 Model Reformulation 100
A.2 Proof for Theorem 2 100

Appendix B: Supplementary Material to Chapter 6 104
B.1 Proof for Theorem 3 104
B.2 PJM Performance Index Simplification 104

Appendix C: Supplementary Material to Chapter 5 106
C.1 Numerical example 112

Appendix D: Supplementary Material to Chapter 6 116
D.1 Nomenclature 116
D.2 Single-Level Equivalent Problem Formulation 118

D.3 ES Profit Constraint Transformation 120
D.4 ES Subgradient Derivation at B^{E} Buses 121
D.5 ES Subgradient Derivation for B^{N} Buses 121
D.6 Exact Relaxation of ES Dispatch Constraints 122

LIST OF FIGURES

Figure Number Page

1.1 Overview of the Participation of Battery Energy Storage in Electricity Markets. 4

2.1 Market price daily variation examples (Source: ISO New England). 8

2.2 Using the rainflow algorithm to identify battery cycle depths. 10

3.1 Proposed control policy illustration. The policy keeps track the current maximum and minimum SoC level. When the distance in between reaches the calculated threshold $\hat{u}$, the policy starts to constrain the response. 16

3.2 Illustration of the optimal cycle depth when responding to regulation instructions. During a single cycle, the participant avoids a mismatch penalty that is linear with respect to the cycle depth, and undertakes a nonlinear cycle aging cost. Hence there exists an optimal cycle depth the maximizes the operating profit which is the area between the two curves. 18

3.3 Example illustration of the policy optimality under different price settings. The value of + is the same in all cases and the round-trip efficiency is assumed to be one, so $\hat{u}$ is the same in all cases. 23

3.4 Distribution of optimality gaps for Case 5 and Case 8. Although Case 8 has twice the duration of Case 5, their optimality gaps are similar. This validates that the worst-case optimality gap is independent of the regulation operation duration. 25

3.5 Regulation operating cost break-down comparison between the proposed policy and the simple policy. Although the proposed policy has higher penalties, the cost of cycle aging is significantly smaller, so it achieves better trade-offs between degradation and mismatch penalty. 25

4.1 Flow chart of the regulation market and control processes. The control policy inputs the clearing prices for determining the optimal response, while the bidding policy submits offers to the market while considering the control policy. 30

4.2 Full year revenue analysis of a 1 MWh BES participating in the regulation market with di erent regulation capacities. (a) With the proposed control policy; (b) With the simple control policy. 36

4.3 PJM case study. (a) The relative regulation capacity vs. di erent from simulating historical regulation signals in 2013 and 2016; (b) Histogram of all cleared regulation capacities under di erence con dence 38
4.4 PJM case study risk analysis. (a) Annual prorated operating pro t vs. performance con dence ; (b) Average annual performance index vs. performance con dence 39
5.1 Upper-approximation to the cycle depth aging stress function. 42
5.2 BES dispatch for different cycle aging cost models (ISO New England SEMASS Zone, Jan 5th & 6th, 2015). 49
5.3 Difference between the cycle aging cost calculated using the predictive model and an ex-post calculation using the benchmark rainflow method for a full-year 5-minute RTM dispatch simulation. 52
6.1 Flowchart of the solution algorithm 62
6.2 LMO battery cycle life curve and fitting to 70% DoD. 72
6.3 Computation test results of the 16 test cases. 73
6.4 AA-CAES planning in different market scenarios. 76
6.5 LiBES planning with decreasing investment cost. 77
7.1 Wholesale market with local aggregation. 84
7.2 Distributed energy resource management system. 85
A.1 Illustration for Lemma 4. The largest half cycle is between s_4 and s_5, other half cycles are in strictly decreasing order either to the left- or to the right-hand side direction of this largest half cycle. 101
A.2 Illustration for Lemma 3. 103
C.1 Cycle counting example. 112
C.2 An example of SoC profile. 113

ACKNOWLEDGMENTS

My PhD study has been a wonderful time thanks to the people around me. I give my most sincere acknowledgement to my PhD advisor Professor Daniel Kirschen, for his utmost guidance and support during my research. Professor Kirschen granted my the best research environment and encouragement, and helped me expanding my connection inside and outside University of Washington. Despite research, I also appreciate his way of working with people and managing the research group, which serves as an extraordinary role model for my future career development.

I'm fortunate to have Professor Baosen Zhang as my PhD co-advisor. It is under his guidance that I excelled my understanding in control and optimization, and it was through our numerous discussions that I expanded my vision beyond power system, and elevated my pursue to cutting edge research challenges.

Thanks to my PhD committee members Professor Miguel Ortega-Vazquez and Professor Venkat Subramanian, for their insightful suggestions during my general exam and dissertation. I also want to send my thanks to Professor Richard Christie for being on my qualify exam committee, and guided me through my teaching assistant periods.

My internship at ISO New England was a turning point for my career, where I got the opportunity to combined my research with practical market requirements. This could not have been possible without the guidance from my mentors there, Dr. Jinye Zhao, Dr. Tongxin Zheng, and Dr. Eugene Litvinov. I give them and all members in the BAT group my most sincere gratitude.

My appreciation to Dr. Tess Williams during my internship at Doosan Gridtech, for treating my as an equal member in the company and offering me opportunities to work on projects based on my interest. I also want to send my thanks to everyone that worked with me there, including Daejin Choi, Dan Sowder, Daniel Malarkey, Jared Slivia, Patrick Leslie,

Troy Negaard, Jason Yedinak, Farshid Shariatzadeh, Sam Zuckerman, and Jiyun Jung.

My thanks to the faculties and staffs at the UW Clean Energy Institute, particularly Dr. Daniel T. Schwartz, Dr. David S. Ginger, Shaun Taylor, and Sara Carlson. Thanks for sponsoring my research, and for awarding me the scientific achievement award. I also want to thank the staffs at the UW Electrical Engineering department for helping me with administrative issues, and the Grainger Foundation for funding my first year PhD study.

My acknowledgement to my research collaborators outside University of Washington and ISO New England: Dr. Di Wang from Microsoft Research, Dr. Cesar Silva-Monroy from Demand Energy, and Dr. Jean-Paul Waston from Sandia National Laboratory.

During my study at UW, I'm pleased to have collaborated with Yishen Wang, Ting Qiu, Yury Dvorkin, Ricardo Fernndez-Blanco, Yushi Tan, Yuanyuan Shi, Yao Long, Hao Wang, Yi Luan, Mathew Murbach, and Sergio Diaz. Thanks for the great works and those helpful discussions. My thanks to all the friends and colleagues there, in no particular order: Zeyu Wang, Zhongming Ye, Ruiyi Li, Yize Chen, Pan Li, Yang Wang, Yi Wang, Yao Chang, Jingkun Liu, Chenghui Tang, Hao Wu, Chuhui Zhang, Tongxi Pan, Jesus Contreras, Ahmad Milyani, Abeer Almainouni, Rya Elliott, Daniel Olsen, Nam Song, Mareldi Ahumada, Ahlmahz Negash, Tu Nguyen, Remy Rigo-Mariani, Mushfiqur Sarker, Kelly Kozdras, Anna Edwards, Kevin Morrissey, Ryan Hay, James Miller, Agustina Gonzalez, Rebecca Breiding. I also want to give my thanks to my internship colleagues at ISO New England: Xuan Zhang, Yufeng Cao, Meng Wu, and Christoph Lackner.

I want to thank all my family friends in Seattle for all the wonderful moments we shared together, in no particular order: Fangmin Yu, George Yu, Bruce Yu, Can Tang, Zoe Mei, Chen Li, Kai Shen, Weicong Ding, Wei Si, Lu Zhou, Long Ren.

I'm most grateful to my parents and my in-laws, for their unconditional love and support. And finally, I am lucky to be accompanied by my wife, Minwen Weng, during my PhD study. And we are so fortunate to have welcomed our daughter into this workd, Hanna Xu, who slept over my chest during the writing of this thesis.

DEDICATION

to Hanna and Minwen

Chapter 1

INTRODUCTION

1.1 Batteries for Grid-scale Energy Storage

Current power systems need more energy storage to increase operation flexibility and improve renewable penetrations [62], and electrochemical batteries are the most promising candidate for building new grid-scale storage systems [39]. The Federal Energy Regulatory Commission (FERC) issued Order No. 784 [50] in 2013 that opens access for energy storage in ancillary services markets. While in 2018, FERC issued another Order. 841 to remove barriers to the participation of electric storage resources in the capacity, energy and ancillary services markets operated by Regional Transmission Organizations and Independent System Operators. The International Renewable Energy Agency (IREA) estimates that 150 GW of battery capacity are required to double the current global renewable penetration, while the National Renewable Energy Laboratory concludes that California needs 20 GW of storage capacity to reach a 50% photovoltaic (PV) penetration [34]. As for 2016, about 200 MW of stationary lithium-ion batteries were operating in grid-connected installations worldwide [46]. In PJM Interconnections, batteries have provided 41% of the frequency regulation capacity in 2016 [8]. In addition to grid-scale battery energy storage, electric vehicles (EV) are also substantial battery resources for the power system [128]. The global EV stock has reached 1.26 million in 2015 [2], equivalent to more than 30 GWh of battery storage capacity[1]. With the surging demand for new batteries, it is expected that global annual production capacity for lithium-ion battery cells will exceed 100 GWh by 2020 [81].

Energy storage provides valuable operation flexibilities to the power system. A critical task in power system operations is to maintain the instantaneous balance between generations and demands [127]. In a traditional power system, the system operator schedules

[1] This estimation assumes each EV has a 30 kWh battery installed.

generations to match demand variations. However, when intermittent renewable generations such as wind and solar are integrated into the system, maintaining the power balance becomes challenging because existing generators in the system are not fast enough to compensate variations from renewable injections. With energy storage, a system operator can store excessive generations, and re-dispatch the stored energy when the system needs additional generations. For example, in a system with a high share of solar generations, energy storage stores excessive solar power during the daytime and discharge electricity into the grid at night when there is no sunlight. Hence energy storage enables more solar energy to be utilized and reduces the generation from fossil fuels.

Although energy storage are vital resources for improving renewable penetration, increasing storage capacity in a power system was not easy before batteries become commercially viable. Traditional energy storage systems are dominated by pumped hydroelectric (PHS) [39]. A PHS stores electricity in the form of gravitational potential energy of water, pumped from a lower elevation reservoir to a higher elevation. PHS units are geographically dependent and can only be installed in mountain areas with sufficient terrain elevation differences. Besides PHS, compressed air energy storage (CAES) also use mechanical means to store electricity. Traditional CAES design uses salt dome to store compressed air, and only two CAES units have been built in history [60], while new above-ground CAES designs hare not commercially viable yet [150].

Battery energy storage systems are geographically unrestricted and can be installed anywhere in a power system, hence batteries are very suitable for accommodating distributed renewable generations. Electrochemical batteries also have faster ramp speed than PHS. PHS units typically take minutes to start up [79], while batteries ramp instantaneously and do not require minimum stable generation or consumption. Besides, batteries are more flexible to dispatch since PHS units must be scheduled according to weather conditions. So far, technologies for building and controlling grid-scale battery energy storage systems (BESS) have been well established [60].

Yet it remains an open question that how to design and operate battery storage economically while addressing their unique degradation characteristics. The life time of electrochemical batteries are extremely sensitive to operation [136, 147], hence their wear-and-tear cost

cannot be neglected when operating the battery and degradation must be incorporated into their planning and operation strategies. However, electricity markets typically model operating cost based on thermal generator heat rate curves, which are inaccurate to model the unique aging mechanisms of electrochemical batteries. Several studies [1, 54, 61, 72, 89, 135] have proposed battery planning and operation strategies that incorporates battery degradation mechanism, however all of these approaches assume certain operation pattern that either constraints the operational flexibility of batteries, or the proposed method become inaccurate if applied to other scenarios.

1.2 Participation of Battery Energy Storage in Electricity Markets

The participation of battery energy storage (BES) in an electricity market can be characterized into three stages:

- The planning stage: BES investors must determine the location to deploy the BES. The power rating and energy rating of each BES unit must also be determined. The deployed BES is then registered for market participation.

- The scheduling stage: The BES owner determines which market (wholesale energy market, frequency regulation market, reserve market) to participate, and submits bid prices and quantities into the corresponding markets. The system operator clears the market based on demand forecast and system security operation constrains. Market clearing prices are published after market clearance.

- The dispatch stage: The system operator issues dispatch instructions to each participation units. The response from these units are recorded, which is later compared with the issued instructions for calculating the ex-post settlement.

Fig. 1.1 includes an overview of the BES participation in electricity markets.

1.3 Thesis Outline

This dissertation aims at improving the planning and operation of battery storage in participating electricity markets. It provides solutions to the following questions:

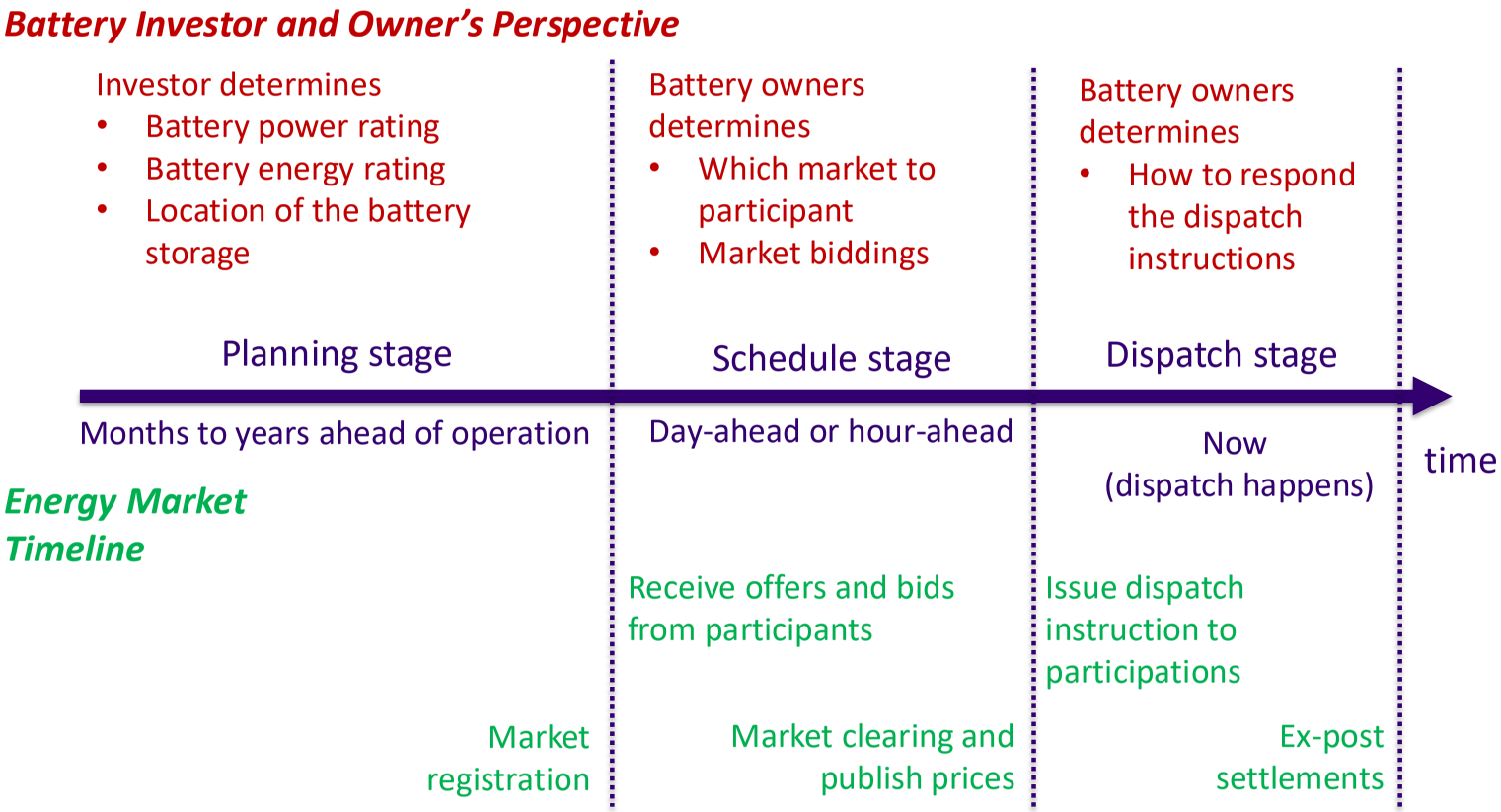

Figure 1.1: Overview of the Participation of Battery Energy Storage in Electricity Markets.

- How to balance the cost of degradation and deviation penalties in real-time stochastic battery operations such as providing frequency regulation or assisting renewable integration.

- How to design optimal bids into the regulation market to maximize battery owner's profit while maintaining satisfactory performance.

- How to accurately model the battery aging mechanism when dispatching batteries in electricity markets.

- How to efficiently identify the location as well as the power and energy rating for battery energy storage in a vertically integrated power system.

Chapter 2

COST OF BATTERY DEGRADATION

2.1 Battery Operating Cost

Previous BES economic studies typically assume that battery cells have a fixed lifetime and do not include the cost of replacing the battery in the BES variable operating and maintenance (O&M) cost [70]. The Electricity Storage Handbook from Sandia National Laboratories assumes that a BES performs only one charge/discharge cycle per day, and that the variable O&M cost of a lithium-ion BES is constant and about 2 $/MWh [5]. Similarly, Zakeri *et al.* [150] assume that battery cells in lithium-ion BES are replaced every five years, and assume the same 2 $/MWh O&M cost. Other energy storage planning and operation studies also assume that the operating cost of BES is negligible and that they have a fixed lifespan [109, 116, 119]. These assumptions are not valid if the BES is cycled multiple times per day because more frequent cycling increases the rate at which battery cells degrade and hasten the time at which they need to be replaced. To secure the battery lifespan, Mohsenian-Rad [89] caps the number of cycles a battery can operate per day. However, artificially limiting the cycling frequency prevents operators from taking advantage of a BES's operational flexibility and significantly lessens its profitability. To take full advantage of the ability of a BES to take part in energy and ancillary markets, its owner must be able to cycle it multiple times per day and to follow irregular cycles. Under these conditions, its lifetime can no longer be considered as being fixed and its replacement cost can no longer be treated as a capital expense. Instead, the significant part of the battery degradation cost that is driven by cycling should be treated as an operating expense.

A BES performs temporal arbitrage in an electricity market by charging with energy purchased at a low price, and discharging this stored energy when it can be sold at a higher price. The profitability of this form of arbitrage depends not only on the price difference but also on the cost of the battery cycle aging caused by these charge/discharge cycles.

When market prices are stable, the expected arbitrage revenue is small and the BES owner may therefore opt to forgo cycling to prolong the battery lifetime and reduce its cycle aging cost. On the other hand, if the market exhibits frequent large price fluctuations, the BES owner could cycle the BES multiple times a day to maximize its profits. Fig. 2.1 shows that the price profile in a given market can change significantly from day to day. Although the average market price is higher in Fig. 2.1a, arbitrage is not profitable in this case because the price fluctuations are small, and the aging cost from cycling is likely to be higher than the revenue from arbitrage. On the other hand, a BES owner is likely to perform three arbitrage cycles if the price profile is similar to the one shown on Fig. 2.1b, because the revenue opportunities arising from the large price fluctuations are likely to be larger than the associated cycle aging cost. It is thus crucial to accurately incorporate the cost of cycle aging into the optimal operation of a BES.

2.2 Electrochemical Battery Degradation Mechanisms

Electrochemical batteries have limited cycle life [39] because of the fading of active materials caused by the charging and discharging cycles. This cycle aging is caused by the growth of cracks in the active materials, a process similar to fatigue in materials subjected to cyclic mechanical loading [48, 76, 77, 136, 138]. Chemists describe this process using partial differential equations [121]. These models have good accuracy but cannot be incorporated in dispatch calculations. On the other hand, heuristic battery lifetime assessment models assume that degradation is caused by a set of stress factors, each of which can be represented by a stress model derived from experimental data. The effect of these stress factors varies with the type of battery technology. In this paper, we focus on lithium-ion batteries because they are widely considered as having the highest potential for grid-scale applications. For our purposes, it is convenient to divide these stress factors into two groups depending on whether or not they are directly affected by the way a grid-connected battery is operated:

- Non-operational factors: ambient temperature, ambient humidity, battery state of life, calendar time [67].

- Operational factors: Cycle depth, over charge, over discharge, current rate, and aver-

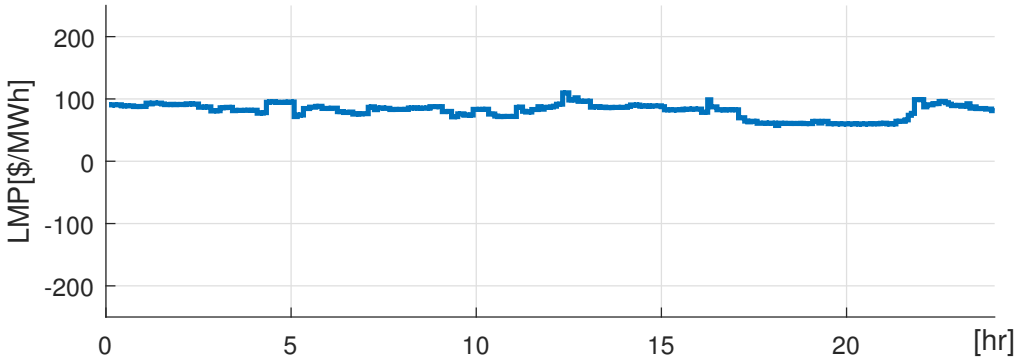

(a) An example of stable market prices (Jan 7, 2015).

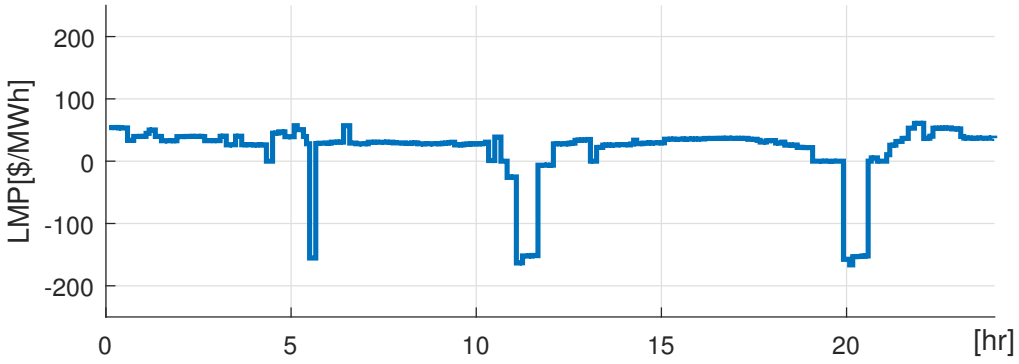

(b) An example of highly variable market prices (Jan 2, 2015).

Figure 2.1: Market price daily variation examples (Source: ISO New England).

age state of charge (SoC) [136].

2.2.1 Cycle depth

Cycle depth is an important factor in a battery's degradation, and is the most critical component in the BES market dispatch model. A 7 Wh Lithium Nickel Manganese Cobalt Oxide (NMC) battery cell can perform over 50,000 cycles at 10% cycle depth, yielding a lifetime energy throughput (i.e. the total amount of energy charged and discharged from the cell) of 35 kWh. If the same cell is cycled at 100% cycle depth, it can only perform 500 cycles, yielding an lifetime energy throughput of only 3.5 kWh [43]. This nonlinear aging property with respect to cycle depth is observed in most static electrochemical batteries [23,

124, 139, 146].

2.2.2 Current rate

While high charging and discharging currents accelerate the degradation rate, grid-scale BES normally have capacities greater than 15 minutes. The effect of current rate on degradation is therefore small in energy markets according to results of laboratory tests [139]. We will therefore not consider the current rate in our model. If necessary, a piecewise linear cost curve can be used to model the current rate stress function as a function of the battery's power output.

2.2.3 Over charge and over discharge

In addition to the cycle depth effect, extreme SoC levels significantly reduce battery life [136]. However, over-charging and over-discharging are avoided by enforcing upper and lower limits on the SoC either in the dispatch or by the battery controller.

2.2.4 Average state of charge

The average SoC level in each cycle has a highly non-linear but slight effect on the cycle aging rate [43, 85]. Therefore we do not consider this stress factor in the proposed model.

2.3 The Rainflow Counting Algorithm

The rainflow counting algorithm is used extensively in materials stress analysis to count cycles and quantify their cumulative impact. It has also been applied to battery life assessment [90, 146]. Given a SoC profile with a series of local extrema (i.e. points where the current direction changed) s_0, s_1, $\therefore$, etc, the rainflow method identifies cycles as [7]:

1. Start from the beginning of the profile (as in Fig. 2.2a).

2. Calculate $\Delta s_1 = |s_0 - s_1|$, $\Delta s_2 = |s_1 - s_2|$, $\Delta s_3 = |s_2 - s_3|$.

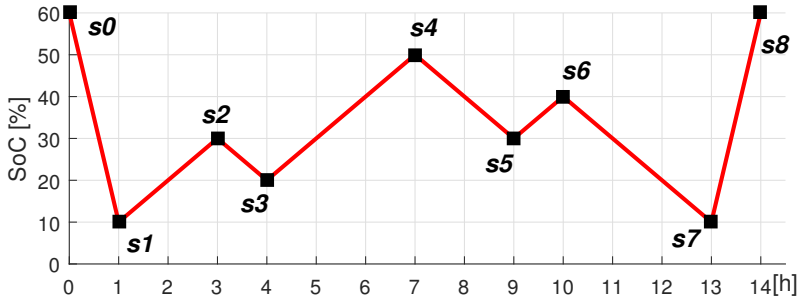

(a) An example of SoC pro le.

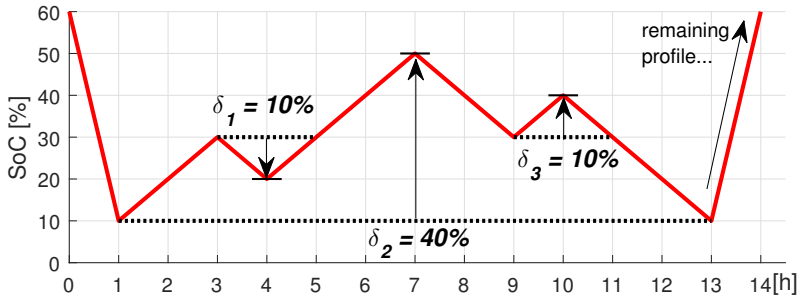

(b) The cycle counting result.

Figure 2.2: Using the rainflow algorithm to identify battery cycle depths.

3. If $\Delta s_2 \leq \Delta s_1$ and $\Delta s_2 \leq \Delta s_3$, then a full cycle of depth Δs_2 associated with s_1 and s_2 has been identified. Remove s_1 and s_2 from the profile, and repeat the identification using points s_0, s_1, s_4, s_5...

4. If a cycle has not been identified, shift the identification forward and repeat the identification using points s_1, s_2, s_3, s_4...

5. The identification is repeated until no more full cycles can be identified throughout the remaining profile.

The remainder of the profile is called the rainflow residue and contains only half cycles [82]. A half cycle links each pair of adjoining local extrema in the rainflow residue profile. A half cycle with decreasing SoC is a discharging half cycle, while a half cycle with increasing SoC is a charging half cycle. For example, the SoC profile shown on Fig. 2.2b has two full cycles

of depth 10% and one full cycle of depth 40%, as well as a discharging half cycle of depth 50% and charging half cycle of depth 50%.

The rainflow algorithm does not have an analytical mathematical expression [13] and cannot be integrated directly within an optimization problem. Nevertheless, several efforts have been made to optimize battery operation by simplifying the rainflow algorithm. Abdulla *et al.* [1] and Tran *et al.* [135] simplify the cycle depth as the BES energy output within each control time interval. Koller *et al.* [72] define a cycle as the period between battery charging and discharging transitions. These model simplifications enable the incorporation of cycle depth in the optimization of BES operation, but introduce additional errors in the degradation model. He *et al.* [61] decompose the battery degradation model and optimize BES market offers iteratively. This method yields more accurate dispatch results, but is too complicated to be incorporated in an economic dispatch calculation.

We will use the rainflow algorithm as the basis for an ex-post benchmark method for assessing battery cycle life. In this model, the total life lost L from a SoC profile is assumed to be the sum of the life loss from all I number of cycles identified by the rainflow algorithm. If the life loss from a cycle of depth $\quad$ is given by a cycle depth stress function $\Psi(\ )$ of polynomial form, we have:

$$L = \sum_{i=1}^{I} \Psi(\ _i): \tag{2.1}$$

Chapter 3

BATTERY REAL-TIME CONTROL

3.1 Motivation

In U.S. frequency regulation markets, a participant's payment for providing the regulation service depends not only on the regulation capacity it provides, but also on the accuracy of its response to the regulation instruction [147]. The instruction takes the form of a signal that is sent every 2 to 6 seconds, representing the amount of active power a participant should inject or withdraw. A participant is penalized if it deviates from the received regulation signal. Since batteries have much faster ramp rates compared to traditional generators, they are among the most competitive providers in these fast regulation markets (in 2016 41% of regulation in PJM was provided by batteries [114]). The importance of batteries is likely to increase further as the size of the fast regulation markets grows in response to the growing penetration of renewable generation.

Although batteries can achieve near perfect accuracy in the provision of regulation [114], it is not always clear that a battery should exactly follow the regulation signal to maximize its gain from participating in the regulation markets. The optimal action of a battery should balance the profit from providing regulation with its operating cost, which is mainly driven by the degradation caused by the charge and discharge cycles [39, 150]. In particular, deep cycles–charging/discharging cycles that use a significant amount of active materials–tend to dramatically reduce battery life [136]. Indeed, a naive battery controller that attempts to follow regulation signals without considering cycle degradation could destroy a battery in a matter of months. Instead, a controller should strategically choose to suffer some performance penalty to avoid deep cycles. However, designing a better controller is not a trivial task, since it is difficult to tell whether the battery is undergoing a deep or a shallow cycle without future knowledge. Most commercial controllers sidestep this issue by setting hard limits on the battery state of charge, which can limit the profitability of batteries and

artificially increase the need for more regulation resources.

3.2 Contribution

In this chapter, we overcome the challenge of balancing regulation performance and reducing battery degradation by designing an online control policy that is nearly optimal:

1. It achieves a bounded optimality gap compared with an optimal offline policy that has full information about future regulation signals.

2. This gap is independent of the duration of operation and can be characterized exactly.

The key to this control policy is a more thorough *algorithmic understanding* of the battery aging process with respect to charge/discharge cycles.

3.3 Modeling

3.3.1 Battery Operations

We consider an operation defined over finite discrete control time intervals $n \in \{1;:::;N\}$, $N \in \mathsf{N}$. Each control time interval has a duration of T, and the entire operation has a duration of TN. Let e_n be the energy stored in the battery–the state of charge (SoC)–at time step n. The battery can either charge an amount c_n or discharge an amount d_n during each interval. Its state of charge is given by the following linear difference equation:

$$e_{n+1} - e_n = T\ _{\mathsf{c}}c_n - (T=\ _{\mathsf{d}})d_n: \tag{3.1}$$

For a given battery, it has the following operation constraints

$$\underline{e} \le e_n \le \bar{e} \tag{3.2}$$

$$0 \le c_n \le P \tag{3.3}$$

$$0 \le d_n \le P \tag{3.4}$$

$$c_n = 0 \text{ or } d_n = 0 \tag{3.5}$$

where $\underline{e}$ and $\bar{e}$ are the minimum and maximum energy capacity of the battery, $_c$ and $_d$ are the charge and discharge efficiency, P is the battery power rating, and (3.5) avoids trivial solutions by preventing the battery from charging and discharging at the same time.

3.3.2 Battery Degradation Cost

The cycle aging model employs a cycle depth stress function $\Phi(u) : [0; 1] \to \mathsf{R}^+$ to model the life loss from a single cycle of depth u. This function indicates that if a battery cell is repetitively cycled with depth u, then it can operate $1=\Phi(u)$ number of cycles before reaching its end of life. $\Phi(u)$ is a convex function for most types of electrochemical batteries [23, 43, 85, 124, 139], an example polynomial form of $\Phi(u)$ is as u [76]. Because cycle aging is a cumulative fatigue process [43, 85], the total life loss ΔL is the sum of the life loss from all cycles

$$\Delta L(\mathbf{u}; \mathbf{v}; \mathbf{w}) = \sum_{i=1}^{|\mathbf{u}|} \Phi(u_i) + \sum_{i=1}^{|\mathbf{v}|} \frac{\Phi(v_i)}{2} + \sum_{i=1}^{|\mathbf{w}|} \frac{\Phi(w_i)}{2} \tag{3.6}$$

where $|\mathbf{u}|$ is the cardinality of $\mathbf{u}$. Let R be the battery cell replacement price in \$/MWh and hence ER is the replacement cost. The cycle aging cost function $J_{\mathsf{cyc}}(\mathbf{c}; \mathbf{d})$ is

$$J_{\mathsf{cyc}}(\mathbf{c}; \mathbf{d}) = \Delta L(\mathbf{c}; \mathbf{d}) ER : \tag{3.7}$$

3.3.3 Market Settlement Model

We assume the system operator charges a constant positive over-response price $\in R^+$ (\$=MWh) for surplus injections or deficient demands during each dispatch interval, and a constant under-response price $\in R^+$ (\$=MWh) for deficient injections or surplus demands. The performance penalty model J_{reg} calculates the market settlement cost for performance the regulation

$$\begin{aligned} J_{\mathsf{reg}}(\mathbf{c}; \mathbf{d}) = & T \sum_{n=1}^{N} |c_n - d_n - r_n|^+ \\ & + T \sum_{n=1}^{N} |r_n - c_n + d_n|^+ ; \end{aligned} \tag{3.8}$$

where $r_n \in [-P; P]$ is the regulation instructed dispatch set-point for the dispatch interval n, with the convention positive values in r_n represents charge instructions.

3.3.4 Optimization Problem

If the regulation instruction $\mathbf{r}$ is known, then the optimization problem is:

$$\min_{\mathbf{c};\mathbf{d}} J(\mathbf{c};\mathbf{d};\mathbf{r}) := J_{\text{cyc}}(\mathbf{c};\mathbf{d}) + J_{\text{reg}}(\mathbf{c};\mathbf{d};\mathbf{r}) \tag{3.9a}$$

$$\text{s.t. } (3.2) - (3.5): \tag{3.9b}$$

However, this problem is inherently online: the charging and discharging decisions must be made at each time step without knowing the future realization of the regulation instruction $\mathbf{r}$. Therefore we seek an *online policy* that will determine c_n and d_n at time step n with only past information. Note we do not assume any information about the future realization of the regulation signal is known (e.g., it need not come from a stochastic process).

3.4 Proposed Online Control Policy

We propose an online battery control policy that balances the cost of deviating from the regulation signal and the cycle aging cost of batteries while satisfying operation constraints. This policy takes a *threshold form* and achieves an optimality gap that is *independent of the total number of time steps*. Therefore in term of regret, this policy achieves the strongest possible result: the regret do not grow with time. Note we assume the regulation capacity has already been fixed in the previous capacity settlement stage [148].

3.4.1 Control Policy Formulation

The key part of the control policy is to calculate thresholds that bounds the SoC of the battery as functions of the deviation penalty and degradation cost. Let $\hat{u}$ denote this bound on the SoC, and it is given by:

$$\hat{u} = \dot{\Phi}^{-1}\left(\frac{d+=c}{R}\right) \tag{3.10}$$

where $\dot{\Phi}^{-1}(\cdot)$ is the inverse function of the derivative of the cycle stress function $\Phi(\cdot)$.

The proposed control policy is summarized in Algorithm 1, and Fig. 3.1 shows a control example of the proposed policy, in which the battery follows the regulation instruction until the distance between its maximum and minimum SoC reaches $\hat{u}$. The detailed formulation

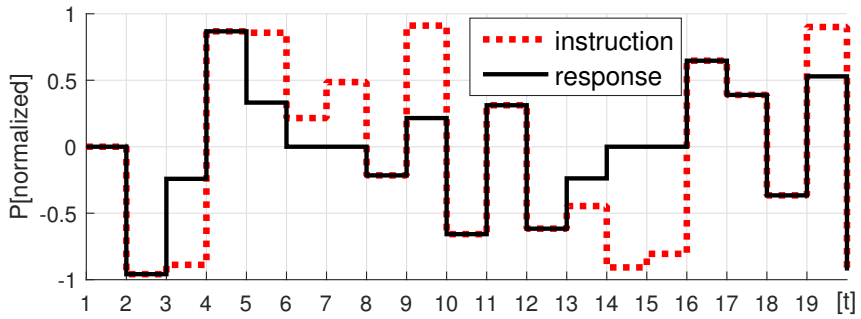

(a) Regulation instruction vs. response

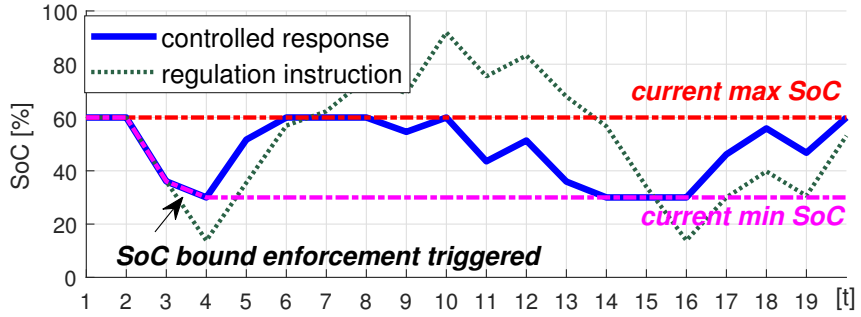

(b) Controlled vs. uncontrolled SoC pro le

Figure 3.1: Proposed control policy illustration. The policy keeps track the current maximum and minimum SoC level. When the distance in between reaches the calculated threshold $\hat{u}$, the policy starts to constrain the response.

is as follows. We assume at a particular control interval n, e_n and r_n are observed, and the proposed regulation policy has the following form: $g_n(e_n; r_n) = \begin{bmatrix} c_n^g & d_n^g \end{bmatrix}$.

The control policy employs the following strategy

$$\text{If } r_n \geq 0,\ c_n^g = \min\left\{\frac{1}{T_c}(\bar{e}^g - e_n);\ r_n\right\} \tag{3.11}$$

$$\text{If } r_n < 0,\ d_n^g = \min\left\{\frac{d}{T}(e_n - \underline{e}^g);\ r_n\right\} \tag{3.12}$$

where $\bar{e}_n^g$ and $\underline{e}_n^g$ are the upper and lower storage energy level bound determined by the controller at the control interval n for enforcing the SoC band $\hat{u}$

$$\begin{aligned} \bar{e}_n^g &= \min\{\bar{e};\ e_n^{\min} + \hat{u}E\} \\ \underline{e}_n^g &= \max\{\underline{e};\ e_n^{\max} - \hat{u}E\} \end{aligned} \tag{3.13}$$

Algorithm 1: Proposed Control Policy

Result: Determine battery dispatch point c_n, d_n

// initialization

set $\dot{\Phi}$ ^{1} $\frac{d+=c}{R}$ $\rightarrow \hat{u}$, $e_0 \rightarrow e_0^{\max}$, $e_0 \rightarrow e_0^{\min}$;

while $n \leq N$ **do**

// read e_n and update controller

set $\max\{e_{n\ 1}^{\max}; e_n\} \rightarrow e_n^{\max}$, $\min\{e_{n\ 1}^{\min}; e_n\} \rightarrow e_n^{\max}$;

set $\min\{\overline{e}; e_n^{\min} + \hat{u}E\} \rightarrow \overline{e}_n^g$;

set $\max\{\underline{e}; e_n^{\max} + \hat{u}E\} \rightarrow \underline{e}_n^g$;

// read r_n and enforce soc bound

if $r_n \geq 0$ **then**

set $\min$ $\left\{\frac{1}{T_c}(\overline{e}^g - e_n); r_n\right\} \rightarrow c_n$, $0 \rightarrow d_n$;

else

set $0 \rightarrow c_n$, $\min$ $\left\{\frac{d}{T}(e_n - \underline{e}^g); r_n\right\} \rightarrow d_n$;

end

// wait until next control interval

set $n+1 \rightarrow n$;

end

and $e_n^{\max}$, $e_n^{\min}$ is the current maximum and minimum battery storage level since the beginning of the operation, which are updated at each control step as

$$\begin{aligned} e_n^{\max} &= \max\{e_{n\ 1}^{\max}; e_n\} \\ e_n^{\min} &= \min\{e_{n\ 1}^{\min}; e_n\}: \end{aligned} \tag{3.14}$$

Fig. 3.2 explains the intuition of the proposed policy. First we consider an arbitrary cycle in the regulation provision. The battery performs a cycle by following the regulation instruction and avoids a penalty cost linear to the cycle depth, but undertakes an aging cost that is convex to the cycle depth. Hence there exists an optimal full cycle depth $\hat{u}$ that maximizes the operating profit over a single cycle. The battery should stop following the regulation

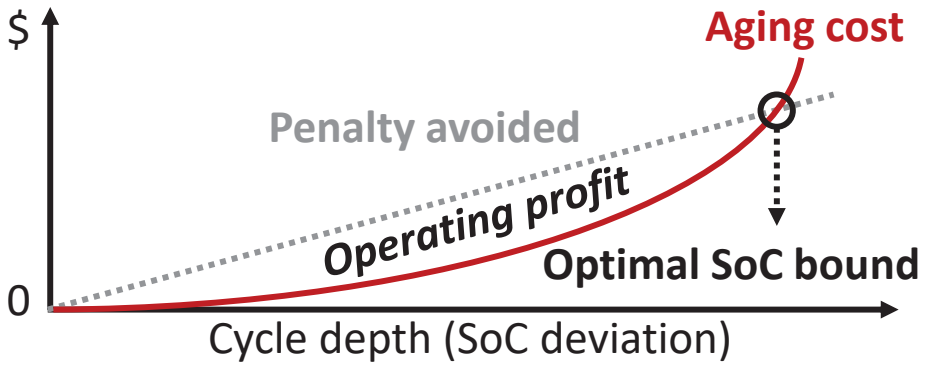

Figure 3.2: Illustration of the optimal cycle depth when responding to regulation instructions. During a single cycle, the participant avoids a mismatch penalty that is linear with respect to the cycle depth, and undertakes a nonlinear cycle aging cost. Hence there exists an optimal cycle depth the maximizes the operating profit which is the area between the two curves.

instruction once this optimal depth is reached, which is equivalent to setting a SoC bound as described in the proposed policy. This policy has a bounded regret since battery operation may contain a residue that can't be matched into cycles. The regret bound is given in the following theorem.

3.4.2 Optimality Gap to O ine Problem

Let $(\mathbf{c}\ ;\mathbf{d}\ )$ be an offline minimizer to the regulation response problem as

$$(\mathbf{c}\ ;\mathbf{d}\ ) \in \arg\min_{\mathbf{c};\mathbf{d}} J(\mathbf{c};\mathbf{d};\mathbf{r})$$
$$\text{subjects to (3.1)–(3.5)} \tag{3.15}$$

and let $g(e_0;\mathbf{r})$ denote the control action of the proposed policy subjects to the initial storage energy level e_0 and the regulation instruction realization $\mathbf{r}$.

Theorem 1. *Suppose the battery cycle aging stress function $\Phi(\cdot)$ is strictly convex. The proposed control strategy $g(\cdot)$ has a worst-case optimality gap (regret) that is independent*

of the operation time duration TN:

$$\exists \quad \in \mathsf{R}^{+} \text{ s.t. } J(g(e_0;\mathbf{r});\mathbf{r}) - J(\mathbf{c}\ ;\mathbf{d}\ ;\mathbf{r}) \leq \tag{3.16}$$

$$\forall\ e_0 \in [\underline{e};\overline{e}],\ \textit{and}\ \forall\ \textit{sequences}\ \{r_n\} \in [-P;P],\ N \in \mathsf{N}.$$

The bound in Theorem 1 can be explicitly characterized. To do this, we transform the objective function $J(\cdot)$ using cycle depths $(\mathbf{u};\mathbf{v};\mathbf{w})$ as control variables instead of $(\mathbf{c};\mathbf{d})$:

$$J_{\mathsf{u}}(u) = ER\Phi(u) - E(\ = _{\mathsf{c}} + \quad _{\mathsf{d}})u \tag{3.17a}$$

$$J_{\mathsf{v}}(v) = (1=2)ER\Phi(v) - (E= _{\mathsf{c}})\ v \tag{3.17b}$$

$$J_{\mathsf{w}}(w) = (1=2)ER\Phi(w) - E\ _{\mathsf{d}}\ w \tag{3.17c}$$

where J_{u} is the cost associated with a full cycle, J_{v} for a charge half cycle, and J_{w} for a discharge half cycle. The detailed transforming procedure is discussed in the appendix.

If we assume the cycle depth stress function $\Phi(\cdot)$ is strictly convex, then it is easy to see that (3.10) is the unconstrained minimizer to (3.17a). Similarly, the unconstrained minimizers of (3.17b) and (3.17c) are:

$$\hat{v} = \dot{\Phi}^{\ 1}\ \frac{= _{\mathsf{c}}}{R}\ ; \quad \hat{w} = \dot{\Phi}^{\ 1}\ \frac{_{\mathsf{d}}}{R}\ : \tag{3.18}$$

The follow theorem offers the analytical expression for

Theorem 2. *If function $\Phi(\cdot)$ is strictly convex, then the worst-case optimality gap for the proposed policy $g(\cdot)$ as in* (3.16) *is*

$$= \begin{cases} \infty & \\ _{\mathsf{w}} & \textit{if} \quad _{\mathsf{d}} > \ = _{\mathsf{c}} \\ 0 & \textit{if} \quad _{\mathsf{d}} = \ = _{\mathsf{c}} \\ _{\mathsf{v}} & \textit{if} \quad _{\mathsf{d}} < \ = _{\mathsf{c}} \end{cases} \tag{3.19}$$

where

$$_{\mathsf{w}} = J_{\mathsf{w}}(\hat{u}) + 2J_{\mathsf{v}}(\hat{u}) - J_{\mathsf{w}}(\hat{w}) - 2J_{\mathsf{v}}(\hat{v}) \tag{3.20}$$

$$_{\mathsf{v}} = 2J_{\mathsf{w}}(\hat{u}) + J_{\mathsf{v}}(\hat{u}) - 2J_{\mathsf{w}}(\hat{w}) - J_{\mathsf{v}}(\hat{v}) : \tag{3.21}$$

We defer the proof of this theorem to the appendix since it is somewhat technically involved. The intuition is that battery operations consist mostly full cycles due to limited storage capacity because the battery has to be charged up before discharged, and vice versa. Enforcing $\hat{u}$–the optimal full cycle depth calculated from penalty prices and battery coefficients–ensures optimal responses in all full cycles. In cases that $\eta_d = \eta_c$, $\hat{u}$ is also the optimal depth for half cycles, and the proposed policy achieves optimal control. In other cases, the optimality gap is caused by half cycles because they have different optimal depths. However, half cycles have limited occurrences in a battery operation because they are incomplete cycles [7], so that the optimality gap is bounded as stated in Theorem 2. Fig. 3.3 shows some examples of the policy optimality when responding to the regulation instruction (Fig 3.3a) under different price settings. The proposed policy has the same control action in all three price settings because of the same $\hat{u}$. The policy achieves optimal control in Fig 3.3b because $\hat{u}$ is the optimal depth for all cycles. In Fig 3.3c and Fig 3.3d, half cycles have different optimal depths and the policy is only near-optimal. However, the offline result also selectively responses to instructions with a zero penalty price (charge instructions in Fig 3.3c, discharge instructions in Fig 3.3d) because it returns the battery to a shallower cycle depth so that the battery have smaller marginal operating cost in future operations.

3.5 Simulation Results

3.5.1 Simulation Setting

We compare the proposed control policy with the offline optimal result and a simple control policy [16]. The maximum storage level $\bar{e}$ is set to 0.95 MWh and the minimum storage level $\underline{e}$ is set to 0.1 MWh. This assumed battery storage consists of lithium-ion battery cells that can perform 3000 cycles at 80% cycle depth before reaching end of life, and these cells have a polynomial cycle depth stress function concluded from lab tests [76]:$\Phi(u) = (5.24 \times 10^{-4})u^{2.03}$, and the cell replacement price is set to 300 \$/kWh.

3.5.2 Optimality Gap

We simulate regulation using random generated regulation traces to exam the optimality of the proposed policy and to validate Theorem 1 and 2. We generate 100 regulation signal traces assuming a uniform distribution between $[-1; 1]$, and design nine test cases. Each test case has different market prices and battery round-trip efficiency $= _d _c$. In order to demonstrate the time-invariant property of the optimality gap, Case 7 to 9 are designed to have twice the duration of Case 1 to 6 by repeating the generated regulation signal trace.

The 100 generated regulation traces are simulated using the proposed policy, the simple policy, and the offline solver for each test case. Table 3.1 summarizes the test results. The penalty prices, round-trip efficiency, and the number of simulation control intervals used in each test case are listed, as well as the control SoC bound $\hat{u}$ and the worst-case optimality gap that are calculated using simulation parameters. The simulation results are recorded under the maximum optimality gap and the average objective value.

This test validates Theorem 2 since is exactly the same as the recorded maximum optimality gap for the proposed policy in all cases (both highlighted in pink), while the gap for the simple policy is significantly larger (highlighted in grey). In particular, the proposed policy achieves exact control results in Case 1 to 3 because $= _c = _d$, while Case 4 to 9 have non-zero gaps because the round-trip efficiency is less than ideal (< 1). We also see that as penalty prices become higher, the control band $\hat{u}$ becomes wider and the battery follows the regulation instruction more accurately. The simple policy also provides better control results at higher penalty prices. Case 7 to 9 have the same parameter settings as to Case 4 to 6, except that the regulation signal is repeated once more time. The proposed policy achieves the same worst-case optimality gap in the two operation duration settings, while the average objective values are approximately doubled as shown in Fig. 3.4.

3.5.3 Simulation using Realistic Regulation Signal

In this simulation we compare the proposed policy with the simple policy using the regulation signal trace published by PJM Interconnection [115]. The control time interval for this signal is 2 seconds and the duration is 4 weeks. We do not use the offline result for

comparison in this case because this problem is beyond the solvability of the implemented numerical solver.

We repeat the simulation using different penalty prices. We let = in each test case and set the round-trip efficiency to 85%. Fig. 3.5 summarizes the simulation results in the form of regulation operating cost versus penalty prices, the cycle aging cost and the regulation mismatch penalty are listed for each policy. Because the simple control does not consider market prices, its control actions are the same in all price scenarios, and the penalty increases linearly with the penalty price. The proposed policy causes significantly smaller cycle aging cost, and have better control results. As the penalty price increases, the gap between the two policies becomes smaller since $\hat{u}$ becomes closer to 100%.

3.6 Summary

In this paper, we proposed an online policy for a battery owner to provide frequency regulation in a pay-for-performance market. It considers the cycle aging mechanism of electrochemical battery cells, and is adaptive to changing market prices. We have shown that the proposed policy has a bounded regret that is dependent of operation durations, and achieves exact control result under certain market scenarios. The proposed policy applies to all battery applications that has constant prices over a specific period and the battery is dispatched in stochastic manners, such as using co-located battery storage to smooth wind farm power productions, or using behind-the-meter batteries to improve the penetration of roof-top photovoltaic generations. In our future work, we will investigate how to incorporate the policy into problems such as optimal battery contracting, and optimal battery sizing.

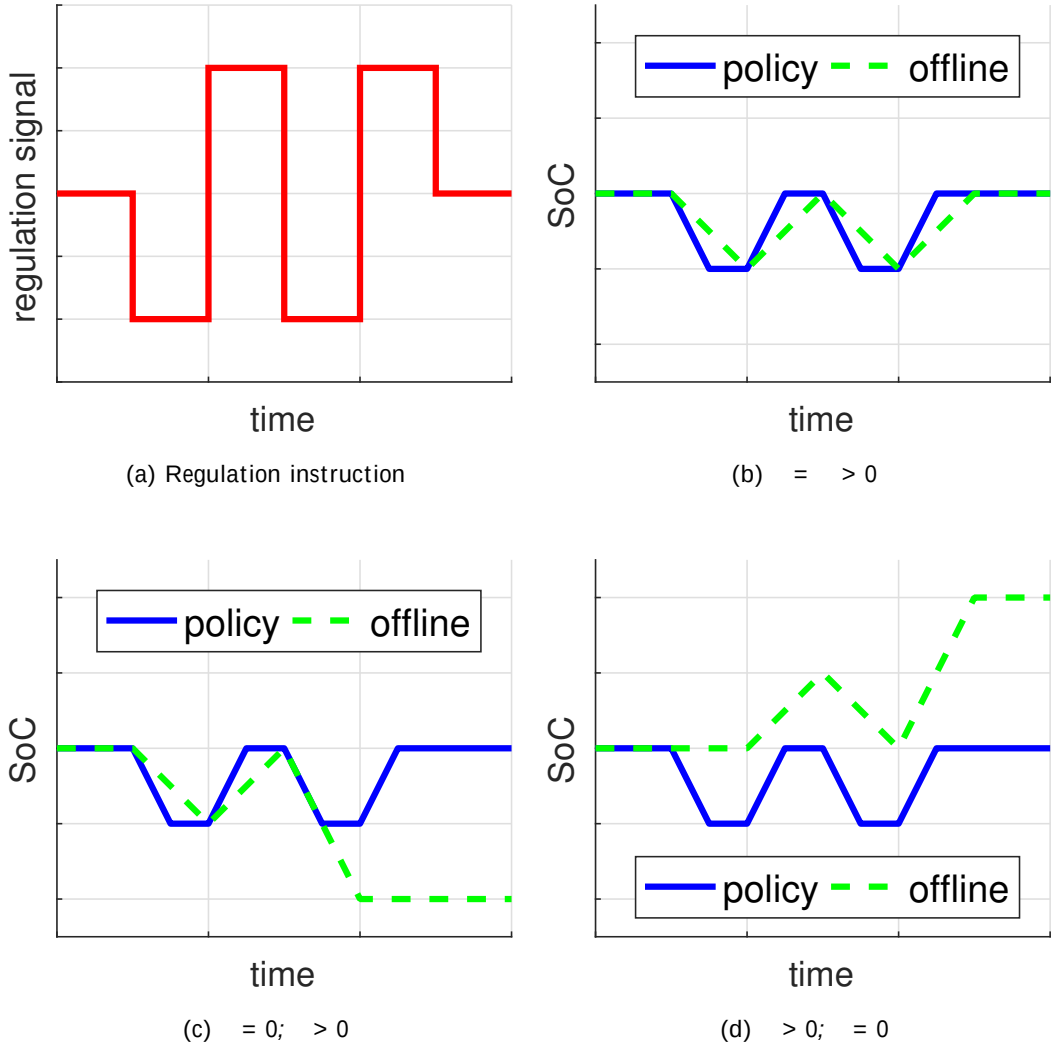

(a) Regulation instruction

(b) = > 0

(c) = 0; > 0

(d) > 0; = 0

Figure 3.3: Example illustration of the policy optimality under different price settings. The value of + is the same in all cases and the round-trip efficiency is assumed to be one, so $\hat{u}$ is the same in all cases.

Table 3.1: Simulation with Random Generated Regulation Signals.

				N	$\hat{u}$		Maximum optimality gap [$]		Average objective value [$]		
Case	[$/MWh]	[$/MWh]	[%]		[%]	[$]	Theoretical	Simple	Offline	Proposed	Simple
1	50	50	100	100	11.1	0.00	0.00	183.9	117.4	117.4	200.2
2	100	100	100	100	21.9	0.00	0.00	127.5	168.7	168.7	209.0
3	200	200	100	100	42.8	0.00	0.00	47.9	219.4	219.4	226.7
4	50	50	85	100	11.2	0.06	0.06	184.9	117.2	117.3	202.9
5	80	20	85	100	11.7	3.83	3.83	181.4	108.0	110.7	198.9
6	20	80	85	100	10.6	2.19	2.19	192.6	122.4	123.8	206.8
7	50	50	85	200	11.2	0.06	0.06	408.8	235.6	235.7	388.3
8	80	20	85	200	11.7	3.83	3.83	400.6	219.5	222.2	375.4
9	20	80	85	200	10.6	2.19	2.19	421.4	247.6	248.9	401.1

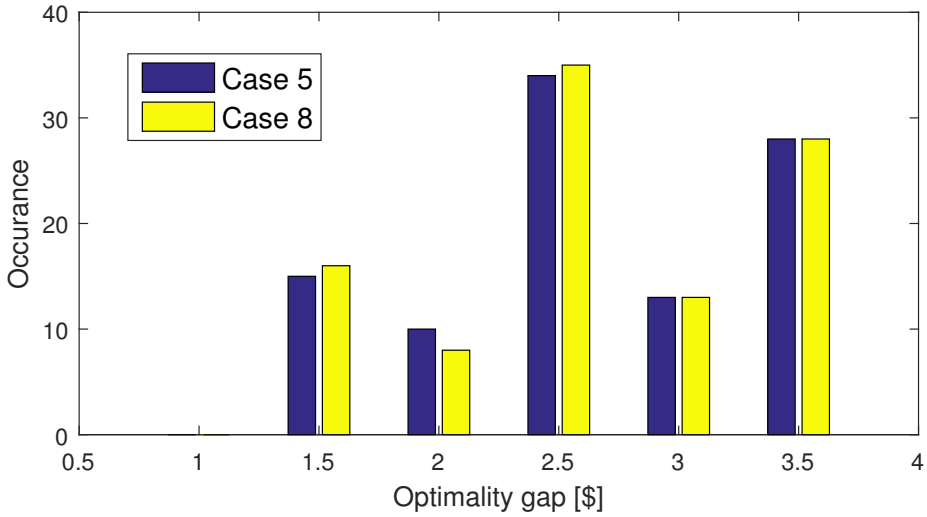

Figure 3.4: Distribution of optimality gaps for Case 5 and Case 8. Although Case 8 has twice the duration of Case 5, their optimality gaps are similar. This validates that the worst-case optimality gap is independent of the regulation operation duration.

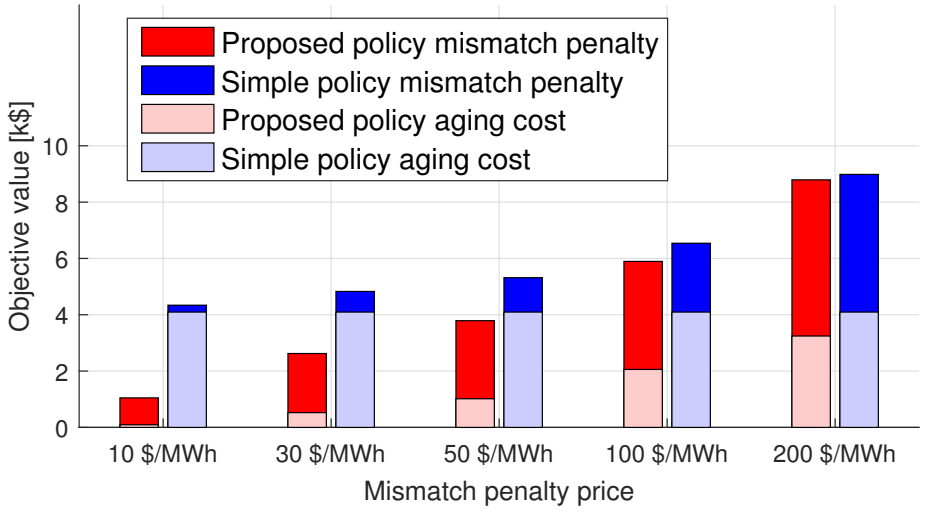

Figure 3.5: Regulation operating cost break-down comparison between the proposed policy and the simple policy. Although the proposed policy has higher penalties, the cost of cycle aging is significantly smaller, so it achieves better trade-offs between degradation and mismatch penalty.

Chapter 4

BATTERY BIDDING IN REGULATION MARKET

4.1 Motivation

Recent regulation market reforms have encouraged numerous BES projects targeted solely at the provision of regulation. These BES units often behave as price-takers by submitting offers at zero price into the market and accepting any clearing prices. If the market prices for regulation are high, these participants can earn considerable profits with naive control strategies. However, since the amount of regulation capacity needed is limited, a market can easily become saturated by too many price-taking participants. Operational evidence shows that the PJM RegD market became saturated in 2016 and its market clearing prices have dropped by two-thirds since 2014 [8, 148], making BES operation hardly profitable with naive bidding and operating strategies.

BES participants must employ more advanced operating and bidding strategies to secure operational profits against dropping market prices and the cost of battery degradation. Previous studies have assessed how providing regulation with batteries affects their aging characteristic under simple SoC control strategies [18,23,73,84,95,131–133,141,142,148,151]. However, few studies have actively incorporated battery aging as part of regulation operation or bidding optimization objectives. References [32,152] take into account the battery lifespan in regulation control optimization, using an aging model that is too simple to reflect properly the complex battery cycle aging mechanisms. The results in [61] incorporate the battery aging cost into regulation bidding strategies, but the proposed method does not optimize real-time operations.

Since regulation instructions are highly stochastic and occur at a very high time resolution, accounting for them explicitly in an optimization problem is computationally challenging. It is thus crucial to reduce the formulation complexity using statistical and analytical derivations, and to jointly optimize the bidding and real-time control strategies. In this

work, we incorporate battery cycle aging into a real-time control policy that ensures profitability under any market clearing result. In addition, we introduce a bidding policy based on the proposed control policy that maximizes profits while satisfying the market performance requirement.

4.2 Contribution

4.3 Regulation Market Model

We consider a pay-for-performance regulation market in which a participant is rewarded based on the regulation capacity it provides, as well as on how much it is instructed to alter dispatch set-points by the system operator, and how accurately it follows the regulation instructions. Most system operators calculate a performance index as the relative error between a participant's regulation response and the regulation instructions [147]. PJM uses a more complicate calculation method [113].

Pay-for-performance regulation markets have two-part offer and payment designs. A participant submits a regulation capacity offer and a regulation mileage offer, and then the system operator unifies the two offer prices into a single modified offer based on the participant's historical performance index and the expected dispatch regulation mileage. In the ex-post market settlement, the capacity payment is calculated using the capacity clearing price and the assigned regulation capacity. The mileage payment is calculated using the mileage clearing price and the instructed mileage. Depending on the market design, the performance index is used to penalize the entire regulation payment, or only the mileage payment. All pay-for-performance regulation markets also have a minimum performance requirement, in which a participant must reach a certain performance index to be eligible for receiving regulation payment, and must maintain a satisfactory performance history to be qualified to participate in the regulation market [148].

The objective of a regulation market participant is to maximize its operational profit, including the expected market payment and the battery aging cost. To formulate this problem, we start by considering a market period with finite discrete dispatch intervals $t \in \{1; \cdots; T\}$ and a single market clearing price which is calculated based on the capacity

clearing price, the mileage clearing prices, and the instructed mileage [147]. We assume that the participant receives regulation instructions that are proportionally scaled with respect to its regulation capacity C based on a set of normalized regulation signals $r = \{r_t \in [-1; 1]\}$. The participant receives the payment $P(Cr; b)\ C$ from the regulation market, where $b = \{b_t\}$ is the participant's response to the regulation instruction, and $P(\cdot)$ is the performance index calculation function. We define $P(\cdot)$ as a linear function of the relative response error:

$$P(Cr; b) = 1 - \frac{||Cr - b||_1}{C||r||_1} \quad : \tag{4.1}$$

where $||Cr - b||_1$ calculates the absolute error in the response, and $C||r||_1$ is the total amount of the instructed regulation signal. $\in [0; 1]$ is the part of the regulation payment that is evaluated based on the relative error of the response. This is a unified performance model that fits all market rules. The value of is specific to each market and can be found in each market manuals.

4.4 Optimization Problem Formulation

If the market clearing price and the regulation signal realization r are known, the participant can find the optimal regulation capacity C and the optimal BES dispatch b by solving the following optimization problem

$$\max_{C; b} \Pi(C; \ ; r; b) := P(Cr; b)\ C - A(b) \tag{4.2a}$$

$$\text{s.t. } P(Cr; b) \geq \ ^{\min} \tag{4.2b}$$

$$C \in [0; B]; \text{constraints (3.2)–(3.4)} \tag{4.2c}$$

where the objective function (4.2a) maximizes the operating profit calculated as the market revenue minus the aging cost, (4.2b) enforces a minimum performance index $^{\min}$ to the regulation response, (4.2c) limits the regulation capacity C to be within the battery power capacity B, and the battery operation must satisfy the operation constraints (3.2)–(3.4).

However, this problem cannot be solved in practice because the realization of r is not known in advance. The participant must therefore decide on a policy g that determines b_t

at time step t based only on past information. The expected profit $J(\cdot)$ corresponding to a particular operational policy and regulation capacity $(g; C)$ is defined as:

$$J(g; C) = \mathsf{E}\left[\Pi(C; \ ; r; b^g)\right]$$
$$= \mathsf{E}\left[C - \frac{||Cr - b^g||_1}{||r||_1} - A(b^g)\right]; \tag{4.3}$$

where the superscript g is included to indicate the dependence on the control policy g. However, the exact value of and $||r||_1$ can only be known after the regulation provision, hence we approximate the formulation using the following expectations

$$= \mathsf{E} \quad ; \quad _r = \mathsf{E}\ ||r||_1 \ : \tag{4.4}$$

To solve this problem, we transform the minimum performance requirement into a chance constraint, and rewrite (4.2) as a chance-constrained stochastic programming problem

$$\max_{g;C} J(g; C) = \quad C - \mathsf{E}\left[\frac{}{r}||Cr - b^g||_1 + A(b^g)\right]$$
$$\text{s.t. } \mathbf{Prob}\ P(Cr; b) \geq \ ^{\min} \ \geq$$
$$g \in \mathcal{G};\ C \in [0; B]: \tag{4.5}$$

where is the confidence level that the performance requirement will be satisfied, and $\mathcal{G}$ is the set of all feasible operation policies g that satisfy (3.2)–(3.4) and the causality condition.

4.5 Optimal Control and Bidding Policy

We propose an online control policy and a bidding policy that solve problem (4.5). Control and bidding in the regulation market are part of a sequential decision-making process because the regulation capacity C is cleared before the actual dispatch. We therefore work backwards by first determining the optimal online control policy g with respect to any cleared regulation capacity (Fig. 4.1)

$$g \ \in \arg\max_{g2G} J(g; C) \tag{4.6}$$

We then derive the optimal bidding policy C based on the optimal control policy:

$$C \ \in \arg\max_{C2[0;B]} \left\{\max_{g2G} J(g; C)\right\}$$
$$\text{s.t. } \mathbf{Prob}\ P(Cr; b) \geq \ ^{\min} \ \geq \ : \tag{4.7}$$

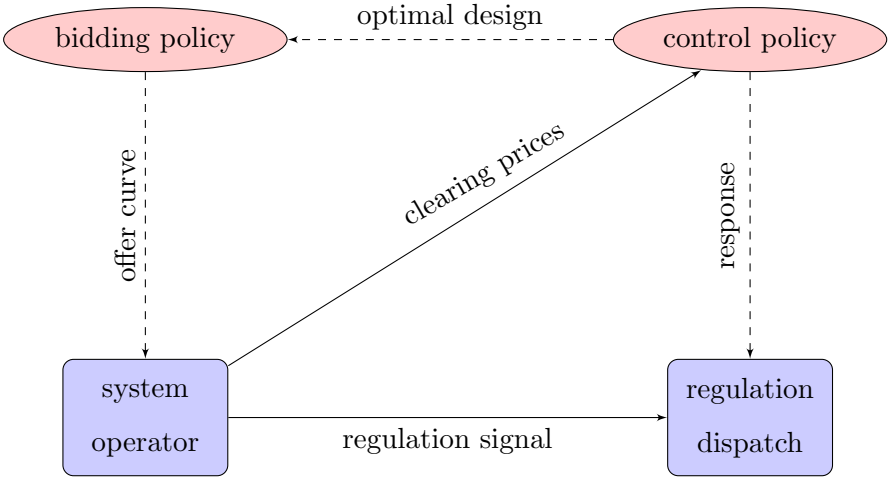

Figure 4.1: Flow chart of the regulation market and control processes. The control policy inputs the clearing prices for determining the optimal response, while the bidding policy submits offers to the market while considering the control policy.

We consider the performance chance constraint at the bidding stage because it depends primarily on the regulation capacity and the battery energy capacity (see Section 4.5.2). We assume that r is energy zero-mean (including efficiency losses) because either the system operator or the participant can employ strategies for controlling the average BES SoC, and these strategies do not effect a participant's objective of minimizing its operating cost.

4.5.1 Optimal Control Policy

We adopt the optimal control policy as described in Algorithm 1 from the previous Chapter. The optimal cycle depth $\hat{u}$ is calculated from the regulation market price and aging cost as

$$\hat{u} = {}' {}^{1} \frac{{}^{2}+1}{R} \quad ; \qquad = \frac{}{{}_{r}M} \tag{4.8}$$

where ${}' {}^{1}(\cdot)$ is the inverse function of the derivative of the cycle stress function ${}'(x) = \mathrm{d}\Phi(x)/\mathrm{d}x$.

4.5.2 Optimal Regulation Capacity

We first show that under the optimal control policy and when *relaxing* the minimum performance constraint, a participant should adopt a price-taker bidding strategy, i.e., it should provide the maximum possible regulation capacity under any market prices. We then incorporate the performance chance constraint and show that the performance-constrained optimal capacity can be explicitly characterized based on statistics of historical regulation signals.

Theorem 3. *When relaxing the minimum performance requirement, the optimal regulation capacity C is equal to the BES power rating B when using the proposed optimal response policy g .*

Proof: See Appendix B.

The intuition for this theorem is that the proposed policy guarantees optimal operating profit under any regulation capacity and signal realization. A higher regulation capacity offers higher profit potential since market payment is capped by C. Therefore under optimal real-time control, a participant will never earn less profit with a higher capacity because the penalty cost never exceeds the market payment.

Stemming from Theorem 2, the solution of (4.7) is reduced to finding the maximum C while satisfying the performance chance-constraint. The challenge is that the regulation signal realization is unknown when determining the regulation capacity. We must therefore characterize a probabilistic function that correlates the performance index with the regulation capacity C. In addition, since the battery regulation response b^g under the proposed policy g is price responsive, we must also take the expected clearing price into consideration.

We start with the performance index calculation with the regulation signal realization r and show that it can be reformed into a function with respect to b^g/C, which is the normalized battery response

$$\begin{aligned} P(Cr; b) &= 1 - \frac{||Cr - b^g||_1}{C||r||_1} \\ &= 1 - \frac{||r - b^g/C||_1}{||r||_1}. \end{aligned} \tag{4.9}$$

Recall that in the proposed policy the battery energy level is constrained between $\overline{E}^g$ and $\underline{E}^g$ that are calculated from battery data and the penalty price. We substitute b^g/C into the proposed policy and show that b^g/C only depends on $\overline{E}_g/C$ and $\underline{E}_g/C$ since the battery operation constraints (3.2)–(3.4) are linear

$$\frac{b_t^g}{C} = \begin{cases} \min \ (\overline{E}^g - e_t)/(M \ C); r_t & \text{if } r_t \geq 0 \\ \max \ (\underline{E}^g - e_t)/(M \ C); r_t & \text{if } r_t < 0. \end{cases} \tag{4.10}$$

We omit the effect of the battery initial energy level e_0 on the performance index because r has a zero mean (i.e. it is energy neutral). The performance index thus depends only on the ratio between the usable energy capacity of the battery $\overline{E}^g - \underline{E}^g$ and the regulation capacity C. We can therefore define this ratio as the normalized regulation energy capacity

$$= \frac{\overline{E}^g - \underline{E}^g}{C} = \frac{\min\{\overline{E} - \underline{E}; \hat{u}E\}}{C} \tag{4.11}$$

where we substitute $\hat{u}$ into $\overline{E}^g - \underline{E}^g$ as in Algorithm 1. Recall that $\hat{u}$ is calculated from the expected market clearing price, hence we represent as a function of and C.

Having shown that the performance index only depends on , we now define a probabilistic function P ( ) of , which means that a battery with a normalized regulation energy capacity of is certain to reach a performance score of P ( ). Hence we can rewrite the performance chance-constraint as

$$\textbf{Prob } P(Cr; b^g) \geq P \ (\ ) \ = \tag{4.12}$$

and P ( ) can be determined by simulating historical regulation signals.

Lemma 1. *P ( ) is monotonic over P ( ) $\in (1 - \ ; 1)$ and has an inverse function $[P \ ]^{-1}( )$ over $\in (1 - \ ; 1)$.*

Proof: This lemma is trivial. First we consider a regulation signal realization set r, the minimum performance index that a battery can possibly score is $1 -$ because the rest is not dependent on the battery's response. Before reaching the perfect performance of 1, an increment in must result in an improvement in the performance index due to that is

the only constraining factor. This is true for any realizations of r, hence it is trivial that $P(\ )$ is monotonic over $P(\ ) \in (1-\ ;1)$.

Following Lemma 1, if a participant wishes to reach a performance score $\in (1-\ ;1)$ with exactly confidence, it must use the following value of :

$$= [P\ ]^{\ 1}(\ );\qquad \in (1-\ ;1) \tag{4.13}$$

We now combine Theorem 2, (4.11) and (4.8) to characterize analytically the optimal regulation capacity when using the proposed optimal response policy:

$$C\ (\quad) = \min\quad B;\ \frac{\min\{\overline{E}-\underline{E};\hat{u}E\}}{[P\ ]^{\ 1}(\ ^{\min})}\ \Bigg)$$
$$\text{where } \hat{u} = {}'^{\ 1}\quad \frac{^2+1}{R\ _rM} \tag{4.14}$$

The only variable in this equation is . The rests are either based on the market policy or the BES design. It is easy to see that if Φ is strictly convex, $C\ (\quad)$ is monotonic over the following range

$$C \in (0;\overline{C})$$
$$\text{where } \overline{C} = \min\ \Big\{B;\ \frac{\overline{E}-\underline{E}}{[P\ ]^{\ 1}(\ ^{\min})}\Big\} \tag{4.15}$$

and $\overline{C}$ is the maximum regulation capacity a participant could provide in order to reach the performance index $^{\min}$ with a confidence of at least .

4.5.3 Optimal Bidding Policy in Regulation Markets

At the bidding stage in the regulation market, each participant must submit a segment bidding curve that specifies how much regulation capacity that it is willing to provide at a given market price. We denote this set $(\ ^{b};C^{b}) = \{(\ ^{b}_{j};C^{b}_{j}) \in \mathbb{R}^2_+ \mid j \in \mathbb{N}\}$. Therefore, each participant needs a bidding policy to calculate ^{b} with respect to the regulation capacity segments C^{b}.

The optimal bidding policy is straightforwardly based on (4.14) and (4.15): a participant uses the inverse function of $C\ (\cdot)$ to calculate the offer price associated with each capacity segment, while the total offered capacity must be smaller than $\overline{C}$ in order to satisfy the performance requirement. This optimal bidding policy is described in Algorithm 2.

Algorithm 2: Optimal Battery Regulation Bidding Policy

Result: Determine the regulation offer price ^{b} associated with capacity segment C^{b}

// starts from the first (cheapest) bid segment

set $1 \rightarrow J$;

// goes through each segment until reaching $\overline{C}$

while $\sum_{j=1}^{J} C_j^b \leq \overline{C}$ **do**

  // total capacity offered so far

  set $\sum_{j=1}^{J} C_j^b \leq \overline{C} \rightarrow C^{total}$;

  // total payment price expected

  set $[C\ ]\ ^{1}(C^{total}) \rightarrow\ ^{total}$;

  // calculate the segment offer price

  set $(\ ^{total}C^{total} - \sum_{j=1}^{J\ 1}\ ^{b}_{j}C_j^b)=C_J^b \rightarrow\ ^{b}_{J}$;

  // go to the next capacity segment

  set $J + 1 \rightarrow J$;

end

4.6 Simulation

4.6.1 Data and Setting

We use the following parameters for the battery energy storage in simulations unless otherwise specified:

- Charging and discharging power rating: 10 MW
- Energy capacity: 3 MWh
- Charging and discharging efficiency: 95%
- Maximum state of charge: 95%
- Minimum state of charge: 10%

- Round-trip efficiency: 92%
- Battery cycle life: 1000 cycles at 80% cycle depth
- Battery shelf life: 10 years
- Cell temperature: maintained at 25 C
- Battery pack replacement cost: \$ 300 /kWh
- Li(NiMnCo)O_2-based 18650 lithium-ion battery cells

These cells have a near-quadratic cycle depth stress function [76]:

$$\Phi(u) = (1.57\text{E-}3)u^{2.03} \tag{4.16}$$

We use a simple control policy as a benchmark in all of the following simulations. The simple policy uses all battery energy capacity $[\underline{E}, \overline{E}]$ for operation and does not consider the penalty price or the cycle aging cost, hence it is equivalent to fixing $\hat{u} = 1$ in the proposed policy. Although this a naive control approach, it has been used in most stochastic real-time battery operation studies [16, 107, 151].

4.6.2 Illustration of Theorem 3

We illustrate Theorem 3 by simulating a 1 MWh BES providing a full-year regulation service with varying regulation capacities in the PJM market using price and signal data from 03/2016 to 02/2017. The minimum performance requirement is not enforced in this example. Fig. 4.2 shows the simulation result for the proposed policy and the simple policy to demonstrate the effectiveness of our method.

The result in Fig. 4.2 includes the aging cost, the performance penalty cost, and the operational profit for regulation capacities up to 10 MW. With the proposed policy, the profits increase with the regulation capacity, which validates Theorem 2. With the simple policy, the BES operation is somewhat profitable when the regulation capacity is below 4 MW, but this profitability disappears completely once the regulation capacity is greater than 8 MW.

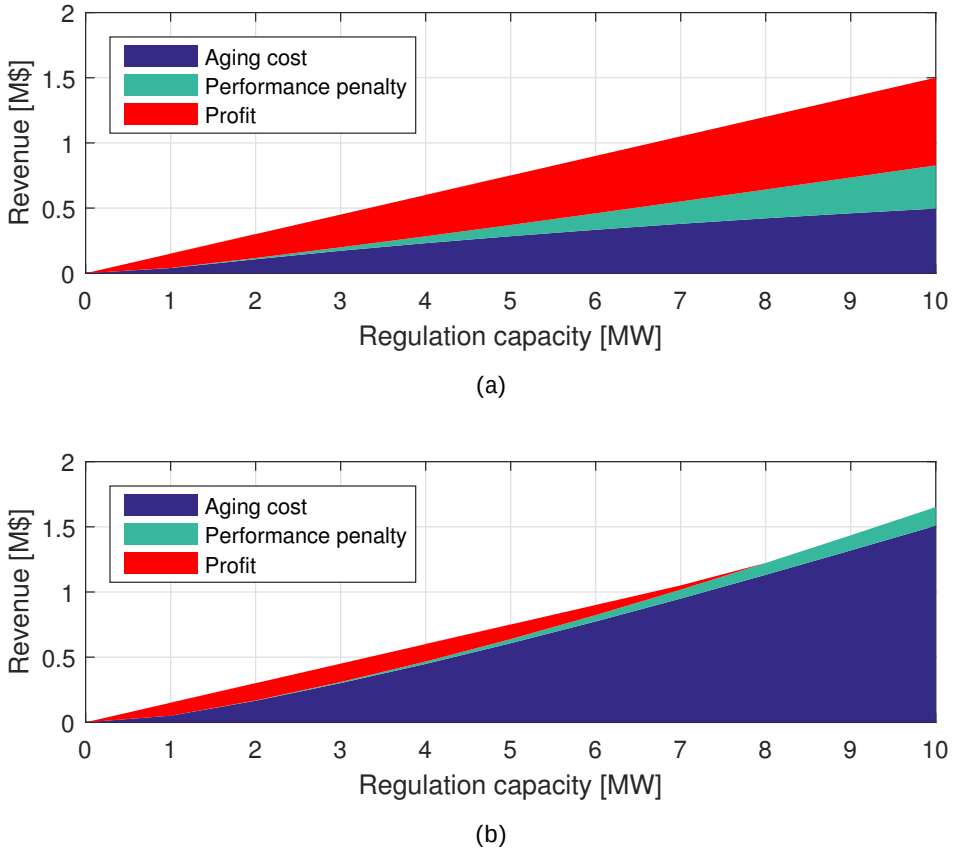

Figure 4.2: Full year revenue analysis of a 1 MWh BES participating in the regulation market with di erent regulation capacities. (a) With the proposed control policy; (b) With the simple control policy.

4.6.3 Case Study

We simulate a BES providing dynamic regulation (RegD) service in the PJM regulation market using signal and price data for a full-year (from 03/2016 to 02/2017). The minimum performance index requirement for this market is 0.7, and the settlement period in one hour. in the performance index model (4.1) is set to 2/3 which models the PJM performance index calculation (see Appendix), while all ex-post performance index calculations are performed according to the PJM manual [113].

The regulation signal is slightly biased to make it energy zero-mean, a realistic assumption in the current market structure [148]. Parameters of the bidding policy, including the value of $_r$ and the function P , are determined using the PJM RegD signal from 06/2013

to 05/2014. The value of is calculated from the PJM capacity and performance clearing prices using a mileage ratio of 3 based on the PJM market clearing manual [147]. We consider 10 1 MW regulation capacity offer segments for a 10MW/3MWh BES. The BES thus offers a total of 10 MW regulation capacity. The offer price associated with each segment is calculated according to the proposed bidding policy using the performance index simulation result from 2013, as shown in Fig. 4.3a. The performance confidence function concluded from 2016 data is slightly different from 2013, in particular, the energy capacity requirement at high confidence levels are higher, possibly due to changes in the dispatch algorithm, unexpected weather conditions, or increased renewable penetration.

For comparison, we include a benchmark strategy, where the 10MW/3MWh BES participates the regulation market as a price taker and always offers 10 MW regulation capacity. Hence over the course of a year this BES provides a total of 87600 MW·h of regulation capacity. The benchmark case uses a simple control strategy that always dispatches the entire BES energy capacity in response to regulation instructions.

Table 4.1 summarizes the case study results, showing that the proposed policy earns more profit than the benchmark strategy for all performance confidence levels. On the other hand, the benchmark strategy has a higher regulation performance because it always dispatches the entire battery energy capacity. The operating profit increases with a lower performance confidence, i.e., a riskier strategy earns more profit. The downside of a riskier strategy is that the BES's offer may become noncompetitive because the system operator considers historical performance when clearing the market. We plot the operating profit (Fig. 4.4a) and the average performance (Fig. 4.4b) to show the trade-off between profit and risk. It is clear that while the average performance index decreases approximately linearly with , the marginal increase in operating profit becomes smaller, i.e., the profit from a riskier regulation market participation saturates. Therefore, a participant must carefully balance profit and risk in actual market scenarios.

4.7 Summary

In this paper, we proposed an optimal control policy and an optimal bidding policy for battery energy storage participating in performance-based regulation market. The proposed

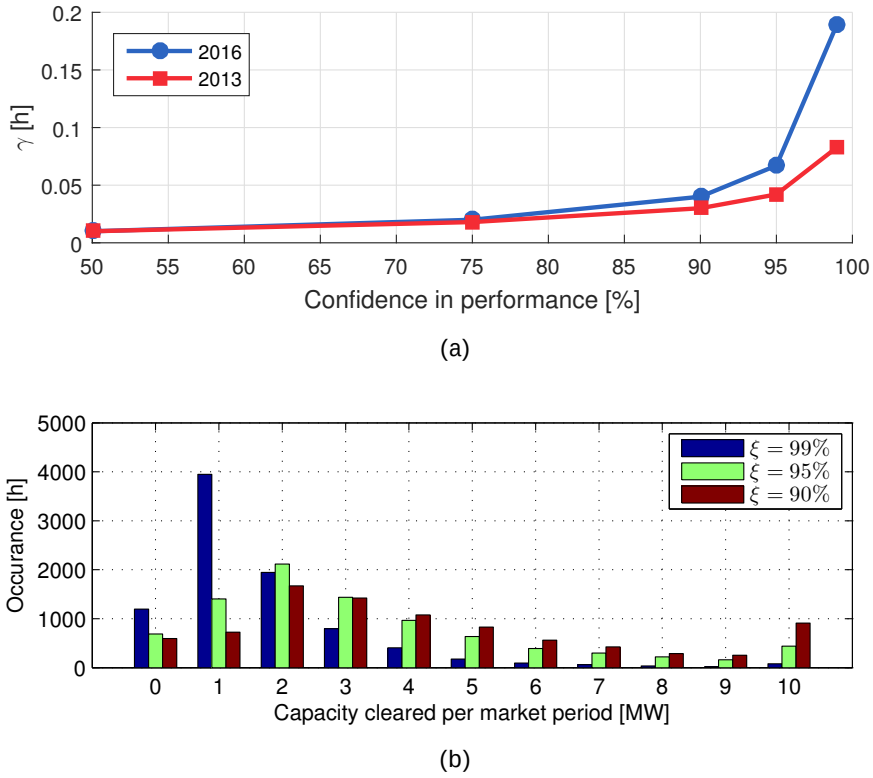

Figure 4.3: PJM case study. (a) The relative regulation capacity vs. different from simulating historical regulation signals in 2013 and 2016; (b) Histogram of all cleared regulation capacities under difference confidence.

policies consider the cycle aging mechanism of electrochemical battery cells, and are adaptive to realistic market settings. We validate the optimality of the proposed policies using simulations, and demonstrate their effectiveness by a case study based on the PJM frequency regulation market.

Performance-based frequency regulation markets have been proposed for around five years and their designs are still maturing. With an increasing number of battery participants, frequency regulation markets are becoming increasingly competitive. As exemplified by the ongoing market revisions in PJM, system operators may also tighten the performance requirements. The proposed approach ensures not only profitability but also the satisfaction of the performance requirements.

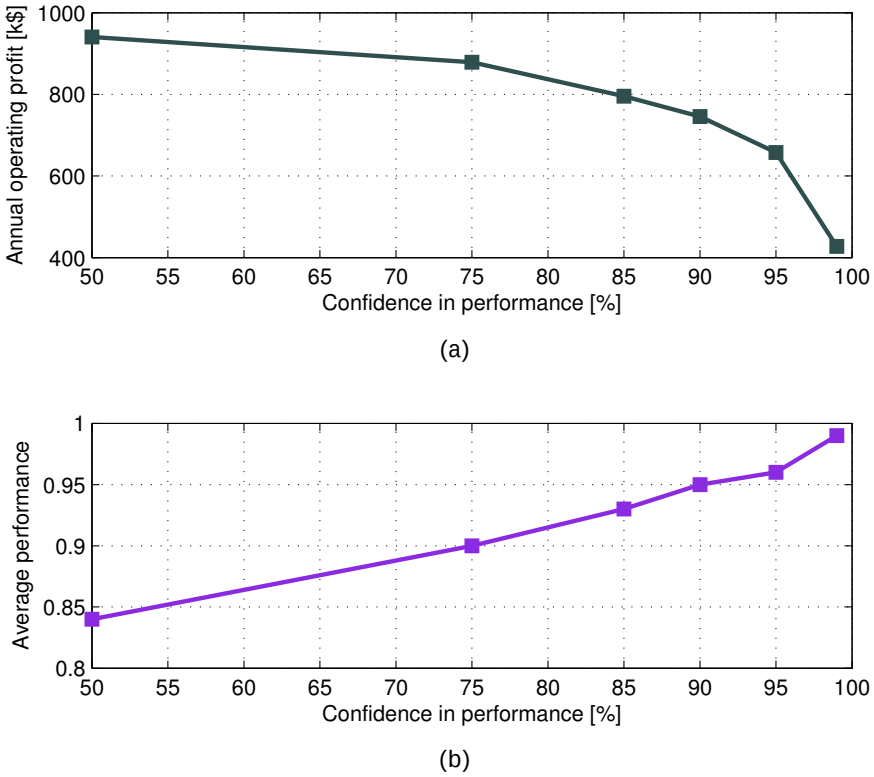

Figure 4.4: PJM case study risk analysis. (a) Annual prorated operating pro t vs. performance con dence ; (b) Average annual performance index vs. performance con dence .

Table 4.1: Case Study Results in PJM RegD Market 03/2016-02/2017.

	Benchmark	Optimal participation under performance confidence					
		= 99%	= 95%	= 90%	= 85%	= 75%	= 50%
Market income [k$]	1472.9	494.8	823.2	958.8	1035.9	1164.9	1266.8
Aging cost [k$]	1091.8	67.5	165.8	213.0	240.3	286	326.3
Prorated operating profit [k$]	381.1	427.3	657.4	745.7	795.6	878.6	940.5
Battery cell life expectancy [month]	9	69	42	35	33	29	26
Annual average performance	0.99	0.99	0.96	0.95	0.93	0.90	0.84
Hours of under-performance	6	81	204	246	297	426	1022
Total regulation capacity cleared [MW·h]	87600	14991	29051	36838	42166	54087	73504

Chapter 5

BATTERY SCHEDULING IN ENERGY MARKET

5.1 Motivation

In order to participate fully in electricity markets, owners of batteries must be able to submit offers and bids that reflect their marginal operating cost. As we argued above, this marginal cost curve should reflect the cost of battery degradation caused by each cycle. In order to keep the model simple, and to obtain a cost function similar to those used in existing market dispatch programs, we assume that battery cycle aging only occurs during the discharge stage of a cycle, so that a discharging half cycle causes the same cycle aging as a full cycle of the same depth, while a charging half cycles causes no cycle aging. This is a reasonable assumption because the amounts of energy charged and discharged from a battery are almost identical when assessed on a daily basis.

5.2 Contribution

This chapter proposes a new and accurate way to model of the cost of battery cycle aging, which can be integrated easily in economic dispatch calculations. The main contributions of this paper can be summarized as follows:

- It proposes a piecewise linear cost function that provides a close approximation of the cost of cycle aging in electrochemical batteries.

- System operators can incorporate this model in market clearing calculations to facilitate the participation of BES in wholesale markets by allowing them to properly reflect their operating cost..

- Since this approach defines the marginal cost of battery cycle aging, it makes it possible for BES owners to design market offers and bids that recover at least the cost of battery life lost due to market dispatch.

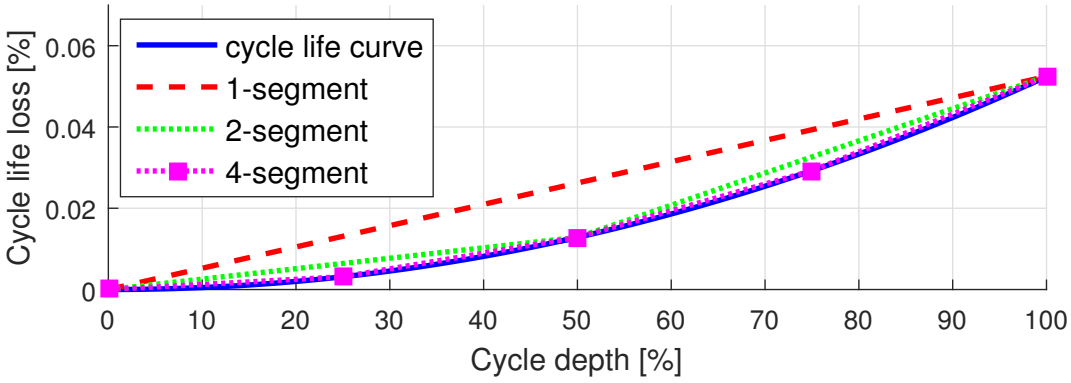

Figure 5.1: Upper-approximation to the cycle depth aging stress function.

- The effectiveness of the proposed model is demonstrated using a full year of price data from the ISO New England energy markets.

- The accuracy of the proposed model in predicting the battery cycle aging cost is demonstrated using an ex-post calculation based on a benchmark model.

5.3 Marginal Cost of Battery Cycling

During a cycle, if the BES is discharged from a starting SoC e^{up} to an end SoC e^{dn} and later charged back (or vice-versa), the depth of this cycle is the relative SoC difference $(e^{\mathsf{up}} - e^{\mathsf{dn}})/E^{\mathsf{rate}}$, where E^{rate} is the energy capacity of the BES. Let a battery be discharged from a cycle depth $_{t\ 1}$ at time interval $t-1$. This battery's cycle depth at time t can be calculated from its output power g_t over time (assuming the time interval duration is one hour):

$$_t = \frac{^{\mathsf{dis}}}{E^{\mathsf{rate}}} g_t + _{t\ 1}; \tag{5.1}$$

where $^{\mathsf{dis}}$ is the BES discharge efficiency, and g_t has non-negative values because we ignore charging for now. The incremental aging resulting from this cycle is $\Psi(_t)$, and the marginal cycle aging can be calculated by taking the derivative of $\Psi(_t)$ with respect to g_t and

substituting from (5.1):

$$\frac{\partial \Psi(\ _i)}{\partial g_t} = \frac{d\Psi(\ _i)}{d\ _i}\frac{\partial\ _i}{\partial g_t} = \frac{^{\text{dis}}}{E^{\text{rate}}}\frac{d\Psi(\ _i)}{d\ _i}\ ; \tag{5.2}$$

To define the marginal cost of cycle aging, we prorate the battery cell replacement cost R ($) to the marginal cycle aging, and construct a piecewise linear upper-approximation function c. This function consists of J segments that evenly divide the cycle depth range (from 0 to 100%)

$$c(\ _t) = \begin{cases} \vdots & \\ c_1 & \text{if } \ _t \in [0; \frac{1}{J}) \\ \vdots & \\ c_j & \text{if } \ _t \in [\frac{j\ 1}{J}; \frac{j}{J}) \\ \vdots & \\ c_J & \text{if } \ _t \in [\frac{J\ 1}{J}; 1] \end{cases}\ ; \tag{5.3}$$

where

$$c_j = R\frac{^{\text{dis}}}{E^{\text{rate}}}J\ \ \Psi(\frac{j}{J}) - \Psi(\frac{j-1}{J})\ \ ; \tag{5.4}$$

and $\ _t$ is the cycle depth of the battery at time t. Fig. 5.1 illustrates the cycle depth stress function and its piecewise linearization with different numbers of segments.

5.4 Optimizing the BES Dispatch

Having established a marginal cost function for a BES, we are now able to optimize how it should be dispatched assuming that it acts as a price-taker on the basis of perfect forecasts of the market prices for energy and reserve. A formal description of this optimization requires the definitions of the following parameters:

- T: Number of time intervals in the optimization horizon, indexed by t
- J: Number of segments in the cycle aging cost function, indexed by j
- M: Duration of a market dispatch time interval
- S: Sustainability time requirement for reserve provision

- E^0: Initial amount of energy stored in the BES
- E^{nal}: Amount of energy that must be stored at the end of the optimization horizon
- $E^{\min}$ and $E^{\max}$: Minimum and maximum energy stored in the BES
- D, G: Discharging and charging power ratings
- c_j: Marginal aging cost of cycle depth segment j
- $\bar{e}_j$: Maximum amount of energy that can be stored in cycle depth segment j
- $\bar{e}_j^0$: Initial amount of energy of cycle depth segment j
- $^{\text{ch}}$, $^{\text{dis}}$: Charge and discharge efficiencies
- $^{\text{e}}_t$, $^{\text{q}}_t$: Forecasts of the energy and reserve prices at t

This optimization uses the following decision variables:

- $p_{t;j}^{\text{ch}}$, $p_{t;j}^{\text{dis}}$: Charge and discharge power for cycle depth segment j at time t
- $e_{t;j}$: Energy stored in marginal cost segment j at time t
- d_t, g_t: Charging and discharging power at time t
- d_t^{q}, g_t^{q}: BES baseline charging and discharging power at time t for reserve provision
- q_t: Reserve capacity provided by the BES at time t
- v_t: Operating mode of the BES: if at time t the BES is charging then $v_t = 0$; if it is discharging then $v_t = 1$. If the BES is idling, this variable can take either value. If some sufficient conditions are satisfied, for example the market clearing prices should not be negative, the binary variable v_t can be relaxed [78]

- u_t: If at time t the BES provides reserve then $u_t = 1$, else $u_t = 0$

The objective of this optimization is to maximize the operating profit Ω of the BES. This profit is defined as the difference between the revenues from the energy and reserve markets and the cycle aging cost C

$$\max_{\mathbf{p};\mathbf{g};\mathbf{d};\mathbf{q}} \Omega := \sum_{t=1}^{T} \left[e_t(g_t - d_t) + q_t q_t \right] - C : \tag{5.5}$$

Depending on the discharge power, the depth of discharge during each time interval extends over one or more segments.

To model the cycle depth in multi-interval operation, we assign a charge power component $p^{ch}_{t;j}$ and an energy level $e_{t;j}$ to each cycle depth segment, so that we can track the energy level of each segment independently and identify the current cycle depth. For example, assume we divide the cycle depth of a 1 MWh BES into 10 segments of 0.1 MWh. If a cycle of 10% depth starts with a discharge, as between s_2 and s_3 in Fig. 2.2a, the BES must have previously undergone a charge event which stored more than 0.1 MWh according to the definition from the rainflow method. Because the marginal cost curve is convex, the BES always discharges from the cheapest (shallowest) available cycle depth segment towards the more expensive (deeper) segments. Thus, the first depth segment must have been fully charged at the beginning of this cycle, and all energy will be discharged from segment e_1 associated with marginal cost c_1 during this cycle. Because the charge and discharge components of a cycle are symmetric, at the end of a cycle, the energy level of each segment e_j is restored to its state at the beginning of the cycle, hence the rest of the operation is not affected. Therefore, the proposed model provides a close approximation to the rainflow cycle counting algorithm.

The cycle aging cost C is the sum of the cycle aging costs associated with each segment over the horizon:

$$C = \sum_{t=1}^{T} \sum_{j=1}^{J} M c_j p^{dis}_{t;j} ; \tag{5.6}$$

This optimization is subject to the following constraints

$$d_t = \sum_{j=1}^{J} p_{t;j}^{\text{ch}} \quad \text{ch} \tag{5.7}$$

$$g_t = \sum_{j=1}^{J} p_{t;j}^{\text{dis}} = \quad \text{dis} \tag{5.8}$$

$$d_t \leq D(1 - v_t) \tag{5.9}$$

$$g_t \leq G v_t \tag{5.10}$$

$$e_{t;j} - e_{t \ \ 1;j} = M(p_{t;j}^{\text{ch}} - p_{t;j}^{\text{dis}}) \tag{5.11}$$

$$e_{t;j} \leq \bar{e}_j \tag{5.12}$$

$$E^{\min} \leq \sum_{j=1}^{J} e_{t;j} \leq E^{\max} \tag{5.13}$$

$$e_{1;j} = e_j^0 \tag{5.14}$$

$$\sum_{j=1}^{J} e_{T;j} \geq E^{\ \text{nal}}; \tag{5.15}$$

Eq. (5.7) states that the BES charging power drawn from the grid is the sum of the charging powers associated with each cycle depth segment, factoring in the charging efficiency. Eq. (5.8) is the equivalent for the discharging power. Eqs. (5.9) - (5.10) enforce the BES power rating, with the binary variable v_t preventing simultaneous charging and discharging [57]. Eq. (5.11) tracks the evolution of the energy stored in each cycle depth segment. Eq. (5.12) enforces the upper limit on each segment while Eq. (5.13) enforces the minimum and maximum SoC of the BES. Eq. (5.14) sets the initial energy level in each cycle depth segment, and the final storage energy level is enforced by Eq. (5.15).

Because the revenues that a BES collects from providing reserve capacity are co-optimized with the revenues from the energy market, it must abide by the requirements that the North American Electric Reliability Corporation (NERC) imposes on the provision of reserve by energy storage. In particular, NERC requires that a BES must have enough energy stored to sustain its committed reserve capacity and baseline power dispatch for at least one hour [97]. This requirement is automatically satisfied when market resources are cleared over an hourly interval, as is the case for the ISO New England day-ahead market. If the dispatch interval is shorter than one hour (e.g.for the five-minute ISO New England real-time market), this one-hour sustainability requirement has significant implications on the dispatch of a BES because of the interactions between its power and energy capacities. For example, let us

consider a 36 MW BES with 3 MWh of stored energy. If this BES is not scheduled to provide reserve, it can dispatch up to 36 MW of generation for the next 5-minute market period. On the other hand, if it is scheduled to provide 1 MW of reserve, its generation capacity is also constrained by the one hour sustainability requirement, therefore it can only provide up to 2 MW baseline generation for the next 5-minute market period.

$$d_t - d_t^q \leq D(1 - u_t) \tag{5.16}$$

$$g_t - g_t^q \leq G(1 - u_t) \tag{5.17}$$

$$d_t^q \leq D u_t \tag{5.18}$$

$$g_t^q \leq G u_t \tag{5.19}$$

$$g_t^q + q_t - d_t^q \leq G u_t \tag{5.20}$$

$$q_t \geq \text{"} u_t \tag{5.21}$$

$$S(g_t^q + q_t - d_t^q) \leq \sum_{j=1}^{J} \bar{e}_j \; ; \tag{5.22}$$

Equations (5.16) - (5.22), enforce the constraints related to the provision of reserve by a BES. In particular, Eq. (5.22) enforces the one-hour reserve sustainability requirement. Depending on the requirements of the reserve market, the binary variable u_t and constraints (5.16) - (5.22) can be simplified or relaxed.

The optimization model described above can be used by the BES owner to design bids and offers or self-schedule based on price forecasts. The ISO can also incorporate this model into the market clearing program to better incorporate the aging characteristic of BES. In this case, the cycle aging cost function should be included in the welfare maximization while constraints (5.7) - (5.22) should be added to the market clearing program constraints. A BES owner should include cycle aging parameters c_j and $\bar{e}_j$ in its market offers, and parameters D, G, $E^{\min}$, E^{nal}, $^{\text{ch}}$, $^{\text{dis}}$ for ISO to manage its SoC and its upper/lower charge limits.

5.5 Case Study

The proposed model has been tested using data from ISO New England to demonstrate that it improves the profitability and longevity of a BES participating in this market. All

simulations were carried out in GAMS using CPLEX solver [123], and the optimization period is 24 hours for all simulations.

5.5.1 BES Test Parameters

The BES simulated in this case study has the following parameters:

- Charging and discharging power rating: 20 MW
- Energy capacity: 12.5 MWh
- Charging and discharging efficiency: 95%
- Maximum state of charge: 95%
- Minimum state of charge: 15%
- Battery cycle life: 3000 cycles at at 80% cycle depth
- Battery shelf life: 10 years
- Cell temperature: maintained at 25 C
- Battery pack replacement cost: 300,000 $/MWh
- Li(NiMnCo)O_2-based 18650 lithium-ion battery cells

These cells have a near-quadratic cycle depth stress function [76]:

$$\Psi(\ ) = (5{:}24\text{E-}4)^{\ 2{:}03}{:} \tag{5.23}$$

Fig. 5.1 shows this stress function along with several possible piecewise linearizations. We assume that all battery cells are identically manufactured, that the battery management system is ideal, and thus that all battery cells in the BES age at the same rate. Since the BES dispatch is performed based on perfectly accurate price forecasts, our results provide an upper bound of its profitability in this market.

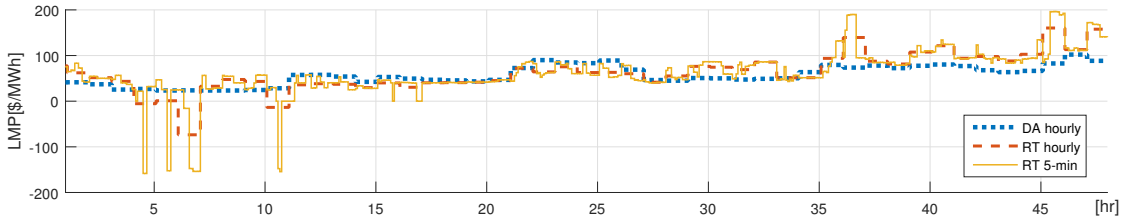

(a) Locational marginal price in the day-ahead market (DAM), in an hourly and a 5-minute real-time market (RTM).

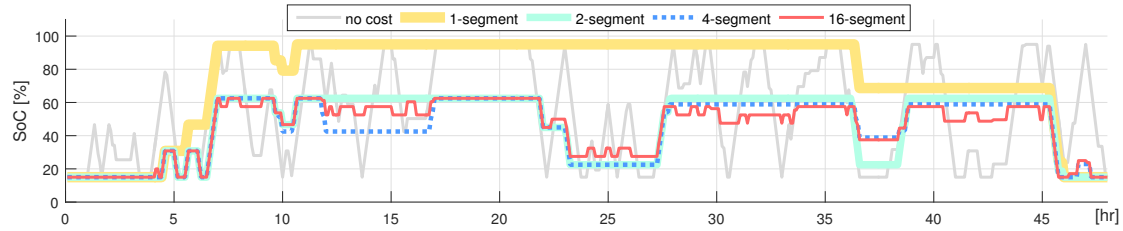

(b) BES SoC pro le in RTM with 5-minute settlement.

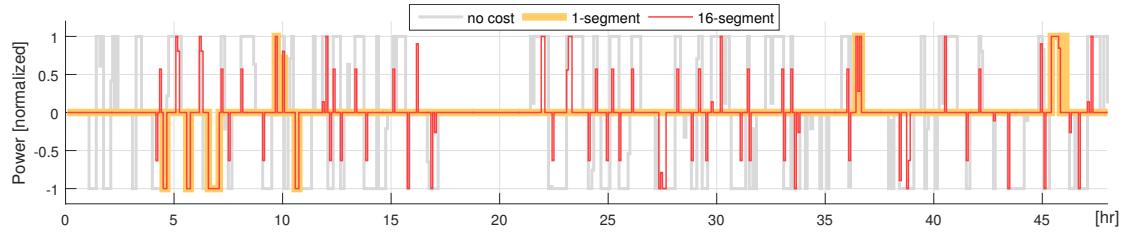

(c) BES output power pro le in RTM with 5-minute settlement.

Figure 5.2: BES dispatch for different cycle aging cost models (ISO New England SE-MASS Zone, Jan 5th & 6th, 2015).

5.5.2 Market Data

BES dispatch simulations were performed using zonal price for Southeast Massachusetts (SE-MASS) region of ISO New England market price data for 2015 [47] because energy storage has the highest profit potential in this price zone [41]. Three market scenarios were simulated:

- *Day-Ahead Market (DAM)*: Generations and demands are settled using hourly day-ahead prices in this energy market. The DAM does not clear operating reserve capacities. DAM is a purely financial market, and is used in this study to demonstrate the BES dispatch under stable energy prices.

- *Real-Time Market (RTM) with 1-hour settlement period*: The real-time energy market clears every five minutes and generates 5-minute real-time energy and reserve prices. Generations, demands, and reserves are settled hourly using an average of these 5-minute prices. The reserve sustainability requirement is one hour.

- *RTM with 5-minute settlement periods*: ISO New England plans to launch the 5-minute subhourly settlement on March 1, 2017 [44]. The reserve sustainability requirement remains one hour.

Fig. 5.2a compares the energy prices in these different markets and shows that the 5-minute real-time prices fluctuate the most, while the day-ahead prices are more stable than real-time prices.

5.5.3 Accuracy of the Predictive Aging Model

Fig. 5.2b and 5.2c compare the BES dispatches for piecewise-linear cycle aging cost functions with different numbers of cycle depth segments. A cost curve with more segments is a closer approximation of the actual cycle aging function. The price signal for these examples is the 5-minute RTM price curve shown in Fig. 5.2a. Fig. 5.2b shows the SoC profile while Fig. 5.2c shows the corresponding output power profile, where positive values correspond to discharging periods, and negative values to charging periods.

The gray curve in Fig. 5.2 shows the dispatch of the BES assuming zero operating cost. This is the most aggressive dispatch, and the BES assigns full power to arbitrage as long as there are price fluctuations, regardless of the magnitude of the price differences. Fig. 5.2c shows that the BES frequently switches between charging and discharging, and Fig. 5.2b that it ramps aggressively. This dispatch maximizes the market revenue for the BES, but not the maximum lifetime profit, because the arbitrage decisions ignore the cost of cycle aging. We will show in Section 5.5.4 that this dispatch actually results in negative profits for all market scenarios.

The yellow curve in Fig. 5.2 illustrates the dispatch of the BES when the cycle aging cost curve is approximated by a single cycle depth segment. In this case, the marginal cost of cycle aging is constant and, as shown in Fig. 5.1, it overestimates the marginal cost of aging over a wide range of cycle depths. Therefore, this dispatch yields the most conservative arbitrage response, and the BES remains idle unless price deviations are very large, as demonstrated in Fig. 5.2c. Consequently, the BES collects the smallest market revenues, but the BES never loses money from market dispatch because the actual cycle aging is always smaller than the value predicted by the model.

As the number of segments increases, the BES dispatch becomes more sensitive to the magnitude of the price fluctuations, and a tighter correlation can be observed between the market price in Fig. 5.2a and the BES SoC in Fig. 5.2b. The red curve shows the dispatch of the BES using a 16-segment linearization of the cycle aging cost curve. When small price fluctuation occurs, the BES only dispatches at a fraction of its power rating, even though it has sufficient energy capacity. This ensures that the marginal cost of cycle aging does not exceed the marginal market arbitrage income.

Besides considering the impact of the piecewise linearization on the BES dispatch, it is also important to compare the cycle aging cost used by the predictive model incorporated in the dispatch calculation with an ex-post calculation of this cost using the benchmark rainflow-counting algorithm. Using the $\hat{e}_{t;j}$ calculated using the optimal dispatch model (5.5), we generate a percentage SoC series:

$$_t = \sum_{j=1}^{J} \hat{e}_{t;j} / E^{\text{rate}} ; \tag{5.24}$$

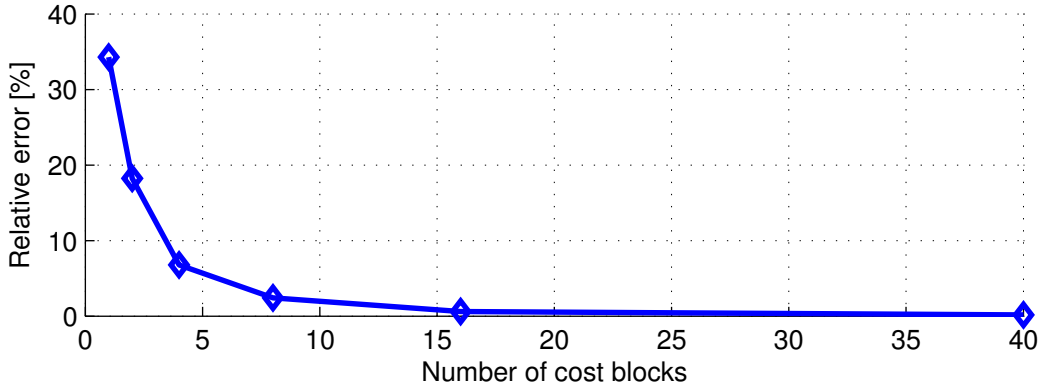

Figure 5.3: Difference between the cycle aging cost calculated using the predictive model and an ex-post calculation using the benchmark rainflow method for a full-year 5-minute RTM dispatch simulation.

This SoC series is fed into the rainflow method as described in Section 2.3, and the cycle life loss L is calculated as in (2.1) with the cycle stress function (5.23). The relative error on the cycle aging cost is calculated as:

$$= |\hat{C} - RL|/(RL); \tag{5.25}$$

where $\hat{C}$ is the cycle aging cost from (5.6). Fig. 5.3 shows the difference between the predicted and ex-post calculations for the simulations based on the RTM with a 5-minute settlement. As the number of segments increases to 16, the error becomes negligible.

5.5.4 BES Market Pro tability Analysis

Table 5.1 summarizes the economics of BES operation under the three markets described in Section 5.5.2 and for three cycle aging cost models: *no operating cost*; *single segment cycle aging cost*; and *16-segment cycle aging cost*. The market revenue, profit, and battery life expectancy calculations are based on dispatch simulations using market data spanning all of 2015. On the fifth row, the life loss due to market dispatch is calculated using the benchmark cycle life loss model of Eqs. (2.1), and (5.23). In the sixth row, we calculate the cycle aging cost by prorating the battery cell replacement cost to the dispatch life loss. In the

seventh row, the cost of cycle aging is subtracted from the market revenue to calculate the operating profit. In the last row, we estimate the battery cell life expectancy assuming the BES repeats the same operating pattern in future years. The life estimation L^{exp} includes shelf (calendar) aging and cycle aging

$$L^{exp} = (100\%)/(\Delta L^{cal} + \Delta L^{cycle}); \tag{5.26}$$

where ΔL^{cal} is the 10% annual self life loss as listed in Section 5.5.1, and ΔL^{cycle} is the annual life loss due to cycle aging as shown in the sixth row in Table 5.1.

The 16-segment model generates the largest profit in all market scenarios. Compared to the 16-segment model, the no cost model results in a more aggressive operation of the BES, while the 1-segment model is more conservative. Because the no-cost model encourages arbitrage in response to all price differences, it results in a very large negative profit and a very short battery life expectancy in all market scenarios. The 1-segment model only arbitrages during large price deviations. In particular, the BES is never dispatched in the day-ahead because these market prices are very stable.

The BES achieves the largest profits in the 5-minute RTM because this market has the largest price fluctuations. The revenue from reserve is lower in the 5-minute RTM than the hourly RTM. This result shows that the proposed approach is able to switch the focus of BES operation from reserve to arbitrage when market price fluctuations become high. In the RTM, the BES collects a substantial portion of its profits from the provision of reserve, especially in the hourly RTM. A BES is more flexible than generators at providing reserves because it does not have a minimum stable generation, it can start immediately, and can remain idle until called. Therefore, the provision of reserve causes no cycle aging. In the hourly RTM, the provision reserve represents about 74% of the market revenue and 90% of the prorated profits for this BES.

5.6 Summary

This paper proposes a method for incorporating the cost of battery cycle aging in economic dispatch, market clearing or the development of bids and offers . This approach takes advantage of the flexibility that a battery can provide to the power system while ensuring

that its operation remains profitable in a market environment. The cycle aging model closely approximates the actual electrochemical battery cycle aging mechanism, while being simple enough to be incorporated into market models such as economic dispatch. Based on simulations performed using a full year of actual market price data, we demonstrated the effectiveness and accuracy of the proposed model. These simulation results show that modeling battery degradation using the proposed model significantly improves the actual BES profitability and life expectancy.

Table 5.1: Dispatch of a 20MW / 12.5MWH BES in ISO-NE Energy Markets (full-year 2015).

Market	DAM			RTM hourly settlement			RTM 5-minute settlement		
Cycle aging cost model	no cost	1-seg.	16-seg.	no cost	1-seg.	16-seg.	no cost	1-seg.	16-seg.
Annual market revenue [k$]	138.8	0	21.3	382.5	197.5	212.5	789.3	303.8	372.3
Revenue from reserve [%]	No price for reserve in DAM			29.6	74.1	73.6	13.8	34.9	29.8
Annual life loss from cycling [%]	24.4	0	0.3	43.6	1.0	1.1	77.0	2.2	2.6
Annual prorated cycle aging cost [k$]	913.8	0	11.3	1626.3	36.3	38.8	2887.5	81.3	96.3
Annual prorated profit [k$]	-775.0	0	10	-1243.8	161.3	173.8	-2101.3	222.5	276.3
Profit from reserve [%]	No price for reserve in DAM			-	90.7	90.0	-	47.7	40.2
Battery life expectancy [year]	2.9	10.0	9.7	1.9	9.1	9.1	1.1	8.2	8.0

Chapter 6

BATTERY PLANNING IN ENERGY AND RESERVE MARKETS

6.1 Motivation

Determining the location and rating of battery energy storage (BES) in a power system is a more complex problem compared to generation or transmission expansion problem because primarily because the number of location candidates is significantly larger. Since BES installations are geographically unrestricted, they can be deployment in almost any location in a power system. Hence, a BES siting problem can involve hundreds or even thousands of nodes, which makes the problem extremely computational challenging to solve. In addition, the power and energy rating of a BES must be jointly optimized to maximize the value of BES investments.

An accurate long-term planning decision must account for its impact on short-term system operations [118]. However, solving a single optimization problem that includes the entire planing horizon (i.e., a full-year operation) is far beyond what is computationally tractable at this point in time. To overcome such computation barriers, heuristic ES planning models [40, 109] split ES siting and sizing into sequential decisions according to heuristic rules. While heuristic models are solvable over longer planning horizons, they may produce suboptimal planning decisions. To obtain more rigorous planning decisions, stochastic programming has been extensively incorporated in power system planning problems [21, 33, 55, 58]. Stochastic planning models co-optimize siting and sizing decisions on ES over a set of selected representative scenarios [11, 21, 33, 52, 101, 119, 144]. The computational complexity of a stochastic planning model depends on the number of scenarios, and a sufficient number of scenarios must be considered for effective representations of the uncertain renewable generation resources and demand. Although a larger number of scenarios improves the robustness of the planning result, such formulated problems can be computationally intractable when applied to large power systems [143]. Besides, adding additional

planning criteria, such as a guarantee of the ES investment payback rates [42, 92], and a co-optimization of energy and reserve markets [75], will further increase the complexity of the planning model.

The aforementioned ES planning approaches aim to trade-off modeling accuracy and computational complexity. Still, solving ES planning problems in realistically large systems is a non-trivial task and the modeling accuracy has been sacrificed for the sake of solvability. Nasrolahpour *et al.* [92] formulated strategic ES sizing in energy markets as a bi-level problem, and adopted a solution algorithm which combines mathematical programming with equilibrium constraints (MPEC) with Benders decomposition. However, their algorithm takes hours to solve the bi-level ES sizing problem on a single bus case study. We propose a decomposition algorithm that provides more accurate and faster solutions to the ES planning problem for a large number of scenarios.

6.2 Contribution

This chapter makes the following contributions:

- It formulates the optimal ES profit-constrained siting and sizing problem in a joint energy and reserve market as a bi-level problem considering the perspectives of the system operator in anticipation that energy storage would act as profit-seeking entities in a market environment

- It describes and tests a solution method which combines primal decomposition with subgradient cutting-planes. This solution method is scalable to any planning scenarios, and has non-heuristic terminating criteria.

- It benchmarks the computational performance of this algorithm against an exact linear programming (LP) approach, and demonstrates the accuracy and scalability of this algorithm.

- It uses compressed air energy storage and lithium-ion batteries to represent two different types of ES technologies, and compares their investment for different regulation

market policies.

- It analyzes the effect of a minimum profit constraint on the ES siting and sizing decisions as well as on the system operating cost.

6.3 Problem Formulation

We formulate the optimal ES siting and sizing as a bi-level problem. The upper-level (UL) problem identifies the ES investment decisions which minimize the overall system cost over a set of typical (or representative) days, while the lower-level (LL) problems minimize the operating cost of each typical day.

6.3.1 Upper-Level Problem: Energy Storage Siting and Sizing

The UL problem minimizes the total system cost (C^S) over all typical days, i.e. the sum of the expected system operating cost and of the ES investment cost:

$$\min_{x^U} C^S(x_j^P) := \sum_{j \in J} \omega_j C_j^P(x^U; x_j^p) + C^E(x^U); \tag{6.1}$$

where x^U are upper-level decision variables, and x_j^p are lower-level decision variables. The system operating cost is the sum of the dispatch cost C_j^P for each typical days weighted by the relative importance ω_j of the days it represents. The ES investment cost C^E is calculated based on both the power rating p_b^R and the energy capacity e_b^R of the ES installed at each bus $b \in B$:

$$C^E(x^U) := \sum_{b \in B} (c^p p_b^R + c^e e_b^R); \tag{6.2}$$

where $x^U = \{p_b^R, e_b^R\}$. This problem is constrained by limits on the power to energy (P/E) ratio of of the ES (which depends on the technology adopted), on the capital available for investment in ES, and by the need to achieve a minimum rate of return on these

investments:

$$\underline{e}_b^{\mathsf{R}} \le p_b^{\mathsf{R}} \le \overline{e}_b^{\mathsf{R}} \; ; \tag{6.3}$$

$$\sum_{b \in B} c^{\mathsf{p}} p_b^{\mathsf{R}} + c^{\mathsf{e}} e_b^{\mathsf{R}} \le c^{\mathsf{ic,max}} ; \tag{6.4}$$

$$C^{\mathsf{R}}(x_j^{\mathsf{P}}; x_j^{\mathsf{D}}) \ge C^{\mathsf{E}}(x^{\mathsf{U}}) ; \tag{6.5}$$

where the ES operational profit C^{R} is calculated as follows:

$$\begin{aligned} C^{\mathsf{R}}(x_j^{\mathsf{P}}; x_j^{\mathsf{D}}) := & \sum_{j \in J} \pi_j \sum_{t \in T} \sum_{b \in B} p_{j,t,b}^{\mathsf{dis}} \, \lambda_{j,t,b}^{\mathsf{lmp}} \, \Delta^{\mathsf{dis}} \\ & - p_{j,t,b}^{\mathsf{ch}} \, \lambda_{j,t,b}^{\mathsf{lmp}} \Delta^{\mathsf{ch}} + r_{j,t,b}^{\mathsf{eu}} \, \lambda_{j,t}^{\mathsf{eu}} \, \Delta^{\mathsf{dis}} + r_{j,t,b}^{\mathsf{ed}} \, \lambda_{j,t}^{\mathsf{ed}} \Delta^{\mathsf{ch}} \\ & - c_b^{\mathsf{dis}} p_{j,t,b}^{\mathsf{dis}} - c_b^{\mathsf{ch}} p_{j,t,b}^{\mathsf{ch}} - c_b^{\mathsf{eu}} r_{j,t,b}^{\mathsf{eu}} - c_b^{\mathsf{ed}} r_{j,t,b}^{\mathsf{ed}} \; : \end{aligned} \tag{6.6}$$

The first two terms calculates the payment the ES receives from the energy market that settles in the locational marginal price (LMP), the third and the fourth term calculates the payment from the regulation market that settles in the system-wide regulation up and down prices, the last four terms represents the operation cost of discharging, charging, as well as providing regulation.

6.3.2 Lower-Level Problem: Economic Dispatch

Each lower-level problem minimizes the system operating cost, C_j^{P}, for a particular typical day using an hourly interval. This economic dispatch takes into account the generation and regulation cost of conventional generators and ES units, as well as the cost associated with spillage of renewable energy. For each typical day j, this problem can be formulated in a compact way as follows:

$$\begin{aligned} \min_{x_j^{\mathsf{P}}} C_j^{\mathsf{P}}(x_j^{\mathsf{P}}) := & \sum_{t \in T} \sum_{b \in B} c^{\mathsf{rs}} p_{j,t,b}^{\mathsf{rs}} \\ & + \sum_{t \in T} \sum_{i \in I} c_i^{\mathsf{g}} p_{j,t,i}^{\mathsf{g}} + c_i^{\mathsf{gu}} r_{j,t,i}^{\mathsf{gu}} + c_i^{\mathsf{gd}} r_{j,t,i}^{\mathsf{gd}} \end{aligned} \tag{6.7}$$

$$+ \sum_{t \in T} \sum_{b \in B} c_b^{\mathsf{dis}} p_{j,t,b}^{\mathsf{dis}} + c_b^{\mathsf{ch}} p_{j,t,b}^{\mathsf{ch}} + c_b^{\mathsf{eu}} r_{j,t,b}^{\mathsf{eu}} + c_b^{\mathsf{ed}} r_{j,t,b}^{\mathsf{ed}} \; ; \tag{6.8}$$

subject to:

$$\mathbf{M}_j^{\mathsf{P}} x_j^{\mathsf{P}} + \mathbf{M}^{\mathsf{E}} x^{\mathsf{U}} \le \mathbf{V}_j^{\mathsf{P}} ; \tag{6.9}$$

where the decision variables are $x_j^{\mathsf{p}} = \{\, p^{\mathsf{ch}}_{j;t;b},\, p^{\mathsf{dis}}_{j;t;b},\, p^{\mathsf{g}}_{j;t;i},\, p^{\mathsf{rs}}_{j;t;b},\, r^{\mathsf{ed}}_{j;t;b},\, r^{\mathsf{eu}}_{j;t;b},\, r^{\mathsf{gd}}_{j;t;i},\, r^{\mathsf{gu}}_{j;t;i},\, e^{\mathsf{soc}}_{j;t;b},\, f_{j;t;l},\ \ _{j;t;b}\}$. $\mathbf{M}_j^{\mathsf{P}}$, $\mathbf{M}^{\mathsf{E}}$, $\mathbf{V}_j^{\mathsf{P}}$ are constraint coefficient matrices. The compact expression of the constraints (6.9) is expanded below and the dual variables associated with each constraint are shown in parentheses after a colon.

Nodal power balance equations ($\forall t \in T; b \in B$)

At each bus, the sum of the power injections and the inflows must be equal to the demand:

$$\begin{aligned} &\sum_{i2I_b} p^{\mathsf{g}}_{j;t;i} - \sum_{ljb2o(l)} f_{j;t;l} + \sum_{ljb2r(l)} f_{j;t;l} + G^{\mathsf{rn}}_{j;t;b} \\ &-p^{\mathsf{rs}}_{j;t;b} + p^{\mathsf{dis}}_{j;t;b}\ ^{\mathsf{dis}} - p^{\mathsf{ch}}_{j;t;b} =\ ^{\mathsf{ch}} = D_{j;t;b} : (\ ^{\mathsf{lmp}}_{j;t;b}) \end{aligned} \tag{6.10}$$

where $^{\mathsf{lmp}}_{j;t;b}$ is the locational marginal price.

Regulation requirement ($t \in T; b \in B_E; i \in I$)

Hourly up/down regulation requirements are expressed as a percentage of the system-wide demand ($^{\mathsf{D}}$) plus a percentage of the system-wide renewable injection ($^{\mathsf{R}}$):

$$\begin{aligned} &\sum_{b2B} r^{\mathsf{eu}}_{j;t;b}\ ^{\mathsf{dis}} + \sum_{i2I} r^{\mathsf{gu}}_{j;t;i} \\ &\geq \sum_{b2B} \ ^{\mathsf{R}}p^{\mathsf{rn}}_{j;t;b} +\ ^{\mathsf{D}}D_{j;t;b}\ : (\ ^{\mathsf{ru}}_{j;t}) \end{aligned} \tag{6.11}$$

$$\begin{aligned} &\sum_{b2B} r^{\mathsf{ed}}_{j;t;b} =\ ^{\mathsf{ch}} + \sum_{i2I} r^{\mathsf{gd}}_{j;t;i} \\ &\geq \sum_{b2B} \ ^{\mathsf{R}}p^{\mathsf{rn}}_{j;t;b} +\ ^{\mathsf{D}}D_{j;t;b}\ : (\ ^{\mathsf{rd}}_{j;t});\end{aligned} \tag{6.12}$$

where $^{\mathsf{ru}}_{j;t}$ and $^{\mathsf{rd}}_{j;t}$ are the hourly up and down regulation prices.

Energy storage constraints ($\forall t \in T; b \in B_E$)

The evolution of the state of charge $e^{\mathsf{soc}}_{j;t;b}$ is calculated from the energy market dispatch schedules:

$$e^{\mathsf{soc}}_{j;t;b} - e^{\mathsf{soc}}_{j;t\ 1;b} = p^{\mathsf{ch}}_{j;t;b} - p^{\mathsf{dis}}_{j;t;b} : (\ ^{\mathsf{e}}_{j;t;b});\tag{6.13}$$

the initial ES SoC is set to zero ($e^{\mathsf{soc}}_{j;0;b} = 0$) for all ES operations, and the end-of-day SoC is not enforced in (6.13). The charging and discharging power must remain within the rated

power:

$$p^{ch}_{j;t;b} + r^{ed}_{j;t;b} \leq p^{R}_{b} : (\ '^{ch}_{j;t;b}) \tag{6.14}$$

$$p^{dis}_{j;t;b} + r^{eu}_{j;t;b} \leq p^{R}_{b} : (\ '^{dis}_{j;t;b}); \tag{6.15}$$

and the ES must sustain the full regulation reserve dispatch for the required time interval (T^{es}):

$$e^{soc}_{j;t;b} + T^{es} r^{ed}_{j;t;b} \leq e^{R}_{b} : (\ '^{soc}_{j;t;b}) \tag{6.16}$$

$$e^{soc}_{j;t;b} - T^{es} r^{eu}_{j;t;b} \geq 0 : (\ ^{soc}_{j;t;b}); \tag{6.17}$$

Other constraints

Appendix D.2 defines the formulation of the generator power rating and ramp constraints, the constrains on renewable spillage, and the dc power flow model used to enforce the network constraints.

6.3.3 Dual Lower-Level Problem

We apply the primal-dual transformation to the primal lower-level (PLL) problem due to its convexity. The dual lower-level (DLL) problem optimizes system prices so that constraint (6.5) is enforced. The DLL objective function is formulated as follows:

$$\begin{aligned}
&\max_{x^{D}_{j}} C^{D}_{j}(x^{U}; x^{D}_{j}) := \sum_{t2T} \sum_{i2I} (\ '^{g}_{j;t;i} G^{max}_{i} + \ ^{g}_{j;t;i} G^{min}_{i}) \\
&+ R^{u}_{i}(\ '^{R}_{j;t;i} + T^{ru}\ '^{gu}_{j;t;i}) + R^{d}_{i}(-\ ^{R}_{j;t;i} + T^{rd}\ '^{gd}_{j;t;i}) \\
&+ \sum_{i2I} (\ '^{R}_{e;1;i} + \ '^{R}_{e;1;i}) G^{0}_{j;t} + \sum_{\substack{t2T \\ l2L}} (\ '^{f}_{j;t;l} - \ ^{f}_{j;t;l}) F^{max}_{l} \\
&+ \sum_{t2T} \sum_{b2B} \Big['^{rs}_{j;t;b} G^{rs}_{j;t;b} + \ ^{lmp}_{j;t;b} (D_{j;t;b} - G^{rn}_{j;t;b}) \\
&+ \sum_{t2T} \sum_{b2B} \ ^{rn} G^{rn}_{j;t;b} (\ ^{ru}_{j;t} + \ ^{rd}_{j;t}) + \ ^{D} D_{j;t;b} (\ ^{ru}_{j;t} + \ ^{rd}_{j;t}) \\
&+ \sum_{t2T} \sum_{b2B} p^{R}_{b} (\ '^{ch}_{j;t;b} + \ '^{dis}_{j;t;b}) + e^{R}_{b}\ '^{soc}_{j;t;b} \ :
\end{aligned} \tag{6.18}$$

subject to:

$$\mathbf{M}^{D}_{j} x^{D}_{j} \leq \mathbf{V}^{D}_{j} : \tag{6.19}$$

where $\mathbf{M}_j^{\mathsf{D}}$ and $\mathbf{V}_j^{\mathsf{D}}$ are the constraint coefficient matrices. The detail of these constraints are given in Appendix D.2. Note that the objective function includes products of UL (x_j^{U}) and DLL variables (x_j^{D}).

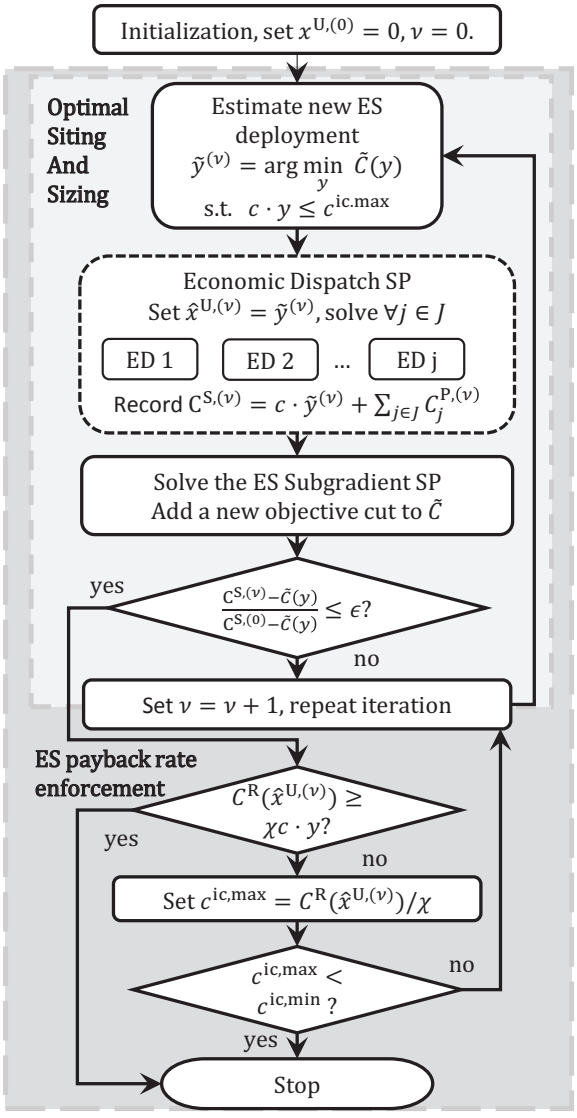

Figure 6.1: Flowchart of the solution algorithm

6.4 Solution Method

Decomposition has been used extensively for solving large-scale programming problems [15, 80, 96, 153], especially for scenario-based stochastic programmings [9, 68, 92, 93, 111]. A stochastic planning problem couples independent scenarios with a few planning decision variables. An effective decomposition breaks each scenario into a subproblem, which can be solved in sequence or in parallel. It is also easier to aggregate subproblem results in such decomposition structures, and the master problem can be solved rapidly and accurately. Fig. 6.1 illustrates the proposed solution algorithm that involves an inner-loop and an outer-loop. The inner-loop identifies the optimal ES locations subject to the maximum ES investment budget, $c^{ic,max}$, and the outer-loop enforces the ES rate of return constraint (6.5).

In the inner-loop, the main problem is decomposed into scenario subproblems by fixing the value of ES planning variables. Each scenario subproblem solves an ED problem. The inner-loop is initialized with no ES installation in the system, and solve the ED for all scenarios. Based on the ED results, the potential benefit of ES installation is calculated for each bus in the system in a subgradient form. ES installations are updated accordingly. Therefore, the inner-loop calculates ES siting and sizing decisions iteratively, until the estimated distance to the exact optimal solution is sufficiently small. The decomposition technique is described in Section 6.4.1. Section 6.4.3 explains how the subgradient of the objective function with respect to ES planning variables is calculated. Section 6.4.2 explains the subgradient cutting-plane method used to update ES planning variables at each iteration and solve the optimal ES location problem.

In the outer-loop, the optimal ES siting and sizing decisions are tested against the ES rate of return constraint (6.5). If it is not satisfied, the maximum ES investment budget, $c^{ic,max}$, is reduced and the inner-loop is repeated (see Section 6.4.4). The algorithm terminates once a current solution satisfy constraint (6.5) or the maximum ES investment budget, $c^{ic,max}$, reaches the minimum ES investment limit, $c^{ic,min}$.

6.4.1 Problem Decomposition

The bi-level problem (6.1)–(6.17) can be recast into a single-level (SL) equivalent. The objective function of this problem is:

$$\min_{x^{U};x_j^{P};x_j^{D}} C^{S}(x^{U};x_j^{P}) := \sum_{j2J} !_j C_j^{P}(x^{U};x_j^{P}) + C^{E}(x^{U}); \tag{6.20}$$

subject to:

UL, PLL, and DLL constraints (6.21)

$$C_j^{P}(x^{U};x_j^{P}) = C_j^{D}(x^{U};x_j^{D}); \; j \in J; \tag{6.22}$$

where (6.22) represents the strong duality constraint. The details of the formulation of this problem are given in Appendix D.2.

When the value of the coupling variables x^{U} is fixed, we can then apply primal decomposition to this problem. For the sake of simplicity, we first ignore the profit constraint (6.5). The subproblem becomes a linear ED problem for each typical day. This decomposed SL problem can then be solved iteratively as follows [19]:

Set initial values for the coupling variables

The solution algorithm starts with $x^{U;(0)} = 0$, indicating no ES deployment.

Solve the subproblems

At iteration , set $x^{U} = x^{U;(\ )}$, solve each EDSP in parallel to obtain $\hat{x}_j^{P;(\ )}$ and $\hat{x}_j^{D;(\ )}$.

Solve the master problem

Calculate the subgradients of C^{S} with respect to x^{U} and update the UL variables accordingly.

Iteration

Check for convergence, and repeat from Step 2) if needed. The convergence criterion is explained in Section. 6.4.2.

While subgradient methods can be easily used to solve the master problem, their convergence is slow and they do not provide a measurement of the optimality of the results. We therefore incorporate the subgradient cutting-plane method in the proposed approach because it converges faster and has a non-heuristic stopping criterion.

6.4.2 The Cutting-plane Method

We apply cutting-plane methods [12, 20, 69] to solve the master problem. Cutting-plane methods incorporate results from previous iterations and form a piece-wise linear approximation ($\tilde{C}^{(\ )}$) of the objective function:

$$\tilde{C}^{(\ +1)}(y) := \max_k \quad [C^S(\tilde{y}^{(\ )}) + (y - \tilde{y}^{(\ )}) \cdot g^{U;(k)}]; \tag{6.23}$$

where y is an inquiry point identical to x^U, and $\tilde{C}^{(\ )}(\tilde{y}^{(\ )})$ is a lower-bound estimate of the optimal objective function value, i.e., the system cost.

At each iteration, the ES subproblems are solved by setting $x^{U;(\ )} = \tilde{y}^{(\ )}$ where $\tilde{y}^{(\ )} \in \arg\min_y \tilde{C}^{(\ )}(y)$ subject to constraints (6.3) and (6.4). The inquiry point $\tilde{y}^{(\ )}$, the current system cost value, and the calculated subgradients are then added to (6.23) as a new objective cut for future iterations. As iterations proceed, $\tilde{C}^{(\ )}$ approaches the actual objective function, and a solution is found when the difference between $C^S(x^{U;(\ )})$ and $\tilde{C}^{(\ )}(\tilde{y}^{(\ )})$ is below a tolerance. We assume that the algorithm terminates based on a relative tolerance with respect to the estimated maximum system cost saving:

$$\tilde{C}^{(\ )}(\tilde{y}^{(\ )}) - C^S(x^{U;(\ )}) \leq \ [C^S(0) - \tilde{C}^{(\ )}(\tilde{y}^{(\ )})]; \tag{6.24}$$

where $C^S(0)$ is the system cost without ES deployments, and is the relative tolerance. Therefore the system cost saving in the algorithm is always greater than $(1 -\ )$ of the optimal system cost saving.

6.4.3 Energy Storage Subgradient Cuts

ES subgradients for B^E buses are calculated directly using dual variables associated with constraints (6.14)–(6.17), this derivation is shown in Appendix D.4. However, the value of $^{soc;(\ )}_{j;t;b}$ is always zero at the first iteration, because energy rating constraints are implicit,

thus (6.16) never binds when the ES power rating is zero. Moreover, $\pi^{ch,(\nu)}_{j,t,b}$ and $\pi^{dis,(\nu)}_{j,t,b}$ cannot reflect the value for arbitrage unless the ES has non-zero SoC evolutions to correlate temporal arbitrage decision between different time intervals. Therefore, we calculate ES subgradients for B^N buses through a subgradient subproblem (SGSP) to correctly identify the value of marginal ES investment. The SGSP provides an initial ES P/E ratio β^0_b, so that solutions to the master problem has reduced perturbations and converges faster. The derivation of the SGSP is shown in Appendix D.5. At iteration ν, the subgradients of C^S with respect to the ES power rating (g^p_b) and energy rating (g^e_b) are calculated as:

$$g^{p,(\nu)}_b = \begin{cases} c^p + \pi^{ch,(\nu)}_{j,t,b} + \pi^{dis,(\nu)}_{j,t,b}; & b \in B^E \\ \hat{g}^{0,(\nu)}_b - \hat{\beta}^{0,(\nu)}_b (1 + \hat{\beta}^{0,(\nu)}_b); & b \in B^N \end{cases} \tag{6.25}$$

$$g^{e,(\nu)}_b = \begin{cases} c^e + \pi^{soc,(\nu)}_{j,t,b}; & b \in B^E \\ \hat{g}^{0,(\nu)}_b - \hat{\beta}^{0,(\nu)}_b; & b \in B^N; \end{cases} \tag{6.26}$$

where $\hat{g}^{0,(\nu)}_b$ and $\hat{\beta}^{0,(\nu)}_b$ are determined by solving the following subgradient subproblem (SGSP):

$$\begin{aligned} &\min_{p^{ch}_{j,t,b}, p^{dis}_{j,t,b}, r^{eu}_{j,t,b}, r^{ed}_{j,t,b}, e^{soc}_{j,t,b}, \beta^0_b} g^{0,(\nu)}_b := \\ &\sum_{j \in J} \Big(\sum_{t \in T} p^{ch}_{j,t,b} \hat{\pi}^{lmp,(\nu)}_{j,t,b} - p^{ch} - p^{dis}_{j,t,b} \hat{\pi}^{lmp,(\nu)}_{j,t,b} \Big) \\ &- r^{eu}_{j,t,b} \hat{\pi}^{ru,(\nu)}_{j,t} - r^{ed}_{j,t,b} \hat{\pi}^{rd,(\nu)}_{j,t} - p^{ch} + c^{dis}_b p^{dis}_{j,t,b} \\ &+ c^{ch}_b p^{ch}_{j,t,b} + c^{eu}_b r^{eu}_{j,t,b} + c^{ed}_b r^{ed}_{j,t,b} + \beta^0_b c^p + c^e; \end{aligned} \tag{6.27}$$

subject to constraints (6.3) and (6.13)–(6.17) by setting $p^R_b = \beta^0_b$ and $e^R_b = 1$. This subproblem maximizes the profit of incremental ES deployments at B^N buses, where ES are price-takes and profit maximization is equivalent to system operating cost minimization [30]. $\hat{\beta}^0_b$ is the optimal P/E ratio for price-taker ES deployments, which is close to the true optimal P/E ratio if the ES has limited price influences. Subgradients at B^N buses are designed to enforce $\hat{\beta}^0_b$ over all new ES deployments. ES deployments with near-optimal P/E ratios have faster convergence due to minimum perturbations between ES power and energy investment decisions.

6.4.4 Incorporating the ES Pro t Constraint

In Appendix D.3, we show that the ES operational revenue can be represented using the ES subgradients:

$$C^{\mathsf{R}} = - \sum_{b2B} (g_b^{\mathsf{p}} - c^{\mathsf{p}}) p_b^{\mathsf{R}} + (g_b^{\mathsf{e}} - c^{\mathsf{e}}) e_b^{\mathsf{R}} \ : \tag{6.28}$$

Because all ES allocation variables must have non-negative values, all p_b^{R} and e_b^{R} with non-zero values must have negative subgradients. we can therefore infer that $C^{\mathsf{R}} \geq C^{\mathsf{E}}$ in all optimal locations, and in unconstrained ES locations, the ES rate of return converges to one. Hence ≥ 1 is guaranteed for all optimal ES locations. For > 1, we can reasonably assume that ES has a limited effect on system prices and that the system-wide ES operating revenue should only increase with ES investment. Therefore, for the optimal ES locations, the ES revenue $\hat{C}^{\mathsf{R}}$ is a concave monotonic increasing function of the ES investment cost C^{E} such that:

$$0 \leq d\hat{C}^{\mathsf{R}}(C^{\mathsf{E}}) / dC^{\mathsf{E}} \leq 1 ; \tag{6.29}$$

where C^{E} is capped by $c^{\mathsf{ic;max}}$ in constraint (6.4). If a rate of return is achievable in the system, then there must be some $C^{\mathsf{E}'}$ that satisfy:

$$\hat{C}^{\mathsf{R}}(C^{\mathsf{E}'}) - \ C^{\mathsf{E}'} \geq 0 : \tag{6.30}$$

When an ES investment cost C^{E} violates (6.4), we can estimate an upper-bound of $C^{\mathsf{E}'}$ as

$$C^{\mathsf{E}'} \leq \hat{C}^{\mathsf{R}}(C^{\mathsf{E}'}) / \ \leq \hat{C}^{\mathsf{R}}(C^{\mathsf{E}}) / \ ; \tag{6.31}$$

because $C^{\mathsf{R}}(C^{\mathsf{E}'}) \leq C^{\mathsf{R}}(C^{\mathsf{E}})$ according to (6.29). Therefore, (6.5) can be satisfied by iteratively solving the optimal ES allocation with a reduced maximum ES investment cost $c^{\mathsf{ic;max}} = C^{\mathsf{R}} / \ $.

Since we use the cutting-plane method to solve the master problem and the feasible region is reduced when setting $c^{\mathsf{ic;max}} = C^{\mathsf{R}} / \ $ (recall that (6.5) only binds when > 1), solving the optimal ES allocations recursively will not add much complexity because the method already has a fairly good estimate of the objective function.

6.4.5 Comparison to Benders Decomposition

Benders decomposition is a classic approach for solving block-structured optimization with coupling (complicating) variables [31], and has been extensively used for solving strategic bi-level planning problems in power system [9, 68, 92]. The proposed algorithm is similar to Benders decomposition because it decomposes the optimization problem by fixing the coupling variables and solves the master problem using cutting planes. However, it incorporates two key improvements over a classic Benders decomposition.

First, it uses coordinated subgradient cuts, which provides more accurate information on the value of marginal ES investments than Benders dual cuts. Since the value of an ES deployment is jointly affected by its power and energy ratings, these planning decisions are not independent, and the P/E ratio must be optimized. However, Benders dual cuts based on the binding conditions of ES rating constraints (6.14) - (6.17) are inefficient at coordinating investments on power and energy ratings, especially during the early iterations where ES ratings are mostly zero. These uncoordinated cuts cause the master problem solution to oscillate around the optimal point, and significantly slow down the convergence. Instead of using dual cuts, the proposed algorithm uses coordinated ES subgradients, which enforces near-optimal P/E ratios over all new ES deployments and thus speeds up the convergence.

Besides using coordinated subgradient cuts, we analytically derived a relationship between the maximum ES investment budget and the profitability, and decomposed the bi-level problem into a recursive structure, as shown in Fig. 6.1. Previous studies [9, 68, 92] follow an approach that combines Benders decomposition with MPEC. This approach first materializes the bi-level problem into a MPEC problem, the MPEC problem is then recast into a MILP structure using the 'big M' method [53], and Benders decomposition is applied to decompose and solve the MILP problem. The 'big M' method uses auxiliary integer variables and a sufficiently large constant M to linearize nonlinear terms. However the accuracy and computational speed of the 'big M' linearization are very sensitive to the value of M, if M is not large enough, the linearization is not accurate, if M is too large, the computation can be extremely slow. Compared to the MPEC+Benders method, our algorithm requires no

auxiliary linearization variables and the size of the master problem does not increase with the number of scenarios. Therefore, the proposed algorithm has better scalability and leads to more robust planning result. In addition, the proposed algorithm generates simpler sub-problems that are solved faster than in the MPEC+Benders method. In Section 6.6.4, we demonstrate that the computational speed of the proposed method surpasses the solution time achieved in a similar previous study.

6.5 Case Study Test System

6.5.1 System Settings

The proposed ES planning model and solution method were tested using a modified 240-bus reduced WECC system [117]. This system includes 448 transmission lines, 71 aggregated thermal plants and renewable sources including hydro, wind, and solar. The maximum expected forecasts of all renewable generations are grouped as $G^{rn}_{j;t;b}$, the maximum allowable spillage for hydro generation is enforced in $G^{rs}_{j;t;b}$, other types of renewable generation have no curtailment limits. Renewable curtailments are necessary in the modified WECC testbed because large renewable generation capacities are installed at some buses with a limited transmission capacity, and the objective of the economic dispatch is to minimize the system operating cost. In certain cases, such as days with strong winds and low demand, a certain amount of wind power generation must be curtailed to maintain secure operation of the system.

We use a '3+5'% reserve policy for setting the requirements for regulation [111], hence $^{D} = 3\%$ and $^{R} = 5\%$. Regulation parameters are adjusted so that the regulation prices are identical to the actual day-ahead regulation clearing prices in CAISO [27]. The value of renewable spillages is set to zero. The modified WECC system has a daily ED operating cost ranging from 15 to 35 M$.

All simulations were carried out in CPLEX under GAMS [123] on an Intel Xenon 2.55 GHz processor with 32 GB of RAM. Typical days and their respective weights from the year-long demand and renewable generation profiles were identified using a hierarchical clustering algorithm [112]. The convergence criterion is set to $= 5\%$.

Table 6.1: Energy Storage Model Parameters.

Energy storage technology	AA-CAES	LiBES
Power rating investment ($/kW-year)	1250 - 20	409 - 20
Energy rating investment ($/kWh-year)	150 - 20	468 - 20
Battery replacement cost ($/kWh)	n/a	406
P/E ratio range (h ^{1})	0.05 to 0.25	0.1 to 4
Round trip efficiency	0.72	0.9
Incremental production cost ($/MWh)	0	87
Incremental consumption cost ($/MWh)	0	0

6.5.2 Energy Storage Cost Model

We consider two types of representative ES technologies: 1) above-ground advanced adiabatic compressed air energy storage (AA-CAES), and 2) lithium-ion battery energy storage (LiBES) [100, 150]. The ES cost model consists of three parts:

- Investment cost of the power equipments (c^{p}) proportional to the ES power rating (unit: $/kW). This investment covers the turbine generator and air compressor in AA-CAES, or the power electronic equipments in LiBES.

- Investment cost of the storage system (c^{e}) proportional to the ES energy rating (unit: $/kWh). This investment covers the storage tank in AA-CAES, or the battery management system in LiBES.

- Marginal production cost (unit: $/kWh). This is the energy production cost of ES units.

Because we consider large-scale ES installations, we assume that the fixed storage installation cost, including the land and construction cost, scales linearly with the ES rating and can therefore be incorporated in the costs proportional to the power and energy ratings. AA-CAES units have high investment cost for power ratings and low investment cost for

the storage capacity, the operation cost is also negligible because AA-CAES consumes no fuel for power generation. Electrochemical battery energy storage such as LiBES [39, 150] has more evenly distributed investment cost components. The lifetime of lithium batteries is very sensitive to operations due to degradation, the marginal production cost of LiBES is therefore defined based on its cell cycle life.

We assume that cycle aging only occurs during battery discharging and has a constant marginal cost. Using cycle life test data set for Lithium manganese oxide (LMO) batteries [146], we apply a linear fit to the LMO cycle life loss per cycle up to 70% depth of discharge (DoD) (Fig. 6.2). The operation region of the LiBES is limited to the range from 20% to 90% of SoC to avoid deep discharges as well as overcharge and overdischarge effects, because these factors severely reduce the battery life [136]. Instead of introducing new SoC constraints, the LiBES is oversized to reflect the increased cost due to a narrowed SoC operation region. We assume that the battery cells in the LiBES are always replaced once reaching their end of life. The marginal discharging cost of LiBES is calculated by prorating the battery cell replacement cost to the cycle life loss curve

$$c^{\text{dis}} = a^{\text{t}} \frac{\text{Cell replacement cost (\$406/kWh)}}{\text{DoD operation range (70\%)}}; \tag{6.32}$$

where a^{t} is the linear fitted slop of the cycle life loss curve in Fig. 6.2.

Table 6.1 shows the capital cost, P/E ratio range, efficiency, and operating cost of these two ES cost models. The battery cells in LiBES are replaced once reaches the end of life. We assume a 5% annual interest rate and calculate the daily prorated cost as in [109]. All 240 buses are considered as ES deployment candidates.

6.5.3 Negative Pricing and Storage Dispatch

In optimal ED solutions, an ES unit may be dispatched to charge and discharge simultaneously during the occurrence of negative LMPs [57]. The storage round-trip efficiency causes energy spillages that are beneficial to the system, and ES units gain additional revenue. Such dispatches are physically achievable for AA-CAES units because the air compressor and generator use separate pipelines [130], so that the compressor and generator can operate at the same time.

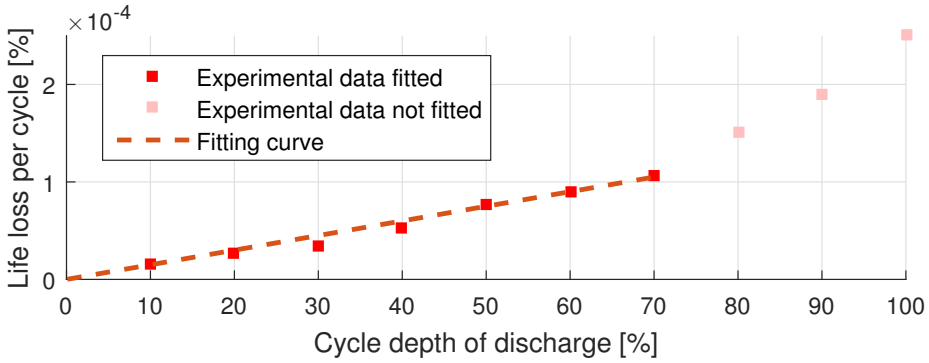

Figure 6.2: LMO battery cycle life curve and fitting to 70% DoD.

LiBES can only charge or discharge at one time and simultaneous dispatches must be avoided. In Appendix D.6 we demonstrated the following sufficient condition for avoiding simultaneous charging and discharging ($\forall b \in B; t \in T; j \in J$):

$$c^{dis} + c^{ch} > -(1 = {}^{dis} - {}^{ch}) \; {}^{lmp}_{j;t;b}. \tag{6.33}$$

The above sufficient condition explains that in optimal ED solutions, an ES unit will not charge and discharge simultaneously as long as the operation cost for a round-trip dispatch is higher than the product of the round trip efficiency loss and the negative LMP value. In other words, the cost of performing simultaneous dispatches is higher than the market payment. In the modified WECC model, the largest negative LMP never exceeds -200 $/MWh, and the round-trip efficiency of LiBES is 90%. Therefore as long as the marginal production cost of LiBES is higher than 20 $/MWh, simultaneous LiBES dispatches are avoided.

6.5.4 Regulation Cost and Dispatch Model

The cost of providing regulation is estimated using normalized CAISO area control error (ACE) data [25, 147]. The provision of regulation does not increase the operating cost for AA-CAES because these units have no marginal operating cost. The average cost for LiBES to provide 1 MW of regulation up for one hour is 10% of the marginal production cost ($c^{eu} = 0{:}1c^{dis}$) under the assumption that an average 100 kWh of energy is generated. The regulation cost scales linearly with the regulation up capacity within the 70% DoD region.

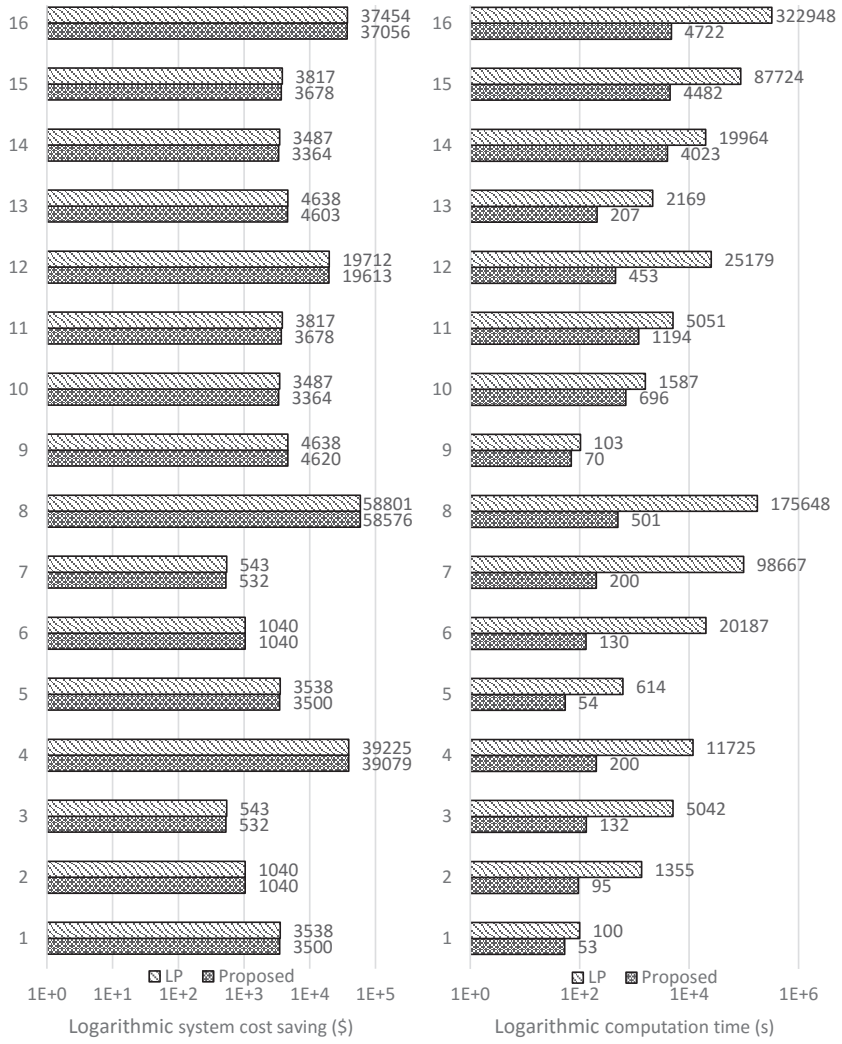

(a) Daily prorated system cost saving. (b) Computation time.

Figure 6.3: Computation test results of the 16 test cases.

The LiBES has no cost for providing regulation down because charging has no marginal cost.

In CAISO, ES units have two options for participating regulation: the regulation energy management program (REM) and the traditional option (non-REM). In the REM program, CAISO co-optimize the ACE with the real-time energy market and generates a regularized regulation signal that has a 15-minute zero-mean in energy. Therefore REM units are only required to have a 15 minute capacity ($T^{es} = 0.25$) and are not deviated from their scheduled SoC levels.

Non-REM units are required to have a continuous full dispatch time requirement of one hour ($T^{es} = 1$). SoC deviations for providing regulation in Non-REM ES units are not accounted in the ED formulation because we primarily evaluate the economic value of ES investment in hourly economic dispatch. In the regulation market, energy deviations caused by regulation provision are settled at the real-time locational marginal prices after the dispatch period [28]. Therefore, from an economic point of view, ES does not gain or loses energy in regulation provision (i.e., ES cannot receive free energy for charging by providing regulation, the charged energy is still settled at market prices), and the proposed planning model leads to sufficiently accurate decisions without considering the real-time regulation energy deviations. In real-time dispatches, ES units can adopt control strategies against large energy deviations [148] and maintain the scheduled dispatch.

6.6 Simulation Results

6.6.1 Computational Performance

We compare the computational performance of the proposed method against solving the problem directly using CPLEX. When the profit constraint (6.5) is ignored, the objective function (6.20) and constraints (6.3), (6.4) and (6.9) become a linear problem (LP), and can be solved by using the solver CPLEX.

We designed 16 test cases with different planning scenarios. Case 1-4 are the optimal ES allocation considering 1, 3, 5, and 10 typical days, subject to a maximum ES investment budget constraint, using the CAES ES model. Case 5-8 are identical to 1-4 except that they

do not include a maximum investment constraint. Case 9-16 are identical to 1-8 except that the LiBES ES model is used.

As shown in Figure. 6.3, the proposed method is significantly faster than solving the LP problem directly using CPLEX, while all system cost saving results are within the set tolerance. CPLEX exhibits an approximately quadratic increase in computation time with the number of typical days, while the proposed method demonstrates a much slower increase. However, the computational speed of the proposed method depends on the renewable and demand profiles because some profiles result in smoother system cost functions, which facilitates the convergence of the subgradient cutting-plane method. When the IC constraint is excluded, the search region for ES allocation expands and thus the computation time of both methods increases. However, this effect is much smaller in the proposed method.

6.6.2 Rate of Return on ES Investment

We performed ES planning on three different days subject to different ES rate of return constraints. Table 6.2 shows the results for the LiBES model with $T^{es} = 0.25$. A higher ES rate of return reduces the installed ES capacity and increases the system operating cost. A return rate of 150% is only achievable in one of the three days.

The computation time of the proposed method increases moderately when the payback rate is greater than 1, because the optimal ES allocation is solved repeatedly. However this will not result in a polynomial or exponential increase in complexity because the cutting-plane method keeps track of historical results. Enforcing a higher rate of return reduces the maximum ES investment budget and hence decreases the feasible region. In turn this reduces the solution time when the problem is solved iteratively.

This table also shows that buses 155 and 285 are the only locations where ES is deployed for day 100, 141 and 285. In other single-day tests that we performed, ES was also located at buses 15, 90, 198, 226, 227, 228. These buses are good locations for performing spatio-arbitrage because they are connected to frequently congested lines and renewable sources, especially hydro units. In particular, LMPs are frequently negative at bus 155.

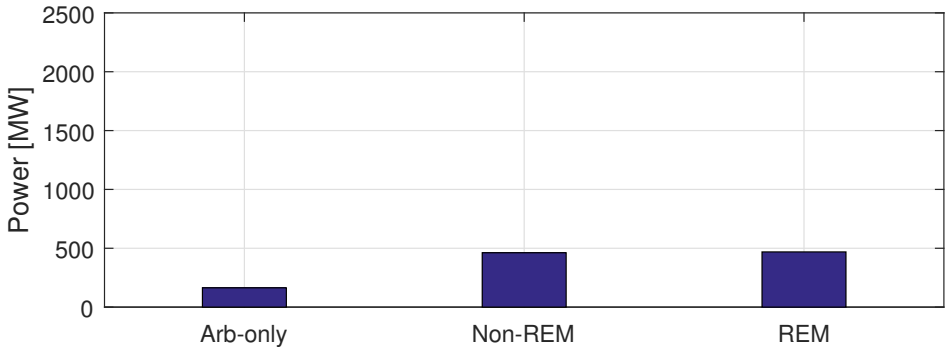

(a) Installed power rating.

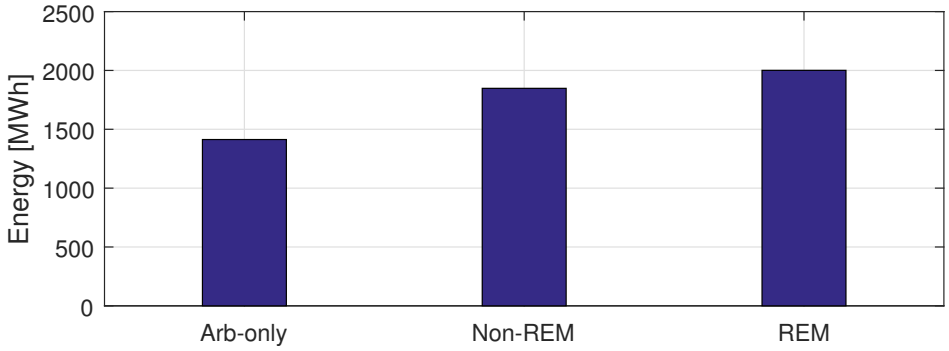

(b) Installed energy rating.

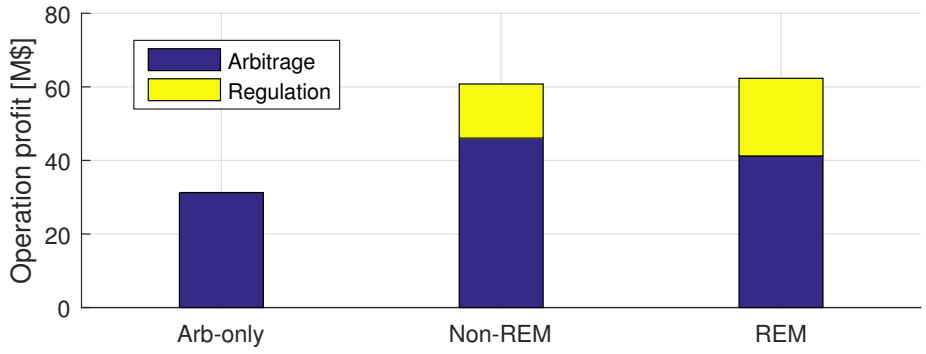

(c) Annual market revenue.

Figure 6.4: AA-CAES planning in different market scenarios.

6.6.3 Stochastic ES Planning

We performed stochastic ES planning considering 20 typical days with no maximum ES investment limit. Three market scenarios are considered: in *Arb-only* AA-CAES only partic-

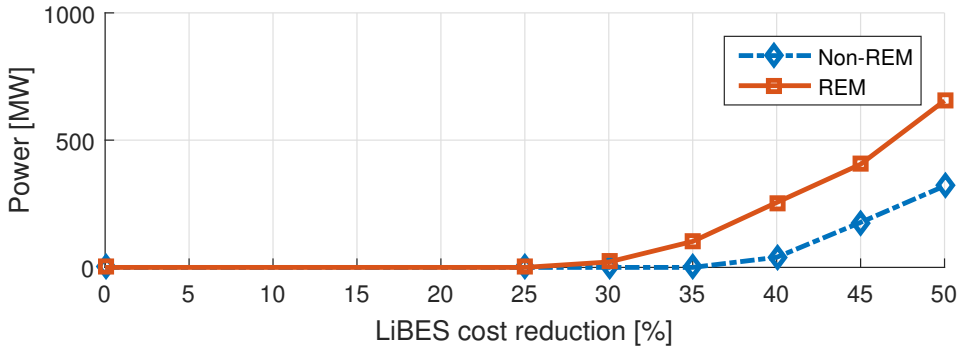

(a) Installed power rating.

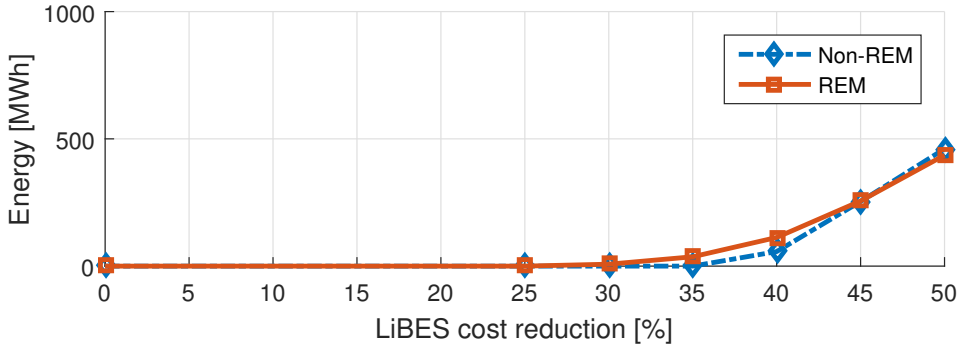

(b) Installed energy rating.

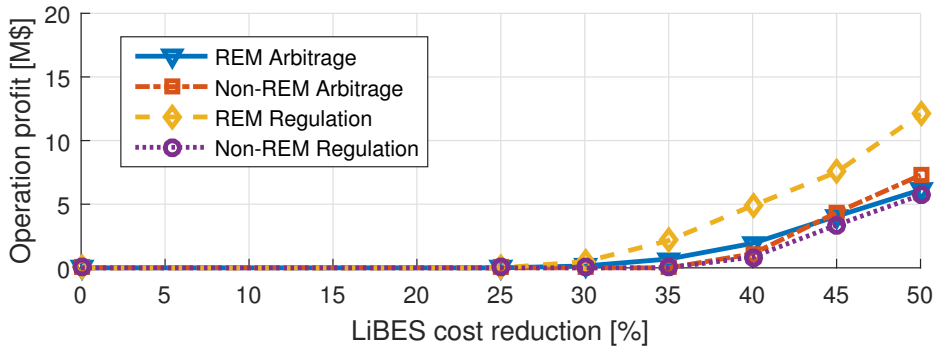

(c) Market revenue from arbitrage and regulation.

Figure 6.5: LiBES planning with decreasing investment cost.

ipates in the energy market, in *Non-REM* AA-CAES can participate energy and regulation markets under traditional regulation requirements, and in *REM* AA-CAES can participate

energy and regulation markets under REM regulation requirements.

AA-CAES Results

Fig. 6.4 shows stochastic planning results for AA-CAES. Because system-wide regulation prices are independent of the location, arbitrage is the sole factor for ES siting. Bus 155 is the optimal choice for all ES allocations, mainly due to its high occurrence of negative LMPs. In the Arb-only market scenario, AA-CAES has a P-to-E ratio of 0.11, equivalent to 9 hours of rated energy capacity. In Non-REM and REM cases, the planning results have larger installation capacities, and the P-to-E ratio also increases. The change in the regulation requirement does not have a significant impact on the planning results, and arbitrage is still the primary market income source.

LiBES Results

No LiBES is installed in any market scenarios under current investment cost as shown in Table 6.1. Since the decreasing trend of LiBES investment cost is expected to continue for the next ten years [39, 100], it is reasonable to assess the planning of LiBES using reduced investment cost. In Fig. 6.5, LiBES planning results are shown for up to 50% investment cost reduction for the Non-REM and REM market scenarios, while in the Arb-only case, no LiBES is installed. The result shows that investments in LiBES will become profitable when the investment cost dropped by at least 30% from its current value , and the installed capacity increases steadily with further cost reductions. At each cost level, the market revenue from arbitrage is roughly the same in the Non-REM and the REM case, while the regulation revenue almost doubles in REM. The difference in revenue also reflects in the installation capacity, while the installed energy capacity is similar in the REM and Non-REM cases, LiBES has a much higher P-to-E ratio with REM.

6.6.4 Computational Speed Comparison

The proposed solution algorithm is faster than solving a bi-level ES planning problem using the combination of Benders decomposition and MPEC. Nasrolahpour *et al.* [92] use the

MPEC+Benders approach to solve a bi-level ES planning problem for optimal ES sizing in a single bus system in an energy market environment. Their solution time range from 3 to 6 hours. By comparison, when our method was applied to the optimization of ES siting and sizing in a 240-bus system considering both energy and regulation markets, the longest simulation finished within one hour, and most simulations finished within 15 minutes.

6.7 Summary

In this paper, we have formulated the optimal ES profit-constrained siting and sizing as a bi-level problem with a minimum rate of return constraint. We have proposed a scalable solution method involving a primal decomposition and subgradient cutting-planes. The proposed method is significantly faster than CPLEX for solving LP ES planning problems.

The proposed solution method has the same order of complexity as conventional economic dispatch, thus making this method computationally tractable for any system with a feasible ED solution. Since the decomposed subproblems are independent of each other, the computation time increases linearly with the number of typical days considered. The solution time could be further improved by solving the subproblems in parallel.

We have analyzed the optimal ES siting in joint energy and reserve markets on a modified WECC 240-bus model. The sensitivity of these siting decisions has been studied with respect to different ES technologies, the rate of return on ES investments, and regulation market policies. The results show that increasing the rate of return requirement greatly reduces the deployment of ES. In the stochastic ES planning, AA-CAES shows a higher potential for reducing system cost than LiBES, which depends on the design of the regulation market for its profitability. However AA-CAES technology is still at the pilot stage, while grid-scale installations of LiBES are happening worldwide.

Table 6.2: Comparison of ES rate of return with a maximum ES investment cost of 50 k$/day.

Selected typical day	Day 100				Day 141				Day 285			
ES rate of return (%)	100	110	120	150	100	110	120	150	100	110	120	150
Runtime (s)	102	164	148	219	86	91	91	113	398	639	551	566
ED operation cost (M$/day)	15.83	15.84	15.85	15.86	22.87	22.87	22.87	22.91	25.19	25.20	25.20	25.20
ES operation revenue (k$/day)	27.2	13.6	10.0	0	60.0	60.0	60.0	36.4	9.2	1.9	0	0
ES investment cost (k$/day)	26.8	12.3	8.0	0	50.0	50.0	50.0	24.1	9.1	1.7	0	0
ES location (bus number)	155	155	155	n/a	155	155	155	155	228	228	n/a	n/a

Chapter 7

CONCLUSION

7.1 Conclusion

This dissertation has addressed the optimal participation of battery energy storage in electricity markets under different operation objectives, such as social welfare maximization or investment profit maximization. It presents a set of generic decision making rules and methods that incorporates the cost of battery degradation into the planning, scheduling, and dispatching stage of market participation. It utilizes varies optimization techniques to fulfill the operation requirement for different participation stages, such as computation speed, complexity, decision sequence, future uncertainty, and the scale of the problem. It guarantees the optimality and computation reliability of the proposed solutions, which have been demonstrated through mathematical proofs.

Theoretical analysis and simulation results from this dissertation have shown that the accuracy of the battery aging model used during decision processes is critical to the economic of battery energy storage investments. Through analysis on the electricity market requirements and lab test results, this thesis have concluded that the cycle aging mechanism unique to solid-state electrochemical batteries is the most critical factor for grid-scale battery energy storage, and must therefore be accurately incorporated into the decision making for battery energy storage operations.

This dissertation introduces varies mathematical programming techniques that provide optimal and scalable solutions to different market participation stages for battery energy storage. It proposes decomposition algorithm reduces the battery energy storage planning problem into solution a set of economic dispatches and the algorithm has linear complexity with respect to number of planning scenarios considered. It designs a piece-wise linear optimization model that accurately incorporates the cost of battery cycle aging into any optimization problems under tractable computation time. It derives bidding and control

policy that balances battery aging cost and performance requirement in frequency regulation markets.

This dissertation concludes that with the proposed participation methods, battery energy storage resources are becoming competitive in electricity market. It shows that the most profitable market for battery energy storage is frequency regulation markets despite the recent price drops due to market saturation. While real-time energy markets possesses vast opportunities for battery energy storage due to high price volatility, new market designs are required to effectively manage batteries' state of charge during real-time operation, and maximize the utilization of batteries' fast ramp speed against transient price spikes.

7.2 Suggestions for Future Work

7.2.1 Real-time Market Design for Energy Storage

In the current market design, energy storage units are allowed to participant in the real-time energy market as a combination of generator and a flexible demand [66]. The storage participant submits a set of hour-ahead generation offers and demand bids. The generation segment quantity is cleared if the market clearing price is higher than submitted offer price, and the demand segment quantity is cleared if the price is lower than the demand bid. The system operator will not monitor the energy storage state of charge, therefore the participant must design offers and bids considering the state of charge constrain.

This market design requires that the storage participants have accurate predictions of the future real-time market prices in order to maintain profitable operation. In detail, the participant need to predict the high and low price ranges for the next hour and submit market bids accordingly. If the participant want to have a certain end-of-operation state of charge level, then it must design market bids carefully to make sure the cleared generation and demand results lead to the desired state of charge level.

However, this market design is unfair for storage participants because it discourages them from submitting true production cost into the market, because it requires that the participant must embed an operating strategy in the market bidding strategy. A good market design should work in a way that when the market has perfect competition, the best,

i.e., most profitable, strategy for the market participants is to submit their true production cost into the market. This proposal suggests to improve the real-time market design for energy storage participation with the following criteria:

- Maintain the energy storage state of charge level during real-time dispatch. The goal is to find out the when to recharge the energy storage in real-time dispatch, which may be accomplished by adding look-ahead functions into the real-time dispatch model. However, a comprehensive look-ahead design with may not be necessary since the energy storage only needs the sufficient future information to determine whether to recharge during the current dispatch interval. In some real-time markets such as NYISO, look-ahead functions have been incorporated to schedule the real-time commitment of gas generators. It is suggested to reference similar designs and incorporate them with energy storage.

- Maximize the utilization of storage's fast ramp speed. Energy storage units are most valuable for their fast ramp speed. However because of their limited energy capacity, they cannot generate power indefinitely. Therefore in the future market design, the system operator should design market signals that help energy storage to be operated when system experiences highest disturbances. Hence, the goal is to find the periods to discharge the energy storage, which might also be accomplished by adding look-ahead into the market.

- Allow storage to submit true cost into the market. The previous two design objectives help to determine the charge and discharge schedule for energy storage in real-time markets. Energy storage participants can therefore submit their true operating cost, and the market dispatch optimization will make sure that the price difference between charge and discharge decisions can recover the energy storage's operating cost.

7.2.2 Wholesale Market Design with Aggregated Participants

Increasing distributed participants are creating huge computation burden for the wholesale market clearing software. These distributed participants include virtual bidders, energy

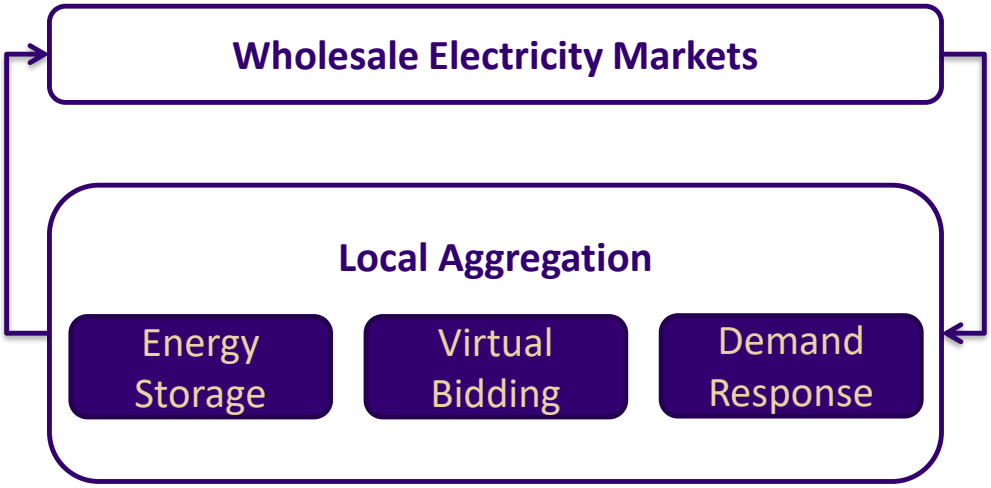

Figure 7.1: Wholesale market with local aggregation.

storage, and demand response. These resources typically submit small quantities into the market and therefore a single participant has negligible impact on the market result. However, these distributed participants may exist anywhere in the system and a single node may contain a large number of such participants, which creates huge burden on data process and computation for the market clearing.

This proposal suggests to develop an local aggregation framework to aggregate these distributed participants at the same market nodes or over several nodes between which transmission capacities in between are not constrained. This proposal covers the following criteria

- Aggregate distributed participant offer and bids for wholesale market clearing. Intuitively, bids that have the same price can be merged into a single bid. To merge bids with different prices, methods such as clustering can be considered.

- Divide the wholesale market result among aggregated participants. This is a more challenging part, especially if clustering methods are used to aggregated participant bids.

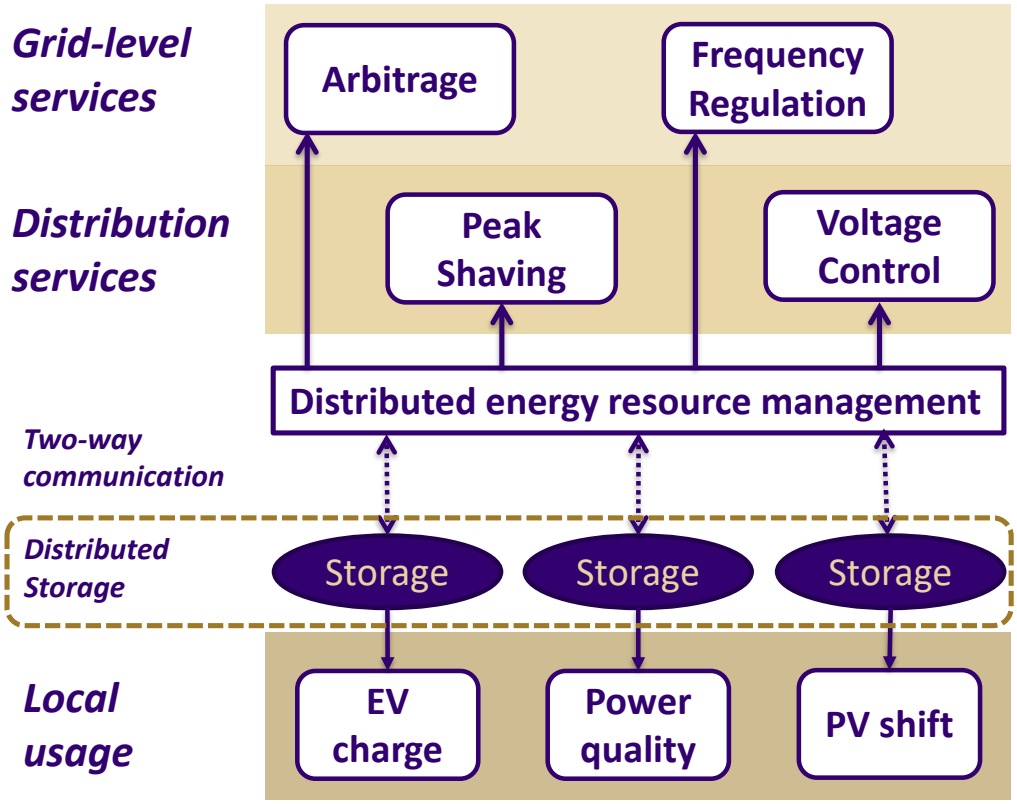

Figure 7.2: Distributed energy resource management system.

- Guaranteeing the security operation of the system. Because the power flow between aggregated resources are absent from the market calculation (such as SCUC), framework must be designed to make sure the outcome of this market design satisfies network security.

7.2.3 Distributed Energy Resource Management System

Distributed energy storage and other types of resources such as electric vehicle and PV can be utilized to assist the distribution grid operation and participant in the wholesale electricity markets. However providing these services require coordination and aggregation of different units, while maintaining individual's privacy of the local usage. Hence, a distributed energy resource management system (DERMS) is required to satisfy these objective. In detail, a DERMS should achieve the following objectives:

- Local services: each energy storage can provide local services based on the owner's interest, such services include charging (electric vehicle), power quality control, and storing excessive PV generation. The key challenge here is to maintain the user's privacy on it's local usage in DERMS, hence a distributed computation structure is of interest here.

- Distribution-level services: distributed energy storage can be coordinated to assist the distribution grid operation. These services include peak shaving, voltage control, and resilience. The challenge here is to coordinate different resources with distributed computation. Also a compensation framework should be designed for services such as voltage control. With distributed resources, the local market power of voltage control may no longer exists so there are sufficient competition for introducing a local market or a compensation framework.

- Grid-level services: distributed energy storage can be aggregated to provide grid-level services to earn extra profit for the storage owners. Such services include arbitrage, frequency regulation, or reserve. All grid-scale services have a capacity requirement, for example, energy market offer and bids must be in 100kWh increments. Hence the challenge here is to aggregated the resource to meet the discrete capacity segment requirement. Vice-verse, it may also be the case that different distributed participants compete for limited market quantities, for example, an aggregation may only qualify to provide 1MW regulation capacity in total, so all the aggregation participates must share this 1MW capacity, which is a very similar problem to channel allocation in communication.

BIBLIOGRAPHY

[1] Khalid Abdulla, Julian De Hoog, Valentin Muenzel, Frank Suits, Kent Steer, Andrew Wirth, and Saman Halgamuge. Optimal operation of energy storage systems considering forecasts and battery degradation. *IEEE Transactions on Smart Grid*, 2016.

[2] International Energy Agency. Global ev outlook 2016: Beyond one million electric cars.

[3] Sanjeev Kumar Aggarwal, Lalit Mohan Saini, and Ashwani Kumar. Electricity price forecasting in deregulated markets: A review and evaluation. *International Journal of Electrical Power & Energy Systems*, 31(1):13–22, 2009.

[4] Hossein Akhavan-Hejazi and Hamed Mohsenian-Rad. Optimal operation of independent storage systems in energy and reserve markets with high wind penetration. *IEEE Transactions on Smart Grid*, 5(2):1088–1097, 2014.

[5] Abbas A Akhil, Georgianne Huff, Aileen B Currier, Benjamin C Kaun, Dan M Rastler, Stella Bingqing Chen, Andrew L Cotter, Dale T Bradshaw, and William D Gauntlett. *DOE/EPRI 2013 electricity storage handbook in collaboration with NRECA*. Sandia National Laboratories Albuquerque, NM, 2013.

[6] JT Alt, MD Anderson, and RG Jungst. Assessment of utility side cost savings from battery energy storage. *IEEE Transactions on Power Systems*, 12(3):1112–1120, 1997.

[7] C Amzallag, JP Gerey, JL Robert, and J Bahuaud. Standardization of the rainflow counting method for fatigue analysis. *International journal of fatigue*, 16(4):287–293, 1994.

[8] Monitoring Analytics. 2016 state of the market report for pjm.

[9] Luis Baringo and Antonio J Conejo. Wind power investment: A benders decomposition approach. *IEEE Transactions on Power Systems*, 27(1):433–441, 2012.

[10] John P Barton and David G Infield. Energy storage and its use with intermittent renewable energy. *IEEE transactions on energy conversion*, 19(2):441–448, 2004.

[11] Islam Safak Bayram, Mohamed Abdallah, Ali Tajer, and Khalid A Qaraqe. A stochastic sizing approach for sharing-based energy storage applications. *IEEE Transactions on Smart Grid*, 2015.

[12] Alexandre Belloni. Introduction to bundle methods. *Lecture Notes for IAP*, 2005.

[13] D Benasciutti and R Tovo. Spectral methods for lifetime prediction under wide-band stationary random processes. *International Journal of fatigue*, 27(8):867–877, 2005.

[14] Dimitris Bertsimas, Eugene Litvinov, Xu Andy Sun, Jinye Zhao, and Tongxin Zheng. Adaptive robust optimization for the security constrained unit commitment problem. *IEEE Transactions on Power Systems*, 28(1):52–63, 2013.

[15] John R Birge. Decomposition and partitioning methods for multistage stochastic linear programs. *Operations Research*, 33(5):989–1007, 1985.

[16] Eilyan Bitar, Ram Rajagopal, Pramod Khargonekar, and Kameshwar Poolla. The role of co-located storage for wind power producers in conventional electricity markets. In *American Control Conference (ACC), 2011*, pages 3886–3891. IEEE, 2011.

[17] Black & Veatch Corporation. Cost and performance data for power generation technologies - prepared for, 2012.

[18] Theodor Borsche, Andreas Ulbig, Michael Koller, and Göran Andersson. Power and energy capacity requirements of storages providing frequency control reserves. In *IEEE PES General Meeting, Vancouver*, 2013.

[19] Stephen Boyd and Lieven Vandenberghe. *Convex optimization*. Cambridge university press, 2004.

[20] Stephen Boyd and Lieven Vandenberghe. Localization and cutting-plane methods. *From Stanford EE 364b lecture notes*, 2007.

[21] M Oloomi Buygi, H Modir Shanechi, G Balzer, and M Shahidehpour. Transmission planning approaches in restructured power systems. In *Proc. 2003 IEEE Power Tech Conf*, volume 2, page 7, 2003.

[22] Raymond H. Byrne and Cesar A. Silva-Monroy. Estimating the maximum potential revenue for grid connected electricity storage: Arbitrage and regulation. *SANDIA REPORT*, 2012.

[23] Raymond H Byrne and Cesar Augusto Silva-Monroy. Estimating the maximum potential revenue for grid connected electricity storage: Arbitrage and regulation. *Sandia National Laboratories*, 2012.

[24] CAISO. Business practice manual for market operations.

[25] CAISO. CAISO Area Control Error Data.

[26] CAISO. Non-generator resource (ngr) and regulation energy management (rem) overview.

[27] CAISO. *CAISO Annual Report on Market Issues and Performance*, 2015.

[28] CAISO. Business practice manual for settlements and billing, 2016.

[29] California ISO. Advancing and maximizing the value of energy storage technology - a california roadmap, 2014.

[30] Alejandro Castillo and Dennice F Gayme. Profit maximizing storage allocation in power grids. In *Decision and Control (CDC), 2013 IEEE 52nd Annual Conference on*, pages 429–435. IEEE, 2013.

[31] Antonio J Conejo, Enrique Castillo, Roberto Minguez, and Raquel Garcia-Bertrand. *Decomposition techniques in mathematical programming: engineering and science applications*. Springer Science & Business Media, 2006.

[32] Tiansong Cui, Yanzhi Wang, Shuang Chen, Qi Zhu, Shahin Nazarian, and Massoud Pedram. Optimal control of pevs for energy cost minimization and frequency regulation in the smart grid accounting for battery state-of-health degradation. In *Proceedings of the 52nd Annual Design Automation Conference*, page 134. ACM, 2015.

[33] Sebastián de la Torre, Antonio J Conejo, and Javier Contreras. Transmission expansion planning in electricity markets. *Power Systems, IEEE Transactions on*, 23(1):238–248, 2008.

[34] Paul Denholm and Robert Margolis. Energy storage requirements for achieving 50% solar photovoltaic energy penetration in california, 2016.

[35] Bern Dibner. *Alessandro Volta and the electric battery*. Franklin Watts, 1964.

[36] KC Divya and Jacob Østergaard. Battery energy storage technology for power systemsan overview. *Electric Power Systems Research*, 79(4):511–520, 2009.

[37] Stephen D Downing and DF Socie. Simple rainflow counting algorithms. *International journal of fatigue*, 4(1):31–40, 1982.

[38] Rodolfo Dufo-López and José L Bernal-Agustín. Multi-objective design of pv–wind–diesel–hydrogen–battery systems. *Renewable energy*, 33(12):2559–2572, 2008.

[39] Bruce Dunn, Haresh Kamath, and Jean-Marie Tarascon. Electrical energy storage for the grid: a battery of choices. *Science*, 334(6058):928–935, 2011.

[40] Krishnamurthy Dvijotham, Misha Chertkov, and Scott Backhaus. Storage sizing and placement through operational and uncertainty-aware simulations. In *2014 47th Hawaii International Conference on System Sciences*, pages 2408–2416. IEEE, 2014.

[41] Y. Dvorkin, R. Fernandez-Blanco, D. S. Kirschen, H. Pandzic, J. P. Watson, and C. A. Silva-Monroy. Ensuring profitability of energy storage. *IEEE Transactions on Power Systems*, PP(99):1–1, 2016.

[42] Y. Dvorkin, R. Fernandez-Blanco, D. S. Kirschen, H. Pandzic, J. P. Watson, and C. A. Silva-Monroy. Ensuring profitability of energy storage. *IEEE Transactions on Power Systems*, PP(99):1–1, 2016.

[43] Madeleine Ecker, Nerea Nieto, Stefan Käbitz, Johannes Schmalstieg, Holger Blanke, Alexander Warnecke, and Dirk Uwe Sauer. Calendar and cycle life study of li (nimnco) o 2-based 18650 lithium-ion batteries. *Journal of Power Sources*, 248:839–851, 2014.

[44] ISO New England. Joint filing of iso new england inc. and new england power pool to implement sub-hourly settlements; docket no. er16-1838-000.

[45] Steven D Eppinger. A planning method for integration of large-scale engineering systems. In *International Conference on Engineering Design*, pages 199–204, 1997.

[46] EUROBAT. Battery Energy Storage in the EU, 2016.

[47] ISO Express. ISO New England Pricing Reports.

[48] A Fatemi and Lianxiang Yang. Cumulative fatigue damage and life prediction theories: a survey of the state of the art for homogeneous materials. *International journal of fatigue*, 20(1):9–34, 1998.

[49] FERC. Frequency Regulation Compensation in the Organized Wholesale Power Markets , 2011.

[50] FERC. Third-Party Provision of Ancillary Services; Accounting and Financial Reporting for New Electric Storage Technologies, 2013.

[51] FERC. Electric Storage Participation in Markets Operated by Regional Transmission Organizations and Independent System Operators, 2018.

[52] R. Fernandez-Blanco, Y. Dvorkin, B. Xu, Y. Wang, and D. S. Kirschen. Optimal energy storage siting and sizing: A wecc case study. *IEEE Transactions on Sustainable Energy*, PP(99):1–1, 2016.

[53] Christodoulos A Floudas. *Nonlinear and mixed-integer optimization: fundamentals and applications*. Oxford University Press on Demand, 1995.

[54] B. Foggo and N. Yu. Improved battery storage valuation through degradation reduction. *IEEE Transactions on Smart Grid*, PP(99):1–1, 2017.

[55] Lina P Garcés, Antonio J Conejo, Raquel García-Bertrand, and Rubén Romero. A bilevel approach to transmission expansion planning within a market environment. *Power Systems, IEEE Transactions on*, 24(3):1513–1522, 2009.

[56] German Trade & Invest. The Energy Storage Market in Germany, 2016.

[57] Roderick S Go, Francisco D Munoz, and Jean-Paul Watson. Assessing the economic value of co-optimized grid-scale energy storage investments in supporting high renewable portfolio standards. *Applied Energy*, 183:902–913, 2016.

[58] BG Gorenstin, NM Campodonico, JP Costa, and MVF Pereira. Power system expansion planning under uncertainty. *IEEE Transactions on Power Systems*, 8(1):129–136, 1993.

[59] Frank Graves, Thomas Jenkin, and Dean Murphy. Opportunities for electricity storage in deregulating markets. *The Electricity Journal*, 12(8):46–56, 1999.

[60] Ioannis Hadjipaschalis, Andreas Poullikkas, and Venizelos Efthimiou. Overview of current and future energy storage technologies for electric power applications. *Renewable and sustainable energy reviews*, 13(6):1513–1522, 2009.

[61] G. He, Q. Chen, C. Kang, P. Pinson, and Q. Xia. Optimal bidding strategy of battery storage in power markets considering performance-based regulation and battery cycle life. *IEEE Transactions on Smart Grid*, 7(5):2359–2367, Sept 2016.

[62] IRC. Emerging technologies: How isos and rtos can create a more nimble, robust bulk electricity system, 2017.

[63] IRENA. Renewables and electricity storage: a technology roadmap for remap 2030, 2016.

[64] ISO New England. 2016 regional electricity outlook, 2016.

[65] ISO New England Inc. 2015 annual market report. *Internal Market Monitor*, 2016.

[66] Daniel R Jiang and Warren B Powell. Optimal hour-ahead bidding in the real-time electricity market with battery storage using approximate dynamic programming. *INFORMS Journal on Computing*, 27(3):525–543, 2015.

[67] Mohammad Kassem, Julien Bernard, Renaud Revel, Serge Pelissier, François Duclaud, and C Delacourt. Calendar aging of a graphite/lifepo 4 cell. *Journal of Power Sources*, 208:296–305, 2012.

[68] S Jalal Kazempour and Antonio J Conejo. Strategic generation investment under uncertainty via benders decomposition. *IEEE Transactions on Power Systems*, 27(1):424–432, 2012.

[69] James E Kelley, Jr. The cutting-plane method for solving convex programs. *Journal of the Society for Industrial and Applied Mathematics*, 8(4):703–712, 1960.

[70] Michael CW Kintner-Meyer, P Balducci, Chunlian Jin, T Nguyen, M Elizondo, V Viswanathan, Xinxin Guo, and F Tuffner. Energy storage for power systems applications: a regional assessment for the northwest power pool (nwpp). *PNNL-19300, Paci c Northwest National Laboratory, Richland, WA*, 2010.

[71] Krzysztof C Kiwiel. Proximity control in bundle methods for convex nondifferentiable minimization. *Mathematical programming*, 46(1-3):105–122, 1990.

[72] Michael Koller, Theodor Borsche, Andreas Ulbig, and Göran Andersson. Defining a degradation cost function for optimal control of a battery energy storage system. In *PowerTech (POWERTECH), 2013 IEEE Grenoble*, pages 1–6. IEEE, 2013.

[73] Michael Koller, Theodor Borsche, Andreas Ulbig, and Göran Andersson. Review of grid applications with the zurich 1mw battery energy storage system. *Electric Power Systems Research*, 120:128–135, 2015.

[74] Dheepak Krishnamurthy, Wanning Li, and Leigh Tesfatsion. An 8-zone test system based on iso new england data: Development and application. *IEEE Transactions on Power Systems*, 31(1):234–246, 2016.

[75] Venkat Krishnan and Trishna Das. Optimal allocation of energy storage in a co-optimized electricity market: Benefits assessment and deriving indicators for economic storage ventures. *Energy*, 81:175–188, 2015.

[76] Izaro Laresgoiti, Stefan Käbitz, Madeleine Ecker, and Dirk Uwe Sauer. Modeling mechanical degradation in lithium ion batteries during cycling: Solid electrolyte interphase fracture. *Journal of Power Sources*, 300:112–122, 2015.

[77] Juchuan Li, Alan K Dozier, Yunchao Li, Fuqian Yang, and Yang-Tse Cheng. Crack pattern formation in thin film lithium-ion battery electrodes. *Journal of The Electrochemical Society*, 158(6):A689–A694, 2011.

[78] Zhengshuo Li, Qinglai Guo, Hongbin Sun, and Jianhui Wang. Sufficient conditions for exact relaxation of complementarity constraints for storage-concerned economic dispatch. *IEEE Transactions on Power Systems*, 31(2):1653–1654, 2016.

[79] Jiaqi Liang and Ronald G Harley. Pumped storage hydro-plant models for system transient and long-term dynamic studies. In *Power and Energy Society General Meeting, 2010 IEEE*, pages 1–8. IEEE, 2010.

[80] Jeff Linderoth and Stephen Wright. Decomposition algorithms for stochastic programming on a computational grid. *Computational Optimization and Applications*, 24(2-3):207–250, 2003.

[81] Luxresearch. The next-generation battery roadmap: Quantifying how solid-state, lithium-sulfur, and other batteries will emerge after 2020.

[82] Gabriel Marsh, Colin Wignall, Philipp R Thies, Nigel Barltrop, Atilla Incecik, Vengatesan Venugopal, and Lars Johanning. Review and application of rainflow residue processing techniques for accurate fatigue damage estimation. *International Journal of Fatigue*, 82:757–765, 2016.

[83] Al McBride. Transmission interface transfer capabilities: 2014 regional system plan assumptions. In *ISO New England Planning Advisory Committee*, 2014.

[84] Pascal Mercier, Rachid Cherkaoui, and Alexandre Oudalov. Optimizing a battery energy storage system for frequency control application in an isolated power system. *IEEE Transactions on Power Systems*, 24(3):1469–1477, 2009.

[85] Alan Millner. Modeling lithium ion battery degradation in electric vehicles. In *Innovative Technologies for an E cient and Reliable Electricity Supply (CITRES), 2010 IEEE Conference on*, pages 349–356. IEEE, 2010.

[86] Milton A Miner et al. Cumulative damage in fatigue. *Journal of applied mechanics*, 12(3):159–164, 1945.

[87] Satchidananda Mishra, Michael Pecht, Ted Smith, Ian McNee, and Roger Harris. Remaining life prediction of electronic products using life consumption monitoring approach. In *Proceedings of the European Microelectronics Packaging and Interconnection Symposium, Cracow*, pages 136–142, 2002.

[88] John E Mitchell. Cutting plane methods and subgradient methods. *Tutorials in operations research*, pages 34–61, 2009.

[89] Hamed Mohsenian-Rad. Optimal bidding, scheduling, and deployment of battery systems in california day-ahead energy market. *IEEE Transactions on Power Systems*, 31(1):442–453, 2016.

[90] Valentin Muenzel, Julian de Hoog, Marcus Brazil, Arun Vishwanath, and Shivkumar Kalyanaraman. A multi-factor battery cycle life prediction methodology for optimal battery management. In *Proceedings of the 2015 ACM Sixth International Conference on Future Energy Systems*, pages 57–66. ACM, 2015.

[91] John M Mulvey and Andrzej Ruszczyński. A new scenario decomposition method for large-scale stochastic optimization. *Operations research*, 43(3):477–490, 1995.

[92] E. Nasrolahpour, S. J. Kazempour, H. Zareipour, and W. D. Rosehart. Strategic sizing of energy storage facilities in electricity markets. *IEEE Transactions on Sustainable Energy*, 7(4):1462–1472, Oct 2016.

[93] National Academies of Sciences, Engineering, and Medicine. *Analytic Research Foundations for the Next-Generation Electric Grid*. The National Academies Press, Washington, DC, 2016.

[94] National Renewable Energy Laboratory. Eastern wind dataset.

[95] Tu A Nguyen, Raymond H Byrne, Ricky J Concepcion, and Imre Gyuk. Maximizing revenue from electrical energy storage in miso energy & frequency regulation markets. In *IEEE PES General Meeting, Chicago*, 2017.

[96] Soren S Nielsen and Stavros A Zenios. Scalable parallel benders decomposition for stochastic linear programming. *Parallel Computing*, 23(8):1069–1088, 1997.

[97] North American Electric Reliability Corporation. Reliability Guideline: Operating Reserve Management, 2013.

[98] Paul WC Northrop, Venkatasailanathan Ramadesigan, Sumitava De, and Venkat R Subramanian. Coordinate transformation, orthogonal collocation, model reformulation and simulation of electrochemical-thermal behavior of lithium-ion battery stacks. *Journal of The Electrochemical Society*, 158(12):A1461–A1477, 2011.

[99] A Nottrott, J Kleissl, and B Washom. Energy dispatch schedule optimization and cost benefit analysis for grid-connected, photovoltaic-battery storage systems. *Renewable Energy*, 55:230–240, 2013.

[100] Björn Nykvist and Måns Nilsson. Rapidly falling costs of battery packs for electric vehicles. *Nature Climate Change*, 5(4):329–332, 2015.

[101] HyungSeon Oh. Optimal planning to include storage devices in power systems. *IEEE Transactions on Power Systems*, 26(3):1118–1128, 2011.

[102] Todd Olinsky-Paul. Energy storage in pjm: Wholesale market rules and requirements, 2016.

[103] GC Oliveira, APC Costa, and S Binato. Large scale transmission network planning using optimization and heuristic techniques. *Power Systems, IEEE Transactions on*, 10(4):1828–1834, 1995.

[104] Miguel A Ortega-Vazquez. Optimal scheduling of electric vehicle charging and vehicle-to-grid services at household level including battery degradation and price uncertainty. *IET Generation, Transmission & Distribution*, 8(6):1007–1016, 2014.

[105] Taku Oshima, Masaharu Kajita, and Akiyasu Okuno. Development of sodium-sulfur batteries. *International Journal of Applied Ceramic Technology*, 1(3):269–276, 2004.

[106] Alexandre Oudalov, Tilo Buehler, and Daniel Chartouni. Utility scale applications of energy storage. In *Energy 2030 Conference, 2008. ENERGY 2008. IEEE*, pages 1–7. IEEE, 2008.

[107] Alexandre Oudalov, Daniel Chartouni, and Christian Ohler. Optimizing a battery energy storage system for primary frequency control. *IEEE Transactions on Power Systems*, 22(3):1259–1266, 2007.

[108] Alexdandre Oudalov, Daniel Chartouni, Christian Ohler, and G_ Linhofer. Value analysis of battery energy storage applications in power systems. In *2006 IEEE PES Power Systems Conference and Exposition*, pages 2206–2211. IEEE, 2006.

[109] Hrvoje Pandzic, Yishen Wang, Ting Qiu, Yury Dvorkin, and Daniel S Kirschen. Near-optimal method for siting and sizing of distributed storage in a transmission network. *Power Systems, IEEE Transactions on*, 30(5):2288–2300, 2015.

[110] Hrvoje Pandžić, Yishen Wang, Ting Qiu, Yury Dvorkin, and Daniel S Kirschen. Near-optimal method for siting and sizing of distributed storage in a transmission network. *IEEE Transactions on Power Systems*, 30(5):2288–2300, 2015.

[111] Anthony Papavasiliou, Shmuel S Oren, and Richard P O'Neill. Reserve requirements for wind power integration: A scenario-based stochastic programming framework. *Power Systems, IEEE Transactions on*, 26(4):2197–2206, 2011.

[112] B Pitt. Applications of data mining techniques to electric load profiling. *University of Manchester*, 2000.

[113] PJM. Pjm manual 12: Balancing operations.

[114] PJM. PJM Regulation Signal and Requirement Update.

[115] PJM. PJMRegulation Market Issues Senior Task Force.

[116] David Pozo, Javier Contreras, and Enzo E Sauma. Unit commitment with ideal and generic energy storage units. *IEEE Transactions on Power Systems*, 29(6):2974–2984, 2014.

[117] James E Price and John Goodin. Reduced network modeling of wecc as a market design prototype. In *Power and Energy Society General Meeting, 2011 IEEE*, pages 1–6. IEEE, 2011.

[118] Danny Pudjianto, Marko Aunedi, Predrag Djapic, and Goran Strbac. Whole-systems assessment of the value of energy storage in low-carbon electricity systems. *IEEE Transactions on Smart Grid*, 5(2):1098–1109, 2014.

[119] T. Qiu, B. Xu, Y. Wang, Y. Dvorkin, and D. Kirschen. Stochastic multi-stage coplanning of transmission expansion and energy storage. *IEEE Transactions on Power Systems*, PP(99):1–1, 2016.

[120] Jay Apta Rahul Walawalkar and Rick Mancinib. Economics of electric energy storage for energy arbitrage and regulation in new york. *Carnegie Mellon Electricity Industry Center Working Paper*, 2007.

[121] Venkatasailanathan Ramadesigan, Paul WC Northrop, Sumitava De, Shriram Santhanagopalan, Richard D Braatz, and Venkat R Subramanian. Modeling and simulation of lithium-ion batteries from a systems engineering perspective. *Journal of The Electrochemical Society*, 159(3):R31–R45, 2012.

[122] Cyrus Reed. Update on storage issues in ercot: Moving forward?, 2016.

[123] Richard E. Rosenthal. *GAMS A Users Guide*, 2016.

[124] Paul Ruetschi. Aging mechanisms and service life of lead–acid batteries. *Journal of Power Sources*, 127(1):33–44, 2004.

[125] Igor Rychlik. A new definition of the rainflow cycle counting method. *International journal of fatigue*, 9(2):119–121, 1987.

[126] Igor Rychlik. Extremes, rainflow cycles and damage functionals in continuous random processes. *Stochastic processes and their applications*, 63(1):97–116, 1996.

[127] Hadi Saadat. *Power system analysis*. WCB/McGraw-Hill, 1999.

[128] Mushfiqur Sarker. *Electric Vehicles as Grid Resources*. PhD thesis, University of Washington, 2016.

[129] Susan M Schoenung and William V Hassenzahl. Long-vs. short-term energy storage technologies analysis. a life-cycle cost study. a study for the doe energy storage systems program. *Sandia National Laboratories*, 2003.

[130] Fernando De Samaniego Steta. Modeling of an advanced adiabatic compressed air energy storage (aa-caes) unit and an optimal model-based operation strategy for its integration into power markets. *EEH Power Systems Laboratory Swiss Federal Institute of Technology (ETH)*, 2010.

[131] Daniel-Ioan Stroe, Maciej Swierczynski, Ana-Irina Stroe, Rasmus Laerke, Philip Carne Kjaer, and Remus Teodorescu. Degradation behavior of lithium-ion batteries based on lifetime models and field measured frequency regulation mission profile. *IEEE Transactions on Industry Applications*, 52(6):5009–5018, 2016.

[132] Daniel-Ioan Stroe, Maciej Swierczynski, Ana-Irina Stroe, Remus Teodorescu, Rasmus Laerke, and Philip Carne Kjaer. Degradation behaviour of lithium-ion batteries based on field measured frequency regulation mission profile. In *Energy Conversion Congress and Exposition (ECCE), 2015 IEEE*, pages 14–21. IEEE, 2015.

[133] Maciej Swierczynski, Daniel Ioan Stroe, Ana-Irina Stan, Remus Teodorescu, and Dirk Uwe Sauer. Selection and performance-degradation modeling of $LiMO_2/Li_4Ti_5O_{12}$ and $LiFePO_4/C$ battery cells as suitable energy storage systems for grid integration with wind power plants: an example for the primary frequency regulation service. *IEEE transactions on Sustainable Energy*, 5(1):90–101, 2014.

[134] Choon Hui Teo, SVN Vishwanthan, Alex J Smola, and Quoc V Le. Bundle methods for regularized risk minimization. *The Journal of Machine Learning Research*, 11:311–365, 2010.

[135] Duong Tran and Ashwin M Khambadkone. Energy management for lifetime extension of energy storage system in micro-grid applications. *IEEE Transactions on Smart Grid*, 4(3):1289–1296, 2013.

[136] J Vetter, P Novák, MR Wagner, C Veit, K-C Möller, JO Besenhard, M Winter, M Wohlfahrt-Mehrens, C Vogler, and A Hammouche. Ageing mechanisms in lithium-ion batteries. *Journal of power sources*, 147(1):269–281, 2005.

[137] Rahul Walawalkar, Jay Apt, and Rick Mancini. Economics of electric energy storage for energy arbitrage and regulation in new york. *Energy Policy*, 35(4):2558–2568, 2007.

[138] John Wang, Ping Liu, Jocelyn Hicks-Garner, Elena Sherman, Souren Soukiazian, Mark Verbrugge, Harshad Tataria, James Musser, and Peter Finamore. Cycle-life model for graphite-lifepo 4 cells. *Journal of Power Sources*, 196(8):3942–3948, 2011.

[139] John Wang, Justin Purewal, Ping Liu, Jocelyn Hicks-Garner, Souren Soukazian, Elena Sherman, Adam Sorenson, Luan Vu, Harshad Tataria, and Mark W Verbrugge. Degradation of lithium ion batteries employing graphite negatives and nickel–cobalt–manganese oxide+ spinel manganese oxide positives: Part 1, aging mechanisms and life estimation. *Journal of Power Sources*, 269:937–948, 2014.

[140] Y. Wang, Y. Dvorkin, R. Fernandez-Blanco, B. Xu, T. Qiu, and D. Kirschen. Look-ahead bidding strategy for energy storage. *IEEE Transactions on Sustainable Energy*, PP(99):1–1, 2017.

[141] D. Watson, C. Hastie, and M. Rodgers. Comparing different regulation offerings from a battery in a wind r d park. *IEEE Transactions on Power Systems*, PP(99):1–1, 2017.

[142] Corey D White and K Max Zhang. Using vehicle-to-grid technology for frequency regulation and peak-load reduction. *Journal of Power Sources*, 196(8):3972–3980, 2011.

[143] Wayne L Winston and Jeffrey B Goldberg. *Operations research: applications and algorithms*, volume 3. Duxbury press Boston, 2004.

[144] Sonja Wogrin and Dennice F Gayme. Optimizing storage siting, sizing, and technology portfolios in transmission-constrained networks. *Power Systems, IEEE Transactions on*, 30(6):3304–3313, 2015.

[145] Allen J Wood and Bruce F Wollenberg. *Power generation, operation, and control*. John Wiley & Sons, 2012.

[146] B. Xu, A. Oudalov, A. Ulbig, G. Andersson, and D. Kirschen. Modeling of lithium-ion battery degradation for cell life assessment. *IEEE Transactions on Smart Grid*, PP(99):1–1, 2016.

[147] Bolun Xu, Yury Dvorkin, Daniel S Kirschen, CA Silva-Monroy, and Jean-Paul Watson. A comparison of policies on the participation of storage in us frequency regulation markets. *PES Genreal Meeting*, 2016.

[148] Bolun Xu, Alexandre Oudalov, Jan Poland, Andreas Ulbig, and Göran Andersson. Bess control strategies for participating in grid frequency regulation. In *19th IFAC World Congress, Cape Town*, 2014.

[149] Fengqi You and Ignacio E Grossmann. Multicut benders decomposition algorithm for process supply chain planning under uncertainty. *Annals of Operations Research*, 210(1):191–211, 2013.

[150] Behnam Zakeri and Sanna Syri. Electrical energy storage systems: A comparative life cycle cost analysis. *Renewable and Sustainable Energy Reviews*, 42:569–596, 2015.

[151] Hongcai Zhang, Zechun Hu, Eric Munsing, Scott J Moura, and Yonghua Song. Data-driven chance-constrained regulation capacity offering for distributed energy resources. *arXiv preprint arXiv:1708.05114*, 2017.

[152] Ying Jun Zhang, Changhong Zhao, Wanrong Tang, and Steven H Low. Profit maximizing planning and control of battery energy storage systems for primary frequency control. *IEEE Transactions on Smart Grid*, 2016.

[153] Feng Zhao, Eugene Litvinov, and Tongxin Zheng. A marginal equivalent decomposition method and its application to multi-area optimal power flow problems. *IEEE Transactions on Power Systems*, 1(29):53–61, 2014.

Appendix A

SUPPLEMENTARY MATERIAL TO CHAPTER 3

A.1 Model Reformulation

We rewrite problem (4.5) when $\quad \geq 0, \quad \geq 0$ as

$$(\mathbf{c}\ ;\mathbf{d}\ ) \in \arg\min_{\mathbf{c};\mathbf{d}} J_{\mathsf{cyc}}(\mathbf{c};\mathbf{d}) - T \sum_{n=1}^{N} \quad c_n + \quad d_n \tag{A.1a}$$

subject to (3.1), (3.2), and

$$0 \leq c_n \leq [r_n]^+ \tag{A.1b}$$

$$0 \leq d_n \leq [-r_n]^+ \tag{A.1c}$$

by observing that a battery's actions would never exceed the regulation signals.

We utilize the rainflow algorithm to transform the problem into a cycle-based form. The rainflow method maps the entire operation uniquely to cycles, the sum of all charge and discharge power can be represented as the sum of cycle depths as (recall that a full cycle has symmetric depth for charge and discharge)

$$\sum_{i=1}^{j\mathbf{u}j} u_i + \sum_{i=1}^{j\mathbf{v}j} v_i = \frac{T_{\mathsf{c}}}{E} \sum_{n=1}^{N} c_n \tag{A.2}$$

$$\sum_{i=1}^{j\mathbf{u}j} u_j + \sum_{i=1}^{j\mathbf{w}j} w_i = \frac{T}{\mathsf{d}E} \sum_{n=1}^{N} d_n : \tag{A.3}$$

We substitute (A.2) and (A.3) into the reformulated objective function (A.1a) to replace c_n and d_n with cycle depths

$$J_{\mathsf{cyc}}(\mathbf{c};\mathbf{d}) + J_{\mathsf{reg}}(\mathbf{c};\mathbf{d};\mathbf{r}) = \sum_{i=1}^{j\mathbf{u}j} J_{\mathsf{u}}(u_i) + \sum_{i=1}^{j\mathbf{v}j} J_{\mathsf{v}}(v_i) + \sum_{i=1}^{j\mathbf{w}j} J_{\mathsf{w}}(w_i) : \tag{A.4}$$

A.2 Proof for Theorem 2

The following lemmas support the proof for Theorem 2

Lemma 2. *Assume a minimizer* $(\mathbf{c}\ ;\mathbf{d}\ )$ *to problem* (4.5) *has the cycle counting results* $(\mathbf{u}\ ;\mathbf{v}\ ;\mathbf{w}\ )$*. Then the depth of each cycle in this result either reaches the optimal cycle depth or bounded by the operation constraints* (3.2), (A.1b), (A.1c) *as*

$$u_i = \min(\hat{u}; \overline{u}_i) \tag{A.5a}$$

$$v_i = \min(\hat{v}; \overline{v}_i) \tag{A.5b}$$

$$w_i = \min(\hat{w}; \overline{w}_i) \tag{A.5c}$$

where $\overline{u}_i$, $\overline{v}_i$, $\overline{w}_i$ *denote constraint bounds.*

Lemma 3. *A cycle depth in the control action of* $g(\cdot)$ *either reaches the depth of* $\hat{u}$ *or is bounded by the operation constraints.*

Lemma 4. *There exists one and only one half cycle with the largest depth in a rain ow residue pro le. Other half cycles are in strictly decreasing order either to the left- or to the right-hand side direction of this largest half cycle.*

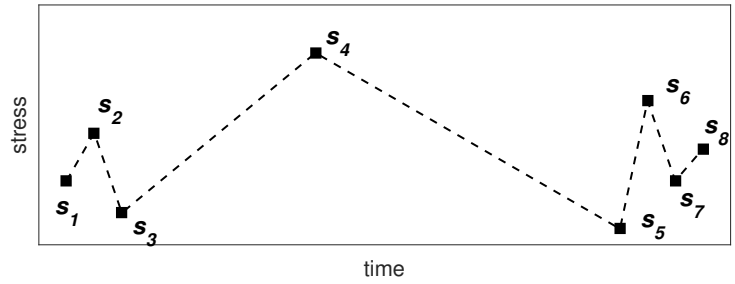

Figure A.1: Illustration for Lemma 4. The largest half cycle is between s_4 and s_5, other half cycles are in strictly decreasing order either to the left- or to the right-hand side direction of this largest half cycle.

It is easy to see now from Lemma 2 and Lemma 3 that the proposed control policy achieves optimal control result for all full cycles, and the optimality gap is caused by half cycle results. Consider the following relationship in a rainflow residue profile as in Lemma 4 assuming the largest half cycle is in the discharging direction

$$\cdots < w_{j-1} < v_{j-1} < w_j > v_j > w_{j+1} > \cdots \tag{A.6}$$

and substitute Lemma 3 into (A.6)

$$\cdots \min\{\hat{v}; \overline{v}_j\} < \min\{\hat{w}; \overline{w}_j\} > \min\{\hat{v}; \overline{v}_{j+1}\} \cdots \tag{A.7}$$

It is easy to see now that if $\hat{w} > \hat{v}$, then the largest possible value for w_j is $\hat{w}$, and the largest possible value for v_j and v_{j-1} is $\hat{v}$, the rest half cycles in (A.6) must have depths smaller than $\hat{v}$, which indicates that their depths are bounded by operation. If $\hat{v} > \hat{w}$, then the largest possible value for w_j is $\hat{w}$, and the rest half cycles must have depths smaller than $\hat{w}$. We repeat this analysis for cases that v_j is the largest cycle, and summarize the half cycle conditions in Table A.1 Hence, the worst-case optimality gap is caused by that

Table A.1: Summarizing Half Cycle Depth Conditions

	$\hat{w} > \hat{v}$	$\hat{w} < \hat{v}$
Half cycles of depth $\hat{w}$	At most one	At most two
Half cycles of depth $\hat{v}$	At most two	At most one
Rest half cycles	must be $< \hat{v}$	must be $< \hat{w}$

some half cycles have depth $\hat{u}$ or $\hat{w}$, while the control policy enforces $\hat{u}$ as the depth of all cycles unbounded by operation. The gap in Theorem 2 is therefore calculated using half cycle depth conditions in Table A.1.

Proof for Lemma 2: This property is trivial because cycles are linear combinations of charge and discharge power, and constraints (3.2), (A.1b), (A.1c) can be transformed into linear constrains with respect to cycle depths. Hence the transformed cycle-based problem also has a convex objective function with linear constraints. Although exact formulations of the transformed constraints are complicated to express, we use $\overline{u}_i$, $\overline{v}_i$, and $\overline{w}_i$ to denote these binds, which are sufficient for the proof for Theorem 2.

Proof for Lemma 3: The rainflow method always identify the largest cycle as between the minimum and the maximum SoC point. In the proposed policy, any operation that goes outside the defined operation zone will cause the largest cycle depth to change instead of

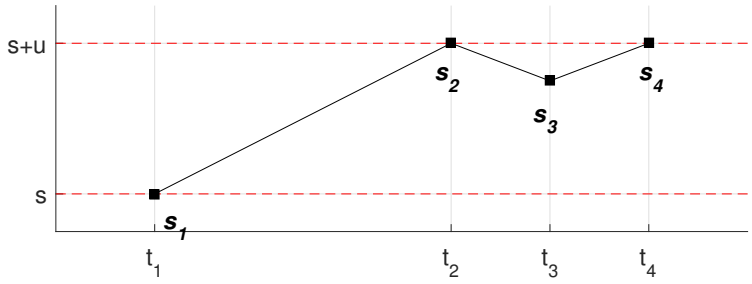

Figure A.2: Illustration for Lemma 3.

the depth of the cycle it was previous in. For example, in Fig. A.2 the maximum cycle is between SoC s and $s+u$, and the battery is at time t_4. If the battery continue to charge and the SoC goes about $s+u$, then this operation will increase the largest cycle depth instead of the shallower cycles assoicated with extrema s_2, s_3 and s_4.

Proof for Lemma 4: Because the rainflow method identifies a cycle from extrema distances if $\Delta s_{i\ 1} \geq \Delta s_i \leq \Delta s_{i+1}$, then all extrema in the rainflow residue must satisfy either $\Delta s_{i\ 1} < \Delta s_i < s_{i+1}$ or $\Delta s_{i\ 1} < \Delta s_i > s_{i+1}$ or $\Delta s_{i\ 1} > \Delta s_i > s_{i+1}$, which proofs this lemma.

Appendix B

SUPPLEMENTARY MATERIAL TO CHAPTER 6

B.1 Proof for Theorem 3

Following the proposed control policy in Algorithm 1. we can rewrite the penalty function as

$$||Cr - b^g||_1 = C||r||_1 - ||b^g||_1 \tag{B.1}$$

because $|b_t| \leq |Cr_t|$ and b_t always has the same sign as r_t. It follows that

$$\begin{aligned} \frac{@J(g;C)}{@C} &= -\mathsf{E}\left[\frac{}{r}||r||_1\right] \\ &= -\frac{\mathsf{E}\ ||r||_1}{r} \\ &= (1- \ ) \quad \geq 0 \end{aligned} \tag{B.2}$$

because $_r = \mathsf{E}\ ||r||_1$ and $\in [0;1]$ and ≥ 0. Since $\frac{@J(g;C)}{@C} \geq 0$, the frequency regulation profit $@J(g;C)$ grows as the bidding capacity C increases. Therefore, the optimal regulation capacity C is equal to maximum possible capacity bidding, which is the BES power rating B. Theorem 3 is hence proved.

B.2 PJM Performance Index Simplification

PJM penalizes the entire regulation payment with the performance index, which is calculated with equal weights on precision, correlation, and delay [113]:

$$\begin{aligned} &\text{PerformanceIndex} = \\ &\frac{1}{3}\ \text{PrecisionScore} + \text{CorrelationScore} + \text{DelayScore} \end{aligned} \tag{B.3}$$

while all scores are valued between 0 to 1. The precision score is the absolute error of the regulation response as

$$\text{Precision} = 1 - \frac{||Cr - b||_1}{||Cr||_1} \tag{B.4}$$

The delay score is evaluated over the delay under which the time-shifted BES response achieves the highest correlation with the regulation instruction, and this correlation coefficient is the correlation score. Because BES responses to dispatch commands instantaneously, the response profile always achieves highest correlation with the instruction at zero delay, hence the BES always has full delay score. However considering the difficulty of incorporating correlation index calculation into a convex programming problem, we approximate the correlation score to be the same as the precision score. The PJM performance index calculation is therefore simplified to

$$\begin{aligned} \text{PerformanceIndex} &= \frac{1}{3}\ \ 2 - 2\frac{||\boldsymbol{C}\boldsymbol{r} - \boldsymbol{b}||_1}{||\boldsymbol{C}\boldsymbol{r}||_1} + 1 \\ &= 1 - \frac{2}{3}\frac{||\boldsymbol{C}\boldsymbol{r} - \boldsymbol{b}||_1}{||\boldsymbol{C}\boldsymbol{r}||_1} \end{aligned} \tag{B.5}$$

which is the same as setting $\quad = 2/3$ in (4.1).

Appendix C

SUPPLEMENTARY MATERIAL TO CHAPTER 5

In this appendix we prove that the proposed piecewise linear model of the battery cycle aging cost is a close approximation of the benchmark rainflow-based battery cycle aging model, and that the accuracy of the model increases with the number of linearization segments. *The proposed model produces the same aging cost as to the benchmark aging model for the same battery operation pro le with an adequate number of linearization segments.* To prove this, we first explicitly characterize the cycle aging cost result calculated using the proposed model (Theorem 1). We then show that this cost approaches the benchmark result when the number of linearization segments approaches infinity (Theorem 2).

We consider the operation of a battery over the period $\mathcal{T} = \{1; 2; \dots; T\}$, the physical battery operation constraints are $(\forall t \in \mathcal{T})$

$$d_t \leq D(1 - v_t) \tag{C.1}$$

$$g_t \leq G v_t \tag{C.2}$$

$$e_t - e_{t\ 1} = M(d_t^{\ \mathrm{ch}} - g_t^{\ \mathrm{dis}}) \tag{C.3}$$

We denote $\mathbf{d} = \{d_1; d_2; \dots; d_T\}$ as the set of all battery charge powers, and $\mathbf{g} = \{g_1; g_2; \dots; g_T\}$ as the set of all discharge powers. Hence, a set in the form of $(\mathbf{d}; \mathbf{g})$ is sufficient to describe the dispatch of a battery over $\mathcal{T}$. Let $\mathcal{P}(e_0)$ denote the set of all feasible battery dispatches that satisfy the physical battery operation constraints (C.1)–(C.3) given an battery initial energy level e_0.

Since we are only interested in characterizing the aging cost calculated by the proposed model for a certain battery operation profile, we will regard the battery operation profile as known variables in this proof. It is easy to see that once the dispatch profile $(\mathbf{d}; \mathbf{g})$ is determined, any battery dispatch problem that involves the proposed model with a linearization segment set $\mathcal{J} = \{1; 2; \dots; J\}$, such as the one formulated in Section 5.4, can be reduced to

the following problem if we neglect any operation prior to the operation interval $\mathcal{T}$

$$\hat{\mathbf{p}} \in \arg\min_{\mathbf{p} \in \mathbb{R}^+} \sum_{t=1}^{T} \sum_{j=1}^{J} M c_j p_{t;j}^{\text{dis}}; \tag{C.4}$$

s.t.

$$d_t = \sum_{j=1}^{J} p_{t;j}^{\text{ch}} \tag{C.5}$$

$$g_t = \sum_{j=1}^{J} p_{t;j}^{\text{dis}} \tag{C.6}$$

$$e_{t;j} - e_{t-1;j} = M(p_{t;j}^{\text{ch}} \eta^{\text{ch}} - p_{t;j}^{\text{dis}} / \eta^{\text{dis}}) \tag{C.7}$$

$$0 \leq e_{t;j} \leq \bar{e}_j \tag{C.8}$$

$$\sum_{j=1}^{J} e_{0;j} = e_0 \tag{C.9}$$

where $(\mathbf{d}; \mathbf{g}) \in \mathcal{P}(e_0)$ is a feasible battery dispatch set, and $\mathbf{p} = \{p_{t;j}^{\text{ch}}; p_{t;j}^{\text{dis}} | t \in \mathcal{T}; j \in \mathcal{J}\}$ denotes a set of the battery charge and discharge powers for all segments during all dispatch intervals. Although the objective is still cost minimization, the problem in (C.4)–(C.9) does not optimize battery dispatch, instead it simulates cycle operations $\mathbf{p}$ and calculates the cycle aging cost with respect to a dispatch profile $(\mathbf{d}; \mathbf{g})$. Hence, the evaluation criteria to this problem is its accuracy compared to the benchmark aging cost model.

Let $\mathbf{c} = \{c_j | j \in \mathcal{J}\}$ denote a set of piecewise linear battery aging cost segments derived as in equation (5.3), so that c_j is associated with the cycle depth range $[(j-1)/J; j/J)$ and $J = |\mathcal{J}|$ is the number of segments. We say that a battery has a *convex* aging cost curve (i.e., non-decreasing marginal cycle aging cost) if a *shallower* cycle depth segment (i.e., indexed with smaller j) is associated with a *cheaper* marginal aging cost such that $c_1 \leq c_2 \leq \cdots \leq c_J$, and let $\mathcal{C}$ denote the set of all convex battery aging cost linearizations.

Theorem 4. *Let* $\hat{\mathbf{p}} = \{\hat{p}_{t;j}^{\text{ch}}; \hat{p}_{t;j}^{\text{dis}} | t \in \mathcal{T}; j \in \mathcal{J}\}$ *and*

$$\hat{p}_{t;j}^{\text{ch}} = \min\ d_t - \sum_{=1}^{j-1} \hat{p}_{t;}^{\text{ch}};\ (\bar{e}_j - \hat{e}_{t-1;j})/(\eta^{\text{ch}} M) \tag{C.10}$$

$$\hat{p}_{t;j}^{\text{dis}} = \min\ g_t - \sum_{=1}^{j-1} \hat{p}_{t;}^{\text{dis}};\ \eta^{\text{dis}} \hat{e}_{t-1;j}/M \tag{C.11}$$

$$\hat{e}_{0;j} = \min\ \bar{e}_j; \max(0; e_0 - \sum_{=1}^{j-1} \hat{e}_{0;}) \tag{C.12}$$

$$\hat{e}_{t;j} = \hat{e}_{t-1;j} + M(p_{t;j}^{\text{ch}} \eta^{\text{ch}} - p_{t;j}^{\text{dis}} / \eta^{\text{dis}}). \tag{C.13}$$

Then $\hat{\mathbf{p}}$ *is a minimizer of the problem* (C.4)–(C.9) *as long as the battery dispatch is feasible*

and the cycle aging cost curve is convex, i.e.,

$$\hat{\mathbf{p}} \in \arg\min_{\mathbf{p} \in \mathbb{R}^+} \ (\text{C.4}) \{ (\text{C.9}); \\ \forall (\mathbf{d}; \mathbf{g}) \in \mathcal{P}(e_0),\ e_0 \in [E^{\min}; E^{\max}],\ \mathbf{c} \in \mathcal{C}: \tag{C.14}$$

Proof. Equations (C.10)–(C.13) describe a battery operating policy over the proposed piecewise linear model. To calculate this policy, we start from (C.12) which calculates the initial segment energy level from the battery initial SoC e_0. (C.12) is evaluated in the order of $j = 0; 1; 2; 3; \dots; J$ such as (note that $\sum_{=1}^{0} \hat{e}_{0;} = 0$)

$$\begin{aligned} \hat{e}_{0;1} &= \min\ \bar{e}_1; \max(0; e_0) \\ \hat{e}_{0;2} &= \min\ \bar{e}_2; \max(0; e_0 - \hat{e}_{0;1}) \\ \hat{e}_{0;3} &= \min\ \bar{e}_3; \max(0; e_0 - \hat{e}_{0;1} - \hat{e}_{0;2}) \\ &\dots; \end{aligned}$$

so that energy in e_0 is first assigned to $\hat{e}_{0;1}$ which corresponds to the shallowest cycle depth range $[0; 1=J]$, the remaining energy is then assigned to the second shallowest segment $\hat{e}_{0;2}$, and the procedure repeats until all the energy in e_0 has been assigned.

We then calculate all battery segment charge power at $t = 1$ in the order of $j = 0; 1; 2; 3; \dots; J$ as

$$\begin{aligned} \hat{p}^{\text{ch}}_{1;1} &= \min\ d_t;\ (\bar{e}_1 - \hat{e}_{0;1}) = (\ ^{\text{ch}}M) \\ \hat{p}^{\text{ch}}_{1;2} &= \min\ d_t - \hat{p}^{\text{ch}}_{1;1};\ (\bar{e}_2 - \hat{e}_{0;2}) = (\ ^{\text{ch}}M) \\ \hat{p}^{\text{ch}}_{1;3} &= \min\ d_t - \hat{p}^{\text{ch}}_{1;1} - \hat{p}^{\text{ch}}_{1;2};\ (\bar{e}_3 - \hat{e}_{0;3}) = (\ ^{\text{ch}}M) \\ &\dots; \end{aligned}$$

and the procedure is similar for segment discharge power $\hat{p}^{\text{dis}}_{1;j}$. We calculate the segment energy level $\hat{e}_{1;j}$ at the end of $t = 1$ using (C.13), and move the calculation to $t = 2$. This procedure repeats until all values in $\hat{\mathbf{p}}$ have been calculated. Therefore in this policy, the battery always prioritizes energy in shallower segments for charge or discharge dispatch. For example, if the battery is required to discharge a certain amount of energy, it will first

dispatch segment 1, then the remaining discharge requirement (if any) is dispatched from segment 2, then segment 3, etc.

Given this policy, this theorem stands if the battery cycle aging cost curve $\mathbf{c}$ is convex, i.e., $\mathbf{c} \in \mathcal{C}$, which means a shallower segment is associated with a cheaper marginal operating cost. Since the objective function (C.4) is to minimize the battery aging cost and the problem involves no market price, then a minimizer for the problem (C.4)–(C.9) will give a cheaper segment a higher operation priority, which is equivalent to the policy described in (C.10)–(C.13). □

Following Theorem 1, the cycle aging cost calculated by the proposed piecewise linear model C^{pwl} for a battery dispatch profile $(\mathbf{d}; \mathbf{g})$ can be written as a function of this profile and the linearization cost set as

$$C^{\mathsf{pwl}}(\mathbf{c}; \mathbf{d}; \mathbf{g}) = \sum_{t=1}^{T} \sum_{j=1}^{J} M c_j \hat{p}_{t;j}^{\mathsf{dis}}; \tag{C.15}$$

where $\hat{\mathbf{p}}$ is calculated as in (C.10)–(C.13).

Let $\Phi(\ )$ be a convex battery cycle aging stress function, and $\mathbf{c}(\Phi)$ be a set of piecewise linearizations of $\Phi(\ )$ determined using the method described in equation (5.3). Let $|\mathbf{c}(\Phi)|$ denote the cardinality of $\mathbf{c}(\Phi)$, i.e. the number of segments in this piecewise linearization.

For a feasible battery dispatch profile $(\mathbf{d}; \mathbf{g}) \in \mathcal{P}(e_0)$, let Δ be the set of all full cycles identified from this operation profile using the rainflow method, Δ^{dis} for all discharge half cycles, and Δ^{ch} for all charge half cycles. The benchmark cycle aging cost C^{ben} resulting from $(\mathbf{d}; \mathbf{g})$ can be written as a function of the profile and the cycle aging function Φ (recall that a full cycle has symmetric depths for charge and discharge)

$$C^{\mathsf{ben}}(\Phi; \mathbf{d}; \mathbf{g}) = R \sum_{i=1}^{j} \Phi(\ _i) + R \sum_{i=1}^{^{\mathsf{dis}}j} \Phi(\ _i^{\mathsf{dis}}): \tag{C.16}$$

Theorem 5. *When the number of linearization segments approaches in nity, the proposed piecewise linear cost model yields the same result as the benchmark rain ow-based cost model:*

$$\lim_{j\mathbf{c}(\ )j\ !\ 1} C^{\mathsf{pwl}}\ \mathbf{c}(\Phi); \mathbf{d}; \mathbf{g}\ = C^{\mathsf{ben}}\ \Phi; \mathbf{d}; \mathbf{g}\ : \tag{C.17}$$

Proof. First we rewrite equation (C.15) as

$$\sum_{j=1}^{J} c_j \sum_{t=1}^{T} M \hat{p}_{t;j}^{\mathsf{dis}} = \sum_{j=1}^{J} c_j \Theta_j; \tag{C.18}$$

where $\Theta_j = \sum_{t=1}^{T} M \hat{p}_{t;j}^{\text{dis}}$ is the total amount of energy discharged at a cycle depth range between $(j-1)/J$ and j/J. Once the number of segments $|\mathbf{c}(\Phi)| = J$ approaches infinity, we can rewrite Θ_j into a function $\Theta(\ )$ indicating the energy discharged at a specific cycle depth $\ $, where $\ \in [0\ 1]$. With an infinite number of segments, we substitute (5.2) in and rewrite the cycle aging function in (C.15) in a continuous form

$$C^{\text{pwl}}(\Phi; \mathbf{d}; \mathbf{g}) = \int_0^1 \frac{R}{{}^{\text{dis}}E^{\text{rate}}} \Theta(\ ) \frac{d\Phi(\ )}{d} d\ \ : \tag{C.19}$$

We define a new function $N_T^{\text{dis}}(\ )$ the number of discharge cycles of depths equal or greater than $\ $ during the operation period from $t = 0$ to $t = T$, accounting all discharge half cycles and the discharge stage of all full cycles. $N_T^{\text{dis}}(\ )$ can be calculated by normalizing $\Theta(\ )$ with the discharge efficiency and the energy rating of the battery

$$N_T^{\text{dis}}(\ ) = \frac{1}{{}^{\text{dis}}E^{\text{rate}}} \Theta(\ ); \tag{C.20}$$

recall that $\Theta(\ )$ is the amount of energy discharged from the cycle depth $\ $. This relationship is proved in Lemma 1 after this theorem.

Now the proposed cost function becomes

$$C^{\text{pwl}}(\Phi; \mathbf{d}; \mathbf{g}) = R \int_0^1 \frac{d\Phi(\ )}{d} N_T^{\text{dis}}(\ ) d\ \ ; \tag{C.21}$$

which is a standard formulation for calculating rainflow fatigue damage [126], and the function $N_T^{\text{dis}}(\ )$ is an alternative way of representing a rainflow cycle counting result. We substitute (C.24) from Lemma 1 into (C.21)

$$\begin{aligned}
&C^{\text{pwl}}(\Phi; \mathbf{d}; \mathbf{g}) \\
&= R \int_0^1 \frac{d\Phi(\ )}{d} \left(\sum_{i=1}^{j_{X^j}} 1_{[\ \ \ _i]} + \sum_{i=1}^{j_{X^{\text{dis}j}}} 1_{[\ \ \ _i^{\text{dis}}]} \right) d \\
&= R \sum_{i=1}^{j_{X^j}} \int_0^1 \frac{d\Phi(\ )}{d} 1_{[\ \ \ _i]} d\ + R \sum_{i=1}^{j_{X^{\text{dis}j}}} \int_0^1 \frac{d\Phi(\ )}{d} 1_{[\ \ \ _i^{\text{dis}}]} d \\
&= R \sum_{i=1}^{j_{X^j}} \Phi(\ _i) + R \sum_{i=1}^{j_{X^{\text{dis}j}}} \Phi(\ _i^{\text{dis}}) \\
&= C^{\text{ben}}(\Phi; \mathbf{d}; \mathbf{g}); \qquad \text{(C.22)}
\end{aligned}$$

then it is trivial to see that this theorem stands if the proposed model yields the same counting result $N_T^{\text{dis}}(\ )$ as the rainflow algorithm. This relationship is proved in Lemma 1. □

Lemma 5. *We assume that the proposed model has an in nite number of segments, then $N_T^{\text{dis}}(\ )$, as de ned in Theorem 2, is the number of discharge cycles of depths equal or greater than during the operation period from $t = 0$ to $t = T$, accounting all discharge half cycles and the discharge stage of all full cycles, hence*

$$N_T^{\text{dis}}(\ ) = \Theta(\ )=(\ ^{\text{dis}}E^{\text{rate}}) \tag{C.23}$$

$$= \sum_{i=1}^{j} {}_{j\ j} 1_{[\quad i]} + \sum_{i=1}^{\text{dis}j} {}^{\text{dis}j} 1_{[\quad \frac{\text{dis}}{i}]}; \tag{C.24}$$

where $1_{[x]}$ has a value of one if x is true, and zero otherwise.

Proof. (C.23) defines $N_T^{\text{dis}}(\ )$ as the number fo times that energy is discharged from the cycle depth , while (C.24) means the number of cycles with depths at least . Therefore in this lemma we prove that these two definitions are equivalent, hence the proposed model has the same cycle counting result as the rainflow method.

Let $N_t^{\text{dis}}(\ )$ be the number of times energy is discharged from the depth during the operation period $[0; t]$, accounting all discharge half cycles and the discharge stage of all full cycles. Similarly, define $N_t^{\text{ch}}(\ )$ accounting all charge half cycles and the charge stage of all full cycles. Because we assume charge dispatches cause no aging cost, we can alternatively model battery initial energy level e_0 as an empty battery being charged to e_0 at the beginning of operation (such as in Fig. C.1), hence at $t = 0$ we have

$$N_0^{\text{ch}}(\ ) = \begin{cases} 1 & \leq e_0 \\ 0 & > e_0 \end{cases}; \quad N_0^{\text{dis}}(\ ) = 0: \tag{C.25}$$

Now assume at time t_1 the battery is switched from charging to discharging, and eventually resulted in a cycle of depth x that ends at t_2, regardless whether it is a half cycle or a full cycle. We also assume that there is no other cycles occuring from t_1 tp t_2, since in the rainflow method The battery must have been previously charged at least depth worth of

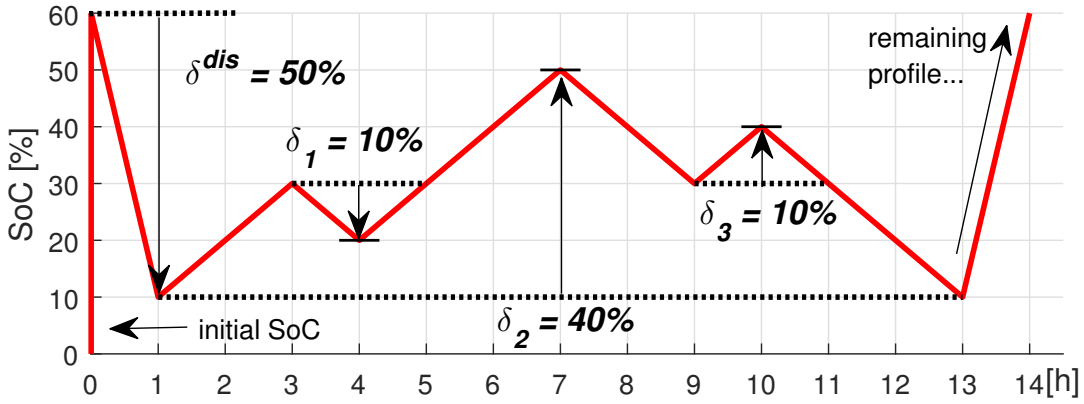

Figure C.1: Cycle counting example.

energy since we now assume the battery starts from empty. Therefore according to Theorem 1, segments in the range $[0; x]$ must be full at t_1, hence

$$N^{\mathrm{ch}}_{t_1}(\ ) - N^{\mathrm{dis}}_{t_1}(\ ) = 1 \quad \forall \ \ \leq x\,; \tag{C.26}$$

which is a sufficient condition for all discharge energy in this cycle being dispatched from segments in the depth range $[0; x]$, according to Theorem 1. After performing this cycle, all and only segments within the range $[0; x]$ are discharged one more time, in other words, all and only cycle depths in the range $[0; x]$ have one more count at end of this cycle t_2 compared to t_1 when the discharge begins, hence

$$N^{\mathrm{dis}}_{t_2}(\ ) - N^{\mathrm{dis}}_{t_1}(\ ) = 1_{[\quad x]}. \tag{C.27}$$

Therefore the proposed model has the same counting result as to the rainflow method for any cycles, which proves this lemma. □

C.1 Numerical example

We include a step-by-step example to illustrate how the proposed model is a close approximation of the benchmark rainflow cost model using the battery operation profile shown in Fig. C.2. To simplify this example, we assume a perfect efficiency of 1 and that the cycle

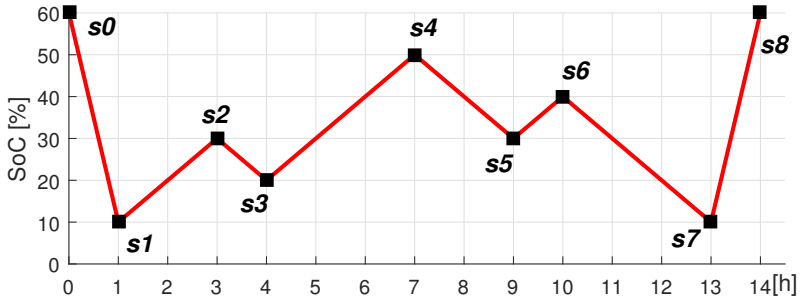

Figure C.2: An example of SoC profile.

aging cost function is 100 ^{2}. We consider 10 linearization segments, with each segment representing a 10% cycle depth range. The proposed model therefore has the following cycle aging cost curve

$$\mathbf{c} = \{1; 3; 5; 7; 9; 11; 13; 15; 17; 19\}. \tag{C.28}$$

According to the rainflow method demostrated in Fig. 2.2 , this example profile has the following cycle counting results

- Two full cycles of depth 10%, each costs 1
- One full cycle of depth 40% that costs 16
- One discharge half cycle of depth 50% that costs 25
- One charge half cycle that costs zero,

hence the total aging cost identified by the benchmark rainflow-based model is 43.

We implement this operation profile using the policy in Theorem 1 and record the marginal cost during each time interval. The results are shown in Table C.1. In this table, the first two columns are the time step and SoC. The third column shows the energy level of each linearization segment represented in a vector from $\mathbf{e}_t$. $\mathbf{e}_t$ is a 10×1 vector, and its energy level segments are sorted from shallower to deeper depths. Segment energy levels are normalized so that one means the segment is full, and zero means the segment is empty.

Table C.1: Battery Operation Example.

t	SoC	energy segments $[\mathbf{e}_t]$	discharge power $[\mathbf{p}_t^{\mathsf{dis}}]$	cost C_t
-	-	→ deeper depth →	→ deeper depth →	-
0	60	1,1,1,1,1,1,0,0,0,0	0,0,0,0,0,0,0,0,0,0	0
1	10	0,0,0,0,0,1,0,0,0,0	1,1,1,1,1,0,0,0,0,0	25
2	20	1,0,0,0,0,1,0,0,0,0	1,1,1,1,1,0,0,0,0,0	0
3	30	1,1,0,0,0,1,0,0,0,0	0,0,0,0,0,0,0,0,0,0	0
4	20	0,1,0,0,0,1,0,0,0,0	1,0,0,0,0,0,0,0,0,0	1
5	30	1,1,0,0,0,1,0,0,0,0	0,0,0,0,0,0,0,0,0,0	0
6	40	1,1,1,0,0,1,0,0,0,0	0,0,0,0,0,0,0,0,0,0	0
7	50	1,1,1,1,0,1,0,0,0,0	0,0,0,0,0,0,0,0,0,0	0
8	40	0,1,1,1,0,1,0,0,0,0	1,0,0,0,0,0,0,0,0,0	1
9	30	0,0,1,1,0,1,0,0,0,0	0,1,0,0,0,0,0,0,0,0	3
10	40	1,0,1,1,0,1,0,0,0,0	0,0,0,0,0,0,0,0,0,0	0
11	30	0,0,1,1,0,1,0,0,0,0	1,0,0,0,0,0,0,0,0,0	1
12	20	0,0,0,1,0,1,0,0,0,0	0,0,1,0,0,0,0,0,0,0	5
13	10	0,0,0,0,0,1,0,0,0,0	0,0,0,1,0,0,0,0,0,0	7
14	60	1,1,1,1,1,1,0,0,0,0	0,0,0,0,0,0,0,0,0,0	0
all	-	-	-	43

The fourth column shows how much energy is discharged from each segment during a time interval, represented by a discharge power vector $\mathbf{p}_t^{\mathsf{dis}}$ and is calculated as (the discharge efficiency is 1)

$$\mathbf{p}_t^{\mathsf{dis}} = [\mathbf{e}_{t\ \ 1} - \mathbf{e}_t]^+ : \tag{C.29}$$

The last column shows the operating cost that arises from each time interval, which is

calculated as

$$C_t = \mathbf{cp}_t^{\mathsf{dis}}. \tag{C.30}$$

This example profile results in the same cost of 43 in both the proposed model and the benchmark model, as proved in Theorem 2.

Appendix D

SUPPLEMENTARY MATERIAL TO CHAPTER 6

D.1 Nomenclature

$B; B^{\mathsf{E}}; B^{\mathsf{N}}$ Set of buses and subset of buses with and without energy storage, indexed by b

$I; I_b$ Set of generators and subset of generators connected to bus b, indexed by i

J Set of typical days, indexed by j

L Set of transmission lines, indexed by l

T Set of time intervals, indexed by t

$o(l); r(l)$ Sending and receiving ends of line l

$C^{[\,]}(\cdot)$ Cost function for different problems, \$

$e_b^{\mathsf{R}}; p_b^{\mathsf{R}}$ Energy storage energy (MWh) and power (MW) rating.

$e_{j;t;b}^{\mathsf{soc}}$ Energy storage state of charge, MWh

$f_{j;t;l}$ Line power flow, MW

$p_{j;t;b}^{\mathsf{ch}}; p_{j;t;b}^{\mathsf{dis}}$ Energy storage charging and discharging rates, MW

$p_{j;t;i}^{\mathsf{g}}$ Generator output power, MW

$p_{j;t;b}^{\mathsf{rs}}$ Renewable spillage, MW

$r_{j;t;b}^{\mathsf{ed}}; r_{j;t;b}^{\mathsf{eu}}$ Regulation down and up provided by energy storage, MW

$r^{gd}_{j;t;i}; r^{gu}_{j;t;i}$ Regulation down and up provided by generator, MW

$x^{[\,]}$ Vector of decision variables

y Cutting-plane method decision variable vector

$_{j;t;b}$ Voltage phase angle

$^{lmp}_{j;t;b}$ Locational marginal price, $/MWh

$^{rd}_{j;t};\ ^{ru}_{j;t}$ Price for down/up regulation, $/MWh

$'^{[\cdot]}_{[\cdot]}, \ ^{[\cdot]}_{[\cdot]}, \ ^{[\cdot]}_{[\cdot]}$ Dual variables associated with upper bounds, lower bounds, and equality constraints

$c^{p}; c^{e}$ Daily prorated capital costs of energy storage, $/MW and $/MWh

$c^{g}_{i}; c^{gd}_{i}; c^{gu}_{i}$ Hourly incremental, regulation up, and regulation down costs of generators, $/MWh

$c^{dis}; c^{ch}$ Hourly incremental discharge and charge cost of ES, $/MWh

$c^{eu}; c^{ed}$ Hourly regulation up and down cost of ES, $/MWh

c^{rs} Value of renewable spillage, $/MWh

$D_{j;t;b}$ Load demands, MW

F_{l} Capacity of transmission lines, MW

$G^{max}_{i}; G^{min}_{i}$ Maximum and minimum power production of generators, MW

$G^{rn}_{j;t;b}; G^{rs}_{j;t;b}$ Renewable power maximum expected forecast and maximum allowable spillage, MW

$R^{u}_{i}; R^{d}_{i}$ Ramp down and ramp up capacity of generators, MW/h

$T^{ru}; T^{rd}$ Ramp down/up speed requirement for down/up regulation, h

T^{es} Continuous full dispatch time requirement for energy storage, h

X_l Transmission line reactance

$!_j$ Weight of typical day

^{min}; ^{max} Minimum and maximum allowable values of the power/energy ratio of storage systems, h ^{1}

^{ch}; ^{dis} Charging and discharging efficiency of energy storage

^{D}; ^{R} Regulation requirement as a percentage of the load and renewable injections

Iteration index

Relative tolerance for system cost savings

D.2 Single-Level Equivalent Problem Formulation

This problem consists of the objective function (6.20), the UL constraints (6.3)–(6.5), and the following constraints:

D.2.1 PLL constraints

Equations (6.10)–(6.17) and the following constraints ($\forall i \in I; j \in J; t \in T; b \in B$):

$$G_i^{min} + r_{j;t;i}^{gd} \le p_{j;t;i}^{g} \le G_i^{max} - r_{j;t;i}^{gu} : (\ ^{g}_{j;t;i};\ '^{g}_{j;t;i}) \tag{D.1}$$

$$0 \le r_{j;t;i}^{gu} \le T^{ru} R_i^{u} : (\ ^{gu}_{j;t;b};\ '^{gu}_{j;t;b}) \tag{D.2}$$

$$0 \le r_{j;t;i}^{gd} \le T^{rd} R_i^{d} : (\ ^{gd}_{j;t;b};\ '^{gd}_{j;t;b}) \tag{D.3}$$

$$-R_i^{d} \le p_{j;t;i}^{g} - p_{j;t\ \ 1;i}^{g} \le R_i^{u} : (\ ^{R}_{j;t;i};\ '^{R}_{j;t;i}) \tag{D.4}$$

$$f_{j;t;l} = (\ _{j;t;o(l)} -\ _{j;t;r(l)})/x_l : (\ ^{f}_{j;t;l}) \tag{D.5}$$

$$-F_l^{max} \le f_{j;t;l} \le F_l^{max} : (\ ^{f}_{j;t;l};\ '^{f}_{j;t;l}) \tag{D.6}$$

$$0 \le p_{j;t;b}^{rs} \le G_{j;t;b}^{rs} : (\ ^{rn}_{j;t;b};\ '^{rn}_{j;t;b});\ \tag{D.7}$$

The minimum and maximum capacity of all generators are enforced in (D.1). (D.2) and (D.3) model the ramp requirement for regulation, and (D.4) models the ramp requirement for dispatch. The DC power flow is modeled in (D.5) and (D.6). The maximum expected forecast for renewable generation and the maximum allowable renewable spillage are enforced in (D.7).

D.2.2 DLL constraints

The DLL problem has the following constraints ($\forall i \in I; j \in J; t \in T; b \in B$):

$$'^{f}_{j;t;l} + {}^{f}_{j;t;l} + {}^{f}_{j;t;l} - {}^{lmp}_{j;t;o(l)} + {}^{lmp}_{j;t;r(l)} = 0 \tag{D.8}$$

$${}^{rn}_{j;t;b} + '^{rn}_{j;t;b} - {}^{lmp}_{j;t;b} + ({}^{ru}_{j;t} + {}^{rd}_{j;t})\ {}^{D} = c^{rs} \tag{D.9}$$

$$'^{g}_{j;t;i} + {}^{g}_{j;t;i} + '^{R}_{j;t;i} - '^{R}_{j;t+1;i} + {}^{R}_{j;t;i} - {}^{R}_{j;t+1;i} + {}^{lmp}_{j;t;b(i)} = c^{g}_{i} \tag{D.10}$$

$$'^{g}_{j;t;i} + {}^{ru}_{j;t} + '^{gu}_{j;t;i} + {}^{gu}_{j;t;i} = c^{gu}_{i} \tag{D.11}$$

$$-{}^{g}_{j;t;i} + {}^{rd}_{j;t} + '^{gd}_{j;t;i} + {}^{gd}_{j;t;i} = c^{gd}_{i} \tag{D.12}$$

$$'^{soc}_{j;t;b} + {}^{soc}_{j;t;b} + {}^{soc}_{j;t;b} - {}^{soc}_{j;t+1;b} = 0 \tag{D.13}$$

$$'^{soc}_{j;n_T;b} + {}^{soc}_{j;n_T;b} + {}^{soc}_{e;n_T;b} = 0 \tag{D.14}$$

$$'^{ch}_{j;t;b} + {}^{ch}_{j;t;b} - {}^{soc}_{j;t;b} - {}^{lmp}_{j;t;b} = {}^{ch} = c^{ch} \tag{D.15}$$

$$'^{dis}_{j;t;b} + {}^{dis}_{j;t;b} + {}^{soc}_{j;t;b} + {}^{lmp}_{j;t;b}\ {}^{dis} = c^{dis} \tag{D.16}$$

$$'^{ch}_{j;t;b} + {}^{rd}_{j;t;b} + T^{es}\ '^{soc}_{j;t;b} - \bar{e}^{ed}\ {}^{soc}_{j;t;b} + {}^{rd}_{j;t} = {}^{ch} = c^{ed} \tag{D.17}$$

$$'^{dis}_{j;t;b} + {}^{ru}_{j;t;b} - T^{es}\ {}^{soc}_{j;t;b} - \bar{e}^{eu}\ {}^{soc}_{j;t;b} + {}^{ru}_{j;t}\ {}^{dis} = c^{eu}; \tag{D.18}$$

where ≥ 0 and $' \leq 0$.

D.3 ES Pro t Constraint Transformation

From DLL constraints (D.15)–(D.16) and (D.17)–(D.18), we obtain the following equalities:

$$\begin{aligned}
&p^{\mathrm{dis}}_{j;t;b}(\ ^{\mathrm{Imp}}_{j;t;b}\ ^{\mathrm{dis}} - c^{\mathrm{dis}}) - p^{\mathrm{ch}}_{j;t;b}(\ ^{\mathrm{Imp}}_{j;t;b} = \ ^{\mathrm{ch}} + c^{\mathrm{ch}}) \\
&= \ ^{\mathrm{soc}}_{j;t;b}(p^{\mathrm{ch}}_{j;t;b} - p^{\mathrm{dis}}_{j;t;b}) - p^{\mathrm{dis}}_{j;t;b}(\ ^{\mathrm{dis}}_{j;t;b} + \ '^{\mathrm{dis}}_{j;t;b}) \\
&- p^{\mathrm{ch}}_{j;t;b}(\ ^{\mathrm{ch}}_{j;t;b} + \ '^{\mathrm{ch}}_{j;t;b}) \qquad \text{(D.19)} \\
&r^{\mathrm{eu}}_{j;t;b}(\ ^{\mathrm{eu}}_{j;t}\ ^{\mathrm{dis}} - c^{\mathrm{eu}}) + r^{\mathrm{ed}}_{j;t;b}(\ ^{\mathrm{ed}}_{j;t} = \ ^{\mathrm{ch}} - c^{\mathrm{ed}}) \\
&= -(\ '^{\mathrm{ch}}_{j;t;b} + \ ^{\mathrm{rd}}_{j;t;b} + T^{\mathrm{es}}\ '^{\mathrm{soc}}_{j;t;b})r^{\mathrm{ed}}_{j;t;b} \\
&- (\ '^{\mathrm{dis}}_{j;t;b} + \ ^{\mathrm{ru}}_{j;t;b} - T^{\mathrm{es}}\ ^{\mathrm{soc}}_{j;t;b})r^{\mathrm{eu}}_{j;t;b} : \qquad \text{(D.20)}
\end{aligned}$$

By using (6.13), (D.13), and (D.14), we derive the following expression:

$$\begin{aligned}
&\sum_{t2T}\ ^{\mathrm{soc}}_{j;t;b}(p^{\mathrm{ch}}_{j;t;b} - p^{\mathrm{dis}}_{j;t;b}) \\
&= \sum_{t=1}^{n_T - 1} e^{\mathrm{soc}}_{j;t;b}(\ ^{\mathrm{soc}}_{j;t;b} - \ ^{\mathrm{soc}}_{j;t+1;b}) + e^{\mathrm{soc}}_{j;n_T;b}\ ^{\mathrm{soc}}_{j;n_T;b} \\
&= \sum_{t2T} e^{\mathrm{soc}}_{j;t;b}(\ ^{\mathrm{soc}}_{j;t;b} + \ '^{\mathrm{soc}}_{j;t;b}) ; \qquad \text{(D.21)}
\end{aligned}$$

We can obtain the linear daily revenue collected by ES by 1) combining and rearranging (D.19)–(D.21), and 2) substituting the complementary slackness condition associated with (6.14)–(6.17).

$$\begin{aligned}
&(p^{\mathrm{ch}}_{j;t;b} + r^{\mathrm{ed}}_{j;t;b})\ '^{\mathrm{ch}}_{j;t;b} + (p^{\mathrm{dis}}_{j;t;b} + r^{\mathrm{eu}}_{j;t;b})\ '^{\mathrm{dis}}_{j;t;b} \\
&+ (e^{\mathrm{soc}}_{j;t;b} + T^{\mathrm{es}} r^{\mathrm{ed}}_{j;t;b})\ '^{\mathrm{soc}}_{j;t;b} + (e^{\mathrm{soc}}_{j;t;b} - T^{\mathrm{es}} r^{\mathrm{eu}}_{j;t;b})\ ^{\mathrm{soc}}_{j;t;b} \\
&= \sum_{t2T}\ (\ '^{\mathrm{ch}}_{j;t;b} + \ '^{\mathrm{dis}}_{j;t;b})p^{\mathrm{R}}_{b} + \ '^{\mathrm{soc}}_{j;t;b} e^{\mathrm{R}}_{b}\ ; \qquad \text{(D.22)}
\end{aligned}$$

which leads to

$$C^{\mathrm{R}} = -\sum_{j2J}\ \sum_{\substack{t2T \\ b2B}}\ (\ '^{\mathrm{ch}}_{j;t;b} + \ '^{\mathrm{dis}}_{j;t;b})p^{\mathrm{R}}_{b} + \ '^{\mathrm{soc}}_{j;t;b} e^{\mathrm{R}}_{b}\ : \qquad \text{(D.23)}$$

Because ES revenue only applies to $b \in B^{\mathrm{E}}$, by comparing (D.23) with (6.25) and (6.26),we can represent ES revenue using ES subgradients:

$$C^{\mathrm{R}} = -\sum_{b2B}\ (g^{\mathrm{p}}_{b} - c^{\mathrm{p}})p^{\mathrm{R}}_{b} + (g^{\mathrm{e}}_{b} - c^{\mathrm{e}})e^{\mathrm{R}}_{b}\ : \qquad \text{(D.24)}$$

D.4 ES Subgradient Derivation at B^E Buses

We calculate the ES subgradients assuming C^S is differentiable. At $(\ )$th iteration, the ES subgradients $g^{U;(\ )}$ includes the subgradients with respect to p_b^R and e_b^R for $b \in B$

$$g^{U;(\ )} = [g_b^{p;(\ )} \quad g_b^{e;(\ )}]^T : \tag{D.25}$$

$g^{U;(\ )}$ can be calculated using either the primal or the dual form of the ED problem with their minimizer (or maximizer):

$$\begin{aligned} g^{U;(\ )} \approx & \nabla_{x^U} C^S(x^{U;(\ )}; \hat{x}^{P;(\ )}) \\ = & \nabla_{x^U} C^E(x^{U;(\ )}) + \sum_{j \in J} \pi_j \nabla_{x^U} C_j^P(x^{U;(\ )}; \hat{x}_j^{P;(\ )}) \\ = & \nabla_{x^U} C^E(x^{U;(\ )}) + \sum_{j \in J} \pi_j \nabla_{x^U} C_j^D(x^{U;(\ )}; \hat{x}_j^{D;(\ )}) : \end{aligned} \tag{D.26}$$

and the subgradients are calculated as follows:

$$\begin{aligned} \lim_{x^U \to 0} || & C_j^D(x^{U;(\ )} + \Delta x^U; \hat{x}_j^{D;(\ )}) - C_j^D(x^{U;(\ )}; \hat{x}_j^{D;(\ )}) \\ & - [g^U]^T \Delta x^U || = || \Delta x^U || = 0 : \end{aligned} \tag{D.27}$$

We use the dual form of the ED problem, and the subgradient for $b \in B^E$ is:

$$\begin{bmatrix} g^{p;(\ )} \\ g^{e;(\ )} \end{bmatrix} = \begin{bmatrix} c^p + \sum_{j \in J} \pi_j \sum_{\substack{t \in T \\ b \in B}} (\mu_{j;t;b}^{ch;(\ )} + \mu_{j;t;b}^{dis;(\ )}) \\ c^e + \sum_{j \in J} \pi_j \sum_{\substack{t \in T \\ b \in B}} \mu_{j;t;b}^{soc;(\ )} \end{bmatrix} : \tag{D.28}$$

D.5 ES Subgradient Derivation for B^N Buses

For $b \in B^N$, let Δp_b^R and Δe_b^R be sufficiently small. We use the strong duality condition and replace C_j^P with C_j^D in C^S. Because $\Delta p_b^R \to 0$, $\Delta e_b^R \to 0$, other decision variables are not affected and are removed, leaving only terms that are directly associated with energy storage at B^N buses and obtain the following problem that calculates the ES gradient at B^N buses at iteration $\ $:

$$\begin{aligned} & \max_x \ C^{0;(\ )}(\hat{x}\ ; \hat{x}_j^D) := \\ & \sum_{j \in J} \pi_j \sum_{\substack{t \in T \\ b \in B}} \Delta p_b^R (\mu_{j;t;b}^{ch} + \mu_{j;t;b}^{dis}) + \Delta e_b^R \mu_{j;t;b}^{soc} \end{aligned} \tag{D.29}$$

we let $\pi^0_b = \Delta p^R_b = \Delta e^R_b$, because all Δp^R_b and Δe^R_b variables are completely independent, thus the problem is equivalent to:

$$\max_x \sum_{j \in J} \omega_j \sum_{t \in T, b \in B} \pi^0_b (\rho^{ch}_{j;t;b} + \rho^{dis}_{j;t;b}) + \rho^{soc}_{j;t;b} \tag{D.30}$$

subject to:

$$\pi^{min} \leq \pi^0_b \leq \pi^{max}; \tag{D.31}$$

and (D.11) to (D.18) by replacing $\pi^{Imp}_{j;t;b}$, $\pi^{ru}_{j;t;b}$, $\pi^{rd}_{j;t;b}$ with $\hat{\pi}^{Imp;(\nu)}_{j;t;b}$, $\hat{\pi}^{ru;(\nu)}_{j;t;b}$, $\hat{\pi}^{rd;(\nu)}_{j;t;b}$ in $X^{D;(\nu)}_j$ because these ES do not affect prices. This subproblem can be transformed into its equivalent primal form

$$\min_x \; C^0(x; \hat{x}^{D;(\nu)}_j) := \sum_{b \in B} g^0(x; \hat{x}^{D;(\nu)}_j); \tag{D.32}$$

which is equivalent to (6.27).

D.6 Exact Relaxation of ES Dispatch Constraints

In the established ED problem, an ES can be enforced to only charge or discharge at a single time step with the following non-convex complementary constraint [78] ($\forall\, j \in J,\, t \in T,\, b \in B$)

$$p^{dis}_{j;t;b} p^{ch}_{j;t;b} = 0; \tag{D.33}$$

Sufficient conditions for an exact relaxation of (D.33) is analyzed using the Karush-Kuhn-Tucker (KKT) condition. In the KKT condition for the ED problem in (6.8) and (6.9), the derivative of the Lagrangian function with respect to ES discharging variables $p^{dis}_{j;t;b}$ must equal to zero, hence the following equation holds ($\forall\, j \in J,\, t \in T,\, b \in B$)

$$c^{dis} - \rho^{dis}_{j;t;b} - \pi^{dis}_{j;t;b} + \pi^{e}_{j;t;b} + \pi^{Imp}_{j;t;b} \eta^{dis} = 0 \tag{D.34}$$

similarly, for ES charging variables $p^{ch}_{j;t;b}$, the following equation holds ($\forall\, j \in J,\, t \in T,\, b \in B$)

$$c^{ch} - \rho^{ch}_{j;t;b} - \pi^{ch}_{j;t;b} - \pi^{e}_{j;t;b} - \pi^{Imp}_{j;t;b} \eta^{ch} = 0 \tag{D.35}$$

Assume there exists $p^{dis}_{j;t;b} > 0$ and $p^{ch}_{j;t;b} > 0$ at bus b at time t during typical day j in the optimal solution of the ED problem. Then $^{dis}_{j;t;b} = 0$, $^{ch}_{j;t;b} = 0$ because of the complementary slackness conditions. Summing (D.34) and (D.35) and the following equation holds

$$c^{dis} + c^{ch} - {}'^{dis}_{j;t;b} - {}'^{ch}_{j;t;b} + (1= {}^{dis} - {}^{ch}) \; {}^{lmp}_{j;t;b} = 0; \tag{D.36}$$

because ${}'^{dis}_{j;t;b} \leq 0$, ${}'^{ch}_{j;t;b} \leq 0$, (D.36) can be reduced to

$$c^{dis} + c^{ch} \leq -(1= {}^{dis} - {}^{ch}) \; {}^{lmp}_{j;t;b}; \tag{D.37}$$

(D.37) describes the necessary condition for $p^{dis}_{j;t;b} > 0$ and $p^{ch}_{j;t;b} > 0$. Hence, the sufficient condition for the exact relaxation of the complementary constraint of (D.33) is

$$c^{dis} + c^{ch} > -(1= {}^{dis} - {}^{ch}) \; {}^{lmp}_{j;t;b}; \tag{D.38}$$

for all $j \in J$, $t \in T$, $b \in B$.

VITA

Bolun Xu received dual B.S. degrees in from Shanghai Jiaotong University, Shanghai, China, and University of Michigan, Ann Arbor, USA, in 2011, all in Electrical and Computer Engineering. He obtained his M.Sc degree in Electrical Engineering from Swiss Federal Institute of Technology,Zurich, Switzerland in 2014. He is currently a PhD Candidate in Electrical Engineering at the University of Washington, Seattle, WA, USA.

Bolun was a research intern in ABB Corporate Research Center Switzerland (2013), China Electric Power Research Institute (2014), ISO New England (2016), and Doosan Gridtech (2017). His research interests include energy storage, power system operations, and power system economics.